DESIGN AND SYNTHESIS OF HYBRID INORGANIC/ORGANIC NETWORKS FOR THE SEQUESTRATION OF POLLUTANTS FROM AQUEOUS ENVIRONMENTS AND THE STABILIZATION OF EMULSIONS

A Dissertation

by

JENIREE ANDREINA FLORES DELGADO

Submitted to the Office of Graduate and Professional Studies of
Texas A&M University
in partial fulfillment of the requirements for the degree of

DOCTOR OF PHILOSOPHY

Chair of Committee,	Karen L. Wooley
Committee Members,	Donald J. Darensbourg
	Jaime C. Grunlan
	Daniel A. Singleton
Head of Department,	Simon W. North

May 2017

Major Subject: Chemistry

ABSTRACT

The contamination of water with hydrocarbons caused by the extraction and transportation of crude oil is a devastating problem for the environment. Typically, mechanical methods are employed to remove the bulk of the oil; however, they cannot efficiently remove oil sheen. Additionally, surfactants are used to break down the oil but the difficulty in their removal from water could cause further contamination.

For these reasons, we have designed magnetically-active hybrid composite materials capable of absorbing oil, and of being removed from the water, known as magnetically-active hybrid networks (MHNs). The MHNs were synthesized from the coupling of amine-functionalized iron oxide nanoparticles and polymeric shell crosslinked knedel-like (SCK) nanoconstructs. An efficiency of *ca.* 400% towards the capture of crude oil was determined, with *ca.* 90% recovery of the oil sequestered, and recyclability of at least 3 cycles without compromising performance.

The performance of the MHNs in solutions that more closely resemble marine environments was also investigated. This was done by sequestering model aromatic (toluene) and aliphatic (dodecane) components of crude oil from water, and a 10% w/w NaCl solution (brine). An increase in the loading capacity of *ca.* 9x was observed, with no preference for either contaminant when sequestering from water. However, lower loadings were found when salts were present in the system; with a preference for toluene over dodecane. Hand shaking of the oil/MHN/water system during remediation led to the formation of emulsion droplets, which led to further examination of the mechanism

of interaction between the pollutants and the MHNs. The data showed that the MHNs operate *via* the mechanisms of absorption and emulsification, with the latter being responsible for the decrease in the loading capacity when sequestering from brine.

The capability of the MHNs to form emulsions was also explored. Stable, magnetically-active toluene-in-water and dodecane-in-water Pickering emulsions were obtained at a water-to-oil ratio of 3 : 1 and MHN concentrations as low as 1 mg/mL. Their magnetic property was explored to separate the emulsified oil phase from the water phase, and they could be used in the extraction of hydrocarbons from unconventional reservoirs.

DEDICATION

To my mother, Ludy Delgado, my father, Jose Flores and my advisor Karen Wooley.

ACKNOWLEDGEMENTS

Five years ago I embarked on this journey of becoming a doctor without really knowing what to expect. I knew it was not going to be easy, and I am extremely grateful to have had, and to still have the support of many people all over the world. I would like to first thank Dr. Karen Wooley, for opening the doors of her laboratory to me, and for having the imagination to create interesting projects like the ones I have worked on over the last five years. During the time she has been my mentor I have learned multiple valuable lessons, both professional and personal. I will forever admire her great imagination that leads to the creation of relevant scientific projects, her passion and dedication to her work, and her high standards. I have always been impressed by her ability to find the best qualities in people even in the worst situations, and her capacity to let people know when they are doing a good job. These two characteristics of her personality have helped me stay motivated over the years, especially during the times when I felt like giving up. Moreover, I want to thank Karen for being a role model not only as a scientist but also as a strong woman. I admire how much she has achieved throughout her career in a field that has been traditionally dominated by men, while still being able to have a family. I thank her for showing all women that we can achieve anything we put our minds to without giving up, just finding the compromise that works for each one of us.

I would also like to thank my committee members Dr. Donald Darensbourg, Dr. Daniel Singleton and Dr. Jaime Grunlan for their invaluable suggestions.

This work would not have been possible without my collaborators. I am thankful to Dr. Yingchao Chen for performing all the cryogenic microscopy work, and for making the technique seem seamless. Her expertise in this area helped us understand the materials we were working with, and made our publications even stronger. To Dr. Adriana Pavía-Sanders, not only for her contributions to my work through countless discussions, editing, and making extraordinary images to illustrate our work; but also for mentoring me during my time in the Wooley laboratory. Adriana not only laid down the ground work for our project, but also guided me through polymerization techniques, nanoparticles synthesis, and instrument training. She has always been there both for scientific and moral support, and for that I am thankful. I would also like to thank Dr. Jennifer Zigmond, a friend and colleague who started this journey with me. Over the years we have built a relationship based on chemistry and fitness. We have been there for each other when times were tough, both mentally and physically, and we have found ways to measure success in non-traditional ways in order to keep pushing through until the end.

I am extremely grateful to Dr. Agustin Diaz, for being a second advisor to me and also my husband. He took a great interest in my project from the very beginning, and always pushed me to reach a deep understanding of every aspect of my research. He taught me new techniques and encouraged me to learn new things even if they were not directly related to my research, helping me become a well-rounded scientist. Agustin has also been there for me when I needed to vent my frustrations and helped me see the

light at the end of the tunnel. I look forward to many more years of discussions and experiences together.

My scientific career began many years ago in the Miller Unit. I am thankful to Dr. Stephen Miller for letting me do research in his laboratory and to my early career mentors Laurent Mialon and Dr. Alexander Pemba. These two individuals not only helped me take my first steps in a laboratory, they also made research fun. They and the other members of the unit, Dr. John Jairo García and Dr. Christian Gorsche showed me that research was challenging and frustrating at times, but having a good team to work with makes all the difference in the world. I would also like to add that Christian was not only a lab friend in the US, but also a mentor and a tour guide in Austria. To him, I am grateful for helping me make the connections to spend my last semester of my undergraduate career in the beautiful city of Vienna, and for sharing his house, friends, and family to make me feel welcome in a completely new environment.

As an international student, I have had financial support from different organizations. I would like to first thank AVEMUNDO for giving me the opportunity to attend Waterford Kamhlaba UWC in Swaziland. This experience completely changed my life, and through the financial support of the Davis Foundation, made my undergraduate studies possible at the University of Florida. I would like to thank my teachers: Neil Cave and Michael Watson, for being friends more than teachers, and to the “spice girls” for helping me get through one of the most challenging experiences in my life.

Lastly, I would like to thank the people I grew up with and whom one way or another, have shaped me into the person I am today. First my parents for instilling in me a great sense of discipline and responsibility, for introducing me to the sports I loved and practiced for so many years, and for always being there for me giving me everything I needed to succeed both in school and in my sports. To my siblings and high school friends, for the e-mails and the text messages that kept us in touch despite the distance. To my cousin William Veloz and my dear friend Valmore Rodriguez, my coaches during a 17 year sports journey that made me the person I am today. They believed in my abilities to become a great athlete even when I could not see it, they pushed me through challenging training sessions to make me stronger both physically and mentally, and stood next to me to make me believe in myself when the nerves got the best of me.

To all of you I just want to say: Thank you! I could not have done it without you.

NOMENCLATURE

AA	Acrylic acid
AIBN	Azobisisobutyronitrile
Amine-IONs	Amine-functionalized iron oxide nanoparticles
ATR	Attenuated total reflectance
AFM	Atomic force microscopy
ATRP	Atom transfer radical polymerization
BTEX	Benzene, toluene, ethylbenzene and xylenes
$CDCl_3$	Deuterated chloroform
Cryo	Cryogenic
CuBr	Cuprous bromide
DLS	Dynamic light scattering
DSC	Differential scanning calorimetry
EDCI	1-(3’-dimethylaminopropyl)-3-ethylcarbodiimide methiodide
FITC	Fluorescein-5-thiosemicarbazide
GC-MS	Gas chromatography- mass spectrometry
GPC	Gel permeation chromatography
ICP-AES	Inductively coupled plasma-atomic emission spectroscopy
IONs	Iron oxide nanoparticles
IR	Infrared
ITF	Interfacial tension

KPS	Potassium persulfate
LCO	Light cycle oil
LGO	Light gas oil
MIC	Microscopy imaging center
MHN	Magnetically-active hybrid networks
MMA	Methyl methacrylate
MSCK	Magnetic shell crosslinked knedel-like
MWCO	Molecular weight cut-off
NMR	Nuclear magnetic resonance spectroscopy
O/W	Oil-in-water
O/W/O	Oil-in-water-in-oil
PAA	Poly(acrylic acid)
PAA-*b*-PS	Poly(acrylic acid)-*block*-polystyrene
PAH	Polycyclic aromatic hydrocarbons
PM	Physical mixture
PMDETA	N,N,N',N",N" – Pentamethyldiethylenetriamine
PMMA	Poly (methyl methacrylate)
PTA	Phosphotungstic acid
P*t*BA	Poly(*tert*-butyl acrylate)
PVP	Polyvinylpyrrolidone
PW	Produced water
PS	Polystyrene

SCK	Shell crosslinked knedel-like
SEM	Scanning electron microscopy
SWNT	Single-walled carbon nanotube
TEM	Transmission electron microscopy
TFA	Trifluoroacetic acid
TGA	Thermogravimetric analysis
THF	Tetrahydrofuran
TICT	Twisted intramolecular charge transfer
TOPO	Tri-*n*-octylphosphine oxide
W/O	Water-in-oil
W/O/W	Water-in-oil-in-water
W : O	Water-to-oil ratio
WSF	Water-soluble fraction

TABLE OF CONTENTS

Page

LIST OF FIGURES

Page

LIST OF SCHEMES

Page

LIST OF TABLES

Page

CHAPTER I

INTRODUCTION

The contamination of marine and fresh aquatic environments with hydrophobic organic pollutants is a problem that gravely affects the balance in our planet's diverse ecological systems. The direct or indirect discharge of chemicals, as well as industrial and residential waste into major bodies of water threatens the growth and development of the planet's diverse flora and fauna. One of the pollutants that severely affect fresh and marine environments is hydrocarbons deposited in the water by oil spills. In 2014 about 20 000 oil spills were reported to the U.S Coast Guard National Response Center;[1] however this number is expected to increase significantly when global spills are taken into consideration. Based on the extent of contamination caused by the exploration, drilling and transport of oil, a remediation routine has been developed with the aim of diminishing the impact of oil spills in the environment. The initial response after a spill is the containment of the pollutants to limit the exposed area; followed by the employment of mechanical methods such as the use of booms, skimmers or even suction to remove the bulk of the oil spilled.[2] Nevertheless, the use these mechanical methods becomes inefficient for the removal of low concentrations of oil better known as *sheen*; which shows as thin layers of *ca*. 0.04 to 50 micrometers of oil on the surface of the water.[3]

An alternative to the mechanical strategy is the use of dispersants, which aim to break the oil slick into smaller droplets that can disperse in water, and which can be processed by natural organisms present in the environment. One of the most common dispersants employed is COREXIT 9500, which is typically composed of surfactants dissolved in one or more solvents.[4] Surfactants, in turn, are composed of a hydrophobic tail and a hydrophilic head, and are capable of reducing the interfacial tension between water and oil by arranging themselves at the oil/water interface.[5] The formation of oil droplets increases the surface area of the oil available, which can be degraded by microorganisms thereby reducing the impact of the oil on the environment (Figure 1.1).[6]

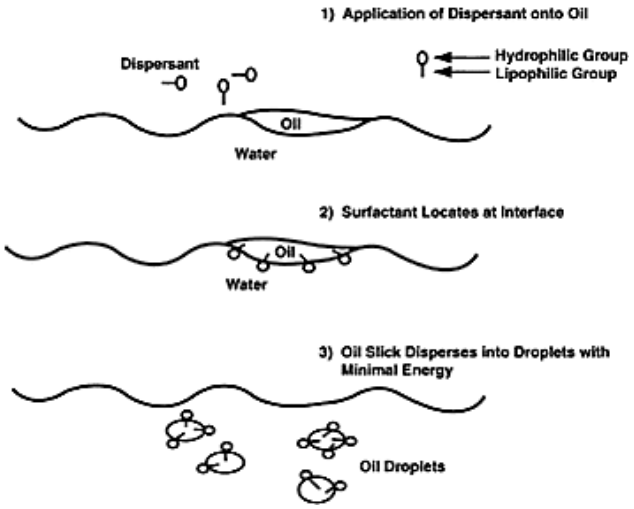

Figure 1.1. Mechanism of interaction between the dispersants and oil. (1) Dispersant is applied onto the oil spilled, (2) the surfactants arrange themselves at the water/oil interface, (3) oil slick is dispersed into smaller droplets after reduction of the interfacial tension between the water and the oil.[5] Reprinted with permission from Lessard, R. R.; DeMarco, G. *Spill. Sci. Technol. B.* **2000**, *6*, 59-68.

The use of surfactants to break down the oil slick can also lead to the formation of stable oil-water emulsions; however, this phenomenon cannot be solely attributed to the presence of surfactants in the water as some components of the oil, as well as the particulate present in the aqueous environments, can also stabilize oil-water emulsions.[4] In general, organic matter and clay minerals can interact with oil droplets by arranging themselves at the oil/water interface to prevent droplet coalescence. These emulsions are known as Pickering emulsions, and were first described by Walter Ramsden in 1903,[7] but their discovery has been attributed to Spencer U. Pickering.[8] The Pickering effect has been recognized as the ability of solid particles to stabilize droplets by adsorbing onto the interface (between the liquid-liquid phase in emulsions and between the gas-liquid phase in foams)[9] in order to prevent coalescence. This type of particle self-arrangement increases the stability of the system, which is determined by the energy required to remove a particle from the interface, given by equation 1.

$$-\Delta G = \pi r^2 \gamma_{OW} (1 - |\cos \theta_{OW}|)^2 \quad (1)$$

In this equation $\boldsymbol{r}$ is the particle's radius, γ_{OW} is the interfacial tension between the oil and the water, and $\boldsymbol{\theta_{OW}}$ is the contact angle that the particle makes with the interface between the oil and the water (also known as the particle's wettability). The contact angle is a highly relevant parameter given that when $\theta_{OW} = 90^{\circ}$, the particle is most strongly held to the interface. This factor also influences the type of emulsion being stabilized:[10] When the contact angle is less than 90˚, oil-in-water (o/w) emulsions are stabilized; however, when the contact angle is greater than 90˚ water-in-oil (w/o) emulsions form and become stable (Figure 1.2). Another parameter of importance is the size of the particles, as the energy necessary to remove the particle from the interface is proportional to the square of the particle's radius.

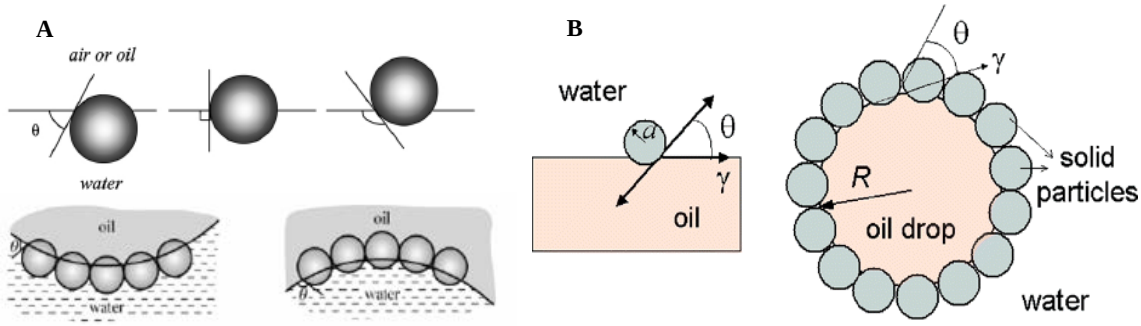

Figure 1.2. Schematic representation of the influence of the particle's wettability on the type of emulsion (A) and positioning of solid particles onto an oil droplet interface giving a solid-stabilized o/w emulsion (B).[10] Reprinted with permission from Melle, S.; Lask, M.; Fuller, G. G. *Langmuir* **2005**, *21*, 2158-2162. Copyright 2005 American Chemical Society.

Although the use of dispersants is a common practice in oil spill remediation, the difficulty associated with their removal from water could lead to further ecological damage; therefore, sorption materials are also employed in oil spill remediation. One of the most commonly utilized materials, particularly for the clean-up of oil sheen, is polypropylene fibers which have shown to be superior to perlite and cellulosic fibers for the absorption of light cycle oils (LCOs) and light gas oils (LGOs).[11] Nevertheless, manipulation of the fibers prior to, and post deployment is cumbersome and limits the ability to recover the loaded materials.

Several other materials such as sponges,[12,13,14] nanowires,[15] hydrogels,[16,17,18] and even nanoparticles[19,20] have been developed for the remediation of polluted water. An outstanding example is the work of Zhu and *et al*,[12] whereby *n*-dodecanoic acid-modified sponges have shown the ability to absorb oil at a ratio of 1 : 13 (material : oil) by weight. These sponges have shown recyclability of up to 9 cycles while maintaining a loading capacity of *ca.* 80%. Despite the remarkable performance of the sponges, the manual manipulation of the loaded materials is expensive and far from practical, making them less desirable for the remediation of contaminated water.

In order to solve the issues related to manipulating remediating materials, nanotechnologies with an added magnetic component have been synthesized to allow for a facile recovery of the loaded materials. In 2012, Zhu and co-workers synthesized polyurethane foams modified with polytetrafluoroethylene and iron oxide nanoparticles (IONs).[13] The foams were successful in the removal of mineral oil from an aqueous

solution *via* manipulation with an external magnetic field. In addition, the Pan group synthesized highly hydrophobic IONs coated with polysiloxane; which showed high absorbing efficiency.[20] These groups demonstrated that the concept of magnetic manipulation of materials for the remediation of aquatic environments could be efficient.[13] Furthermore, our group has ventured into the synthesis of magnetically-active nanostructures that target both buoyant and submerged oil; known as magnetic shell crosslinked knedel-like nanoparticles (MSCKs). The MSCKs are well defined organic/inorganic hybrid materials composed of poly(acrylic acid)-*block*-polystyrene (PAA-*b*-PS) block copolymers, that underwent co-assembly with IONs of *ca.* 8 nm in diameter, to form micellar structures which upon crosslinking exhibited a number-average hydrodynamic diameter of *ca.* 75 nm.[21] The MSCKs were capable of sequestering crude oil at a 1 : 10 (polymer : oil) ratio by weight, and exhibited quantitative recyclability.

In an effort to further increase the loading capacity of the current nanotechnology, and to address the variability in the composition of crude oil; hierarchically-assembled structures that display both magnetic responsivity as well as variable polymeric components are of interest. Our group has a long standing interest in the employment of supramolecular assembly of amphiphilic block copolymers for the development of core-shell nanoparticles, known as shell crosslinked knedel-like (SCK) nanoparticles. These devices have been obtained *via* the employment of controlled radical polymerization techniques such as atom transfer radical polymerization (ATRP), to synthesize amphiphilic block copolymers which upon controlled addition of water

into an organic system and selective crosslinking of the shell, yield the SCKs.[22,23] These nanoconstructs have been typically designed to serve as drug delivery systems due to their ability to host hydrophobic guests;[24-26] therefore, their application could be expanded to the sequestration of hydrophobic pollutants such as crude oil.

This dissertation is focused on the design and synthesis of hierarchically-assembled, magnetically-active materials capable of sequestering hydrophobic pollutants, and on the investigation of the mechanism of interactions between the hydrophobic pollutants and the remediating materials. The original design for these structures consisted of a large ION core that would impart the desired magnetic responsivity, surrounded by multiple SCK nanoparticles obtained from the self-assembly of PAA-*b*-PS block copolymers, which were synthesized *via* ATRP (Figure 1.3). This particular block copolymer was chosen to serve as the initial proof-of-concept; however, multiple SCKs of different polymer compositions could be loaded onto the ION core to target specific components of crude oil, as well as other types of pollutants.

The primary goals of the research in this dissertation were:

1) to synthesize novel magnetically-active composite materials capable of sequestering hydrophobic pollutants from aqueous environments, and to improve on previous successes;
2) to explore the sequestration of pollutants from saline environments to understand the effect of salts on the performance of the materials;
3) to determine the possibility of preferential sequestration for pollutants of differing chemical compositions;

4) to understand the mechanisms of interactions taking place between the composite materials and the hydrophobic contaminants in order to improve their performance and expand their field of applications.

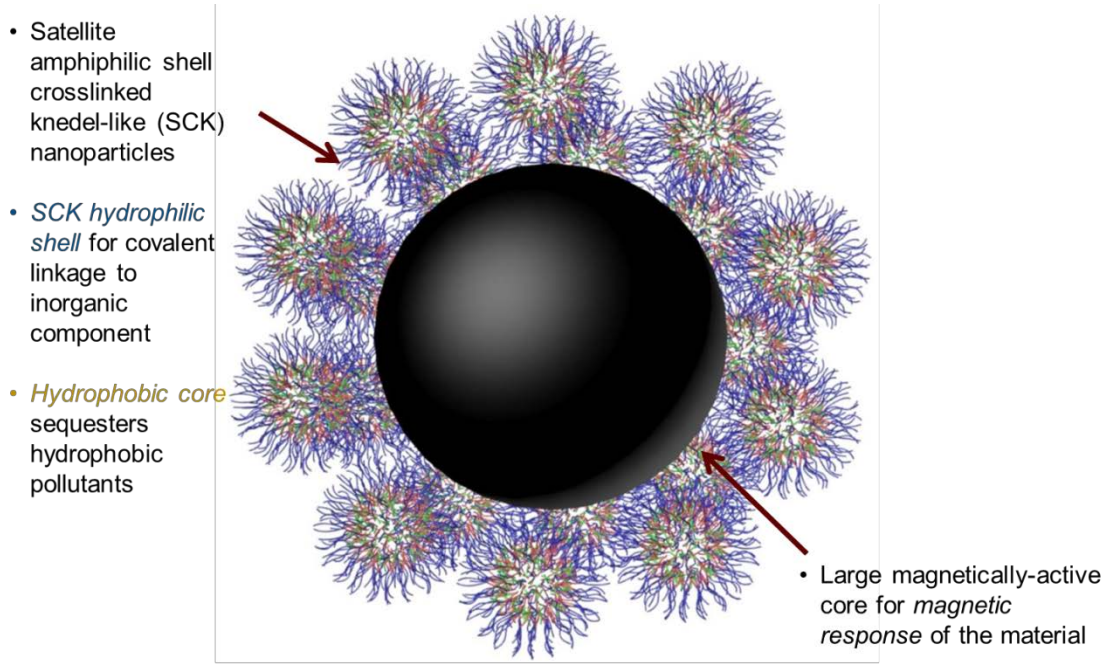

Figure 1.3. Original design of magnetically-active composite materials.

In Chapter II, hybrid inorganic/organic composite materials known as magnetically-active hybrid networks (MHNs) were synthesized from the coupling of amine-functionalized IONs (amine-IONs) and pre-established SCK polymer nanoconstructs. The MHNs displayed a network-like structure composed of several interconnected SCKs bound to agglomerates of magnetically-active amine-IONs, and

were designed for their application in the sequestration of hydrophobic contaminants from polluted environments. An initial assessment of their ability to capture crude oil determined a loading capacity in the range of 3.5 – 4.5 mg of oil sequestered per 1 mg of MHNs. The magnetic component of the hybrid nanoconstructs was exploited as a facile method of manipulation of the loaded networks, which allowed for the recovery of *ca.* 90% of the MHNs deployed in water, as well as *ca.*90% recovery of the oil originally sequestered. Re-utilization of these materials exhibited comparable efficiency after three cycles of remediation, which involved deployment, magnetic recovery, and organic washes to remove the cargo. These studies served as the proof-of-concept and corroborated the ability of the MHNs to sequester contaminants from aqueous environments *via* the expected mechanism of absorption of the hydrophobic pollutants into the hydrophobic core of the SCKs. However, no concrete evidence of this mechanism was obtained, and the performance of the MHNs in saline environments remained unknown. Additionally, the complex chemical composition of crude oil made it impossible to determine the existence of any preferential sequestration of the specific components of this convoluted pollutant.

In Chapter III, the performance of the MHNs in saline solutions that more closely resemble marine environments was investigated. To facilitate the studies, a 10% w/w NaCl (brine) solution was employed in order to fully study the interactions of the MHNs with the salts present in the system. Moreover, in order to determine the possibility of targeting the chemical composition of the polymeric component of these materials towards specific components of crude oil, model aliphatic (dodecane) and aromatic

(toluene) components of crude oil were utilized as contaminants. The results showed a *ca.* 9x increase in the loading capacity of the MHNs towards these less complex pollutants when compared to their loading capacity towards crude oil, with no preference being observed for the sequestration of either toluene or dodecane when the contaminants were deployed in nanopure water. However, significant differences were observed when sequestration was performed in brine. In general, a lower loading capacity of the MHNs was observed when salts were present during the remediation experiments; and under these conditions, higher loadings of toluene were encountered than for dodecane. Hand-shaking of the oil/MHN/water (or brine) system during remediation led to the formation of emulsion droplets which prompted a more detailed examination of the mechanism of interaction between the pollutants and the MHNs. The experiments revealed that the MHNs operate *via* dual mechanisms of interaction, which include the previously hypothesized absorption mechanism, as well as the stabilization of emulsions *via* the Pickering effect. The latter is believed to be responsible for the decrease in the loading capacity of the MHNs when sequestering from brine, and can be explained by the formation of "flocs" of MHNs as a consequence of their interaction with NaCl, which in turn reduces the effective concentration of particles capable of stabilizing the droplets. Overall, it has been concluded that when the mechanism of emulsification is compromised by the presence of salts in the system, the mechanism of absorption dominates. Under these circumstances, it is possible to design the polymeric component of the MHNs to target the sequestration of specific pollutants *via* hydrogen

bonding, van der Waals, or π-π interactions, which could lead to higher loadings and to a more effective remediation approach.

In Chapter IV, the ability of the MHNs to act as Pickering emulsifiers was further explored. These intricate networks were employed to stabilize emulsions between organic solvents and water, upon mechanical stimulus. In these studies, two methods of emulsification, vortex and probe sonication, were employed to yield toluene-in-water and dodecane-in-water emulsions, which were stable for up to two months in the presence of the MHNs. A detailed study of the effect of the water-to-oil (W : O) volume ratio and the MHN concentration on the droplet size of the emulsions revealed that the smallest droplet size, and narrowest dispersity were obtained at a W : O = 3 : 1, for all conditions tested. Additionally, concentrations of MHNs as low as 1 mg/mL and 1.5 mg/mL, for emulsions prepared *via* vortex and probe sonication, respectively, were sufficient to yield the smallest droplets and narrowest distributions. The effects of probe sonication on the structure of the MHNs were investigated, and although retention of the network structure characteristic of the MHNs was observed, the studies revealed partial dissociation of the MHNs into smaller clusters, and of some of the SCKs into individual polymer strands. These observations helped us explain why a slightly higher concentration of MHNs was required to achieve results *via* probe sonication, which were similar to those obtained *via* vortex. Moreover, confocal microscopy was employed to fully understand the stabilization of the emulsions by these complex network structures. To do so, fluorescently-labelled MHNs were used to generate and stabilize the emulsions, and upon excitation of the emulsion droplets with a 488 nm laser source, it

was determined that although the surface of the droplets was not completely covered by the MHNs, the particles did in fact decorate the oil droplets by arranging themselves at the oil/water interface, thus creating a stable barrier against coalescence. Furthermore, due to the presence of amine-IONs within the network structure of the composite materials, the oil droplets stabilized by the MHNs exhibited magnetic character and could be manipulated with an external magnetic field.

CHAPTER II

RECYCLABLE HYBRID INORGANIC/ORGANIC MAGNETICALLY-ACTIVE NETWORKS FOR THE SEQUESTRATION OF CRUDE OIL FROM AQUEOUS ENVIRONMENTS

2.1 Introduction

The deposition of chemicals and particles, as well as industrial, agricultural and residential waste into major bodies of water poses a danger to the growth and development of healthy biological populations. Among the pollutants that severely affect aquatic environments are hydrocarbons deposited in the water during the drilling, extraction and transport of crude oil. One of the main sources of contamination is oil spills, of which *ca*. 20,000 were reported to the U.S. Coast Guard National Response Center in 2014,[1] of varying severities and requiring varying extents of clean-up efforts; higher numbers are expected as global spills are taken into consideration. In cases of large-volume spills, a remediation routine involving the use of mechanical methods, such as booms, skimmers or suction, is utilized to remove the bulk of the oil discharged.[2] However, the use of these mechanical methods becomes inefficient for the removal of low concentrations of oil, better known as sheen, which shows as a thin layer of *ca*. 0.04 to 50 μm of oil on the surface of the water.[3]

---

*Reprinted with permission from Jeniree A. Flores, Adriana Pavía-Sanders, Yingchao Chen, Darrin. J. Pochan, Karen. L. Wooley. *Chem. Mater*. **2015**, *27*, 3775-3782,

An additional source of contamination is produced water (PW), which is a mixture of water trapped in underground formations and the water injected into the reservoir to facilitate drilling and extraction of oil during hydraulic fracturing (fracking) practices. Although this water has a variety of contaminants, the content of hydrocarbons is of primary concern, notably the suspended oil present, which can be reminiscent of sheen. Between 2010 and 2011 the water produced by the Marcellus formation, which encompasses parts of the states of New York, Pennsylvania, Ohio and West Virginia, was estimated to be 1.3 billion gallons in Pennsylvania alone.[27,28] If PW could be cleaned to achieve environmental standards, it could be reutilized in areas such as underground injection, irrigation, and other industrial uses (*e.g.* power plant makeup water and vehicle washing), diminishing its environmental impact.[29]

Recently, many advances have focused on designing materials for the separation of oil/water mixtures, such as sponges,[12-14,30] nanowires,[15] hydrogels,[16-18] fibers,[31] organic-inorganic composite membranes,[32,33] and nanoparticles.[19,20,34] However, despite their remarkable performance, many rely on manual labor for the manipulation and removal of the oil-loaded materials, making them less desirable for the remediation of contaminated water, due to financial and feasibility constraints. To address this issue, nanomaterials with an added magnetic component have been synthesized to allow for their facile recovery once loaded by the oil contaminant. For instance, Zhu and co-workers synthesized polyurethane foams modified with polytetrafluoroethylene and iron oxide nanoparticles (IONs), which were successful in the removal of mineral oil from an aqueous solution *via* the magnetic handling of the foam.[13] Likewise, the Pan group

developed highly hydrophobic IONs coated with polysiloxane which showed a high absorbing efficiency of over ten times the weight of the material.[20]

Despite the remarkable performance of these materials, their hydrophobic nature represented a limitation for the removal of submerged oil. To address this issue, Lead and co-workers synthesized water-dispersable polyvinylpyrrolidone (PVP)-coated IONs capable of removing crude oil from a water/oil mixture at a ratio of 1 : 2.6 (oil : PVP-IONs).[34] Recently, our group has synthesized magnetic shell crosslinked knedel-like (MSCK) nanoparticles, which combined amphiphilic polymers (to allow for aqueous dispersability and crude oil sequestration) with magnetic nanoparticles (to provide for magnetic recovery) in a robust nanoscopic structure. These organic/inorganic crosslinked micellar structures, composed of poly(acrylic acid)-*block*-polystyrene (PAA-*b*-PS) block copolymers and 8-nm IONs, had a core-shell morphology, overall dimensions of *ca*. 70 nm and contained large numbers of IONs within the amphiphilic block copolymer framework. The MSCKs were capable of sequestering crude oil from aqueous dispersions at a 1 : 10 (nanoparticle : oil) ratio by weight and exhibited quantitative recyclability.[21] With the significant advancement in the synthesis of remediating nanomaterials capable of sequestering buoyant and submerged oil made possible by the MSCK amphiphilic character, we anticipated that producing similar polymer-nanoparticle assemblies by a stagewise protocol would allow for definition of the composition and morphology to improve understanding of the structure-property-function relationships and optimize performance.

Consequently, we sought the development of compartmentalized materials assembled from pre-fabricated shell crosslinked knedel-like (SCK) nanoparticles covalently bound to magnetic inorganic substrates. As opposed to the MSCK structure, these hybrid materials were designed initially to present multiple copies of SCK polymer nanoparticles around a central magnetic inorganic nanoparticle core. It was expected that this morphology would allow for the sequestration of a diverse number of complex contaminants through tailoring of the polymeric SCK components. As an initial proof of concept, we report the synthesis of magnetically-active hybrid networks (MHNs) from the conjugation of PAA-*b*-PS SCK nanoparticles to similarly-sized amine functionalized IONs (amine-IONs). Rather than the idealized central inorganic and satellite organic nanoparticle structure, complex multi-particle MHNs were obtained. Their application towards the remediation of water contaminated with complex pollutants such as crude oil is demonstrated, as well as their potential for recovery of the pollutants and recyclability of the materials.

2.2 Materials and Methods

Materials. All chemicals were purchased from Aldrich Chemical Co. and used without further purification unless otherwise noted. *tert*-Butyl acrylate and styrene monomers were purified through an alumina plug to remove the stabilizer. Amine-IONs were purchased from Chemicell GmbH. Nanopure water (18 MΩ•cm) was acquired by means of a Milli-Q water filtration system, Millipore Corp. (Bedford, MA). A

neodymium magnet (90 lbs. pull) was purchased from magnets4less.com. Crude oil for this research was donated by Enbridge Energy Partners, LP.

Characterization Techniques. ^{1}H NMR and ^{13}C NMR spectra were recorded on an Inova 300 or Mercury 300 spectrometer interfaced to a UNIX computer using VnmrJ software. Samples were prepared as solutions in $CDCl_3$ or THF-d_8 and the solvent protons were used as internal standards. IR spectra were recorded on an IR Prestige 21 system (Shimadzu Corp., Japan). A small amount of sample was placed to cover the ATR crystal for IR measurements. Data were analyzed using IRsolution software. Differential scanning calorimetry studies were performed on a Mettler Toledo DSC822 (Mettler-Toledo, Inc., Columbus, OH) calibrated according to the standard procedures using indium. The heating rates were 4 °C/min and cooling rates were 4 °C/min with a temperature range of 25 – 150 °C. The T_g was taken as the midpoint of the inflection tangent, upon the third heating scan. Thermogravimetric analysis was performed under Ar atmosphere using a Mettler Toledo model TGA/DSC1 with a heating rate of 10 °C/min. Measurements were analyzed using Mettler Toledo *STAR*^{e} software v 10.00.

THF gel permeation chromatography (GPC) was conducted on a system equipped with Waters chromatography, Inc. (Milford, MA) model 1515 isocratic pump and a model 2414 differential refractometer with a three-column set of Polymer Laboratories, Inc. (Amherst, MA) Styragel columns (PL_{gel} 5 μm Mixed C, 500 Å, and 10^4 Å, 300 × 7.5 mm columns) and a guard column (PL_{gel} 5 μm, 50 × 7.5 mm). The

system was equilibrated at 40 °C in THF, which served as the polymer solvent and eluent (flow rate set to 1.00 mL/min). The differential refractometer was calibrated with Polymer Laboratories, Inc. polystyrene standards (300 to 467 000 Da). Polymer solutions were prepared at a concentration of *ca.* 3 mg/mL and an injection volume of 200 μL was used. Data were analyzed using *Empower Pro* software from Waters Chromatography Inc. Transmission electron microscopy (TEM) analysis was performed on a JEOL 1200 EX operating at 100 kV and micrographs were recorded at calibrated magnifications using a SLA-15C CCD camera. Samples for TEM were prepared as follows: 5 μL of a solution were deposited onto a formvar-coated copper grid, and after 30 s, the excess of the solution was quickly wicked away by a piece of filter paper. The samples were negatively stained with 1% phosphotungstic acid (PTA) aqueous solution. After 30 s, the excess staining solution was quickly wicked away by a piece of filter paper and the samples were left to dry overnight. Cryogenic TEM (cryo-TEM) measurements were performed on a FEI Tecnai G^2-12 microscope, operated at 120 kV and equipped with a Gatan CCD camera. Cryo-TEM sample grids were prepared using a FEI Vitrobot vitrification system. A droplet of *ca* 1.2 μL assembly suspension was then pipetted onto a lacey carbon grid, several blotting times were used (2 times) with each blot lasting 2 s in order to obtain appropriate liquid film thickness for imaging. The sample was allowed to relax for *ca*. 2 s to release any residual stresses induced by blotting, and then quickly plunged into a liquid ethane reservoir cooled by liquid N_2. The vitrified sample was rapidly moved into a Gatan 626 cryo-holder and cryo-transfer stage cooled by liquid N_2. During the imaging of the vitrified samples, the temperature

of the cryo-holder was maintained at *ca.* -176 °C to limit sublimation of vitreous water. Longer exposure time (3 - 5 s) at a lower dose was used to obtain data and avoid beam damage.

Dynamic light scattering (DLS) measurements were conducted using Delsa Nano C from Beckman Coulter, Inc. (Fullerton, CA) equipped with a laser diode operating at 658 nm. Size measurements were made in water (n = 1.3329, η = 0.890 cP at 25 ± 1 °C; n = 1.3293, η = 0.547 cP at 50 ± 1 °C; n = 1.3255, η = 0.404 cP at 70 ± 1 °C). Scattered light was detected at a 165°C angle and analyzed using a log correlator over 70 accumulations for a 0.5 mL of sample in a glass sizing cell (0.9 mL capacity). The photomultiplier aperture and the attenuator were automatically adjusted to obtain a photon counting rate of *ca*. 10 kcps. The calculations of the particle size distribution and distribution averages were performed using CONTIN particle size distribution analysis routines. Prior to analysis, the samples were passed through a 5 μm syringe filter (Thermo Scientific). The samples in the glass sizing cell were equilibrated at the desired temperature for 5 min before measurements were made. The peak average of histograms from intensity, volume, or number distributions out of 70 accumulations was reported as the average diameter of the particles. Mass balance was performed through the use of a Citizen Scale micro balance (Mumbai, India) with a readability of 1 μg and repeatability of 1 μg. Interfacial tension measurements were conducted using an OCA 25 measuring instrument from DataPhysics Instruments GmbH (Filderstadt, Germany) equipped with a high-speed USB camera (max. 215 images/s sample rate) and a high-speed video system

UpHSV1220 (max. 1120 images/s sample rate). The calculations of the interfacial tension values were performed using SCA 20 software.

Synthesis of Poly(*tert*-butyl acrylate) (P*t*BA$_{90}$) *via* ATRP. A flame dried 100 mL Schlenk flask equipped with a magnetic stir bar was charged with *N*, *N*, *N'*, *N"*, *N"*-pentamethyldiethylenetriamine (PMDETA, 1 equiv, 697.0 mg, 4 mmol), *t*BA (110 equiv, 54.9 g, 0.43 mol), ethyl-2-bromoisobutyrate (1 equiv, 948.5 mg, 5 mmol), and anisole (13 mL). The reaction mixture was degassed by three freeze-pump-thaw cycles. Then, CuBr (1 equiv, 577.1 mg, 4 mmol) was added under a nitrogen flow to the frozen mixture. Following two additional freeze-pump-thaw cycles, the reaction mixture was allowed to return to room temperature and immersed in a preheated oil bath at 55 °C to start the polymerization. The polymerization was monitored by analyzing aliquots collected at predetermined times by ^{1}H NMR spectroscopy. As the expected monomer conversion was reached at *ca*. 18.5 h, the polymerization was quenched by quick immersion of the reaction vessel into liquid N_2 and exposure to air. THF (60 mL) was added to the flask and the polymer was purified by filtration through an alumina plug followed by subsequent precipitation into 500 mL of a methanol/ice mixture (3 times). The precipitate was collected and dried under vacuum overnight to afford 27 g of P*t*BA$_{90}$ as a white solid, giving 50% yield of the 98% conversion polymerization. $M_{n(\mathrm{NMR})}$ = 13.4 kDa, $M_{n(\mathrm{GPC})}$ = 14 kDa, PDI = 1.10, IR: ν = 3040 – 2790, 1725, 1480, 1450, 1390, 1365, 1250, 1140, 845, 750 cm^{-1}. ^{1}H NMR (300 MHz, $CDCl_3$, δ): 4.30 (q, J = 7, 2H), 2.34 – 2.10 (br, 90H), 1.92 – 1.69 (br, 45H), 1.68 – 1.17 (m, 990H), 1.12 (br, 6H) ppm.

^{13}C NMR (75 MHz, $CDCl_3$, δ): 28.3 – 28.4, 36.1 – 37.8, 42.2 – 42.7, 80.4 – 81.0, 165.3, 173.9 – 174.5 ppm. DSC: (T_g) = 44 °C. TGA: T_{onset} = 211 °C. $T_{decomposition}$ = (211 – 220 °C) 47% mass loss; (292 – 433 °C) 38% mass loss; 15% mass remaining.

Synthesis of Poly(*tert*-butyl acrylate)$_{90}$-*b*-polystyrene$_{140}$ (PtBA$_{90}$-*b*-PS$_{140}$) *via* ATRP. A flame dried 10 mL Schlenk flask equipped with a magnetic stir bar was charged with PMDETA (1 equiv, 10.8 mg, 38 µmol), styrene (500 equiv, 2.04 g, 19 mmol) P*t*BA (1 equiv, 516 mg, 38 µmol) and anisole (2 mL). The reaction mixture was degassed by three freeze-pump-thaw cycles. Then, CuBr (3.5 equiv, 23 mg, 0.1 mmol) was added under a nitrogen flow to the frozen mixture. Following two additional freeze-pump-thaw cycles, the reaction mixture was allowed to return to room temperature and immersed in a preheated oil bath at 95 °C to start the polymerization. The polymerization was monitored by analyzing aliquots collected at predetermined times by ^{1}H NMR spectroscopy. As the expected monomer conversion was reached at *ca*. 9 h, the polymerization was quenched by quick immersion of the reaction vessel into liquid N_2 and exposure to air. THF (20 mL) was added to the reaction flask and the polymer was purified by filtration through an alumina plug followed by subsequent precipitation into 250 mL of a methanol/ice mixture (3x). The precipitate was collected and dried under vacuum overnight to afford 660 mg of P*t*BA$_{90}$-*b*-PS$_{140}$ as a white solid, giving 62% yield of the 27% conversion polymerization. $M_{n(NMR)}$ = 28 kDa, $M_{n(GPC)}$ = 34 kDa, PDI = 1.12, IR: ν = 3125 – 2790, 2420 – 2360, 2360 – 2215, 2150 – 2020, 2020 – 1785, 1730, 1600, 1490, 1450, 1390, 1365, 1255, 1145, 1170, 1130, 905, 850, 755, 700 cm^{-1}.

^{1}H NMR (300 MHz, $CDCl_3$, δ): 7.14 – 6.8 (br, 430H), 6.7 – 6.2 (br, 280H), 2.3 – 1.03 (br, m, 1610H) ppm. ^{13}C NMR (75 MHz, $CDCl_3$, δ): 27.8 – 28.2, 40.1 – 40.9, 80.2 – 80.7, 125.3 – 126.4, 127.4 – 128.7, 144.8 – 146, 165.3, 173.8 – 174.5 ppm. DSC: $(T_g)_{PtBA}$ = 46 °C, $(T_g)_{PS}$ = 98 °C. TGA: T_{onset} = 211 °C. $T_{decomposition}$ = (211 – 236 °C) 20% mass loss; (377 – 428 °C) 70% mass loss; 10% mass remaining.

Synthesis of Poly(acrylic acid)$_{90}$-*b*-polystyrene$_{140}$ (PAA$_{90}$-*b*-PS$_{140}$). P*t*BA$_{90}$-*b*-PS$_{140}$ (1 equiv, 392 mg, 14 μmol) was dissolved in dichloromethane (100 mL). Trifluoroacetic acid (TFA) was added in excess and the reaction mixture was allowed to stir overnight. After evaporation of the solvent and TFA, the remaining solid was resuspended in THF, placed in presoaked membrane dialysis tubing (MWCO 12 – 14 kDa) and dialyzed against nanopure water for 3 days. The suspension was lyophilized to obtain a white powder. IR: *v* = 3125 – 2790, 3010 – 2860, 2420 – 2360, 2360 – 2215, 2150 – 2020, 2020 – 1785, 1705, 1600, 1490, 1450, 1365, 1250, 1170, 1065, 1020, 905, 810, 750, 700 cm^{-1}. ^{1}H NMR (300 MHz, THF-d_8, δ): 7.5 – 6.8 (br, 430H), 6.8 – 6.3 (br, 275H), 2.55 – 1.03 (br, m, 915H) ppm. ^{13}C NMR (75 MHz, THF-d_8, δ): 41.0 – 42.4, 125.3 – 127, 127.8 – 129.3, 145.8 – 147.8, 176.4 – 177.0 ppm. DSC: (T_g) = 90 °C. TGA: T_{onset} = 155 °C. $T_{decomposition}$ = (155 – 136 °C) 5% mass loss; (357 – 411 °C) 84% mass loss; 11% mass remaining.

Preparation of PAA$_{90}$-*b*-PS$_{140}$ Micelles. A 250 mL round bottom flask was charged with a stir bar, and PAA$_{90}$-*b*-PS$_{140}$ (80.3 mg, 3.8 μmol) was dissolved in 80 mL

of THF and allowed to stir for *ca.* 15 min. Nanopure water (80 mL) was added with the aid of a syringe pump at a rate of 20 mL/h, the resulting solution was placed in presoaked dialysis membrane tubing (MWCO 6 – 8 kDa) and dialyzed against nanopure water for 2 days. Final concentration of solution *ca*. 0.27 mg/mL, $D_{h\,(N)}$ (DLS) = 20 ± 5 nm; zeta (ζ) = *ca.* -60 mV (pH 5-6).

Preparation of Shell Crosslinked Knedel-like (SCK) Nanoparticles. A 250 mL round bottom flask was charged with a stir bar and a solution of micelles (1 equiv, 100 mL, 0.27 mg/mL, 27.0 mg, 124 μmol of acrylic acid units). A stock solution of 2,2'-(ethylenedioxy)bis(ethylamine) (0.25 equiv, 4.59 mg, 30.9 μmol) was prepared in 100 μL of nanopure water followed by dropwise addition to the reaction mixture, which was allowed to stir for 2 h. A stock solution of EDCI (0.5 equiv, 18.4 mg, 61.8 μmol) was prepared in 100 μL of nanopure water and added dropwise to the vessel, the reaction mixture was allowed to stir overnight. The resulting solution was placed in presoaked membrane dialysis tubing (MWCO 6 – 8 kDa) for 2 days. Final concentration of solution *ca*. 0.27 mg/mL, $D_{h\,(N)}$ (DLS) = 25 ± 10 nm; TEM (18 ± 2 nm); zeta (ζ) = *ca.* -30 mV (pH 5-6).

Synthesis of Magnetically-active Hybrid Networks (MHNs). A 250 mL vial was charged with a stir bar and a solution of SCKs (12 equiv, 70 mL, 0.27 mg/mL, 20 mg, 62 μmol of available acrylic acid units). A solution of amine-functionalized iron oxide nanoparticles (amine-IONs, 1 equiv, 22.6 mL, 0.15 mg/mL, 3.4 mg, 5.2 μmol of

ligand) was added dropwise to the reaction mixture and it was allowed to stir for *ca*. 5 min, after which a solution of EDCI (13.5 mg, 45.4 μmol, 8.8 equiv, as a 7.5 mL aqueous solution at a concentration of 1.8 mg/mL) was added *via* a syringe pump at a rate of 0.25 mL/min. The reaction was allowed to stir for 24 hours, followed by centrifugation at 10000 rpm for 5 min. The brown precipitate was resuspended in 15 mL of nanopure water with the aid of sonication and vortexing, this process was repeated twice. The supernatant was collected and centrifuged 2 more times with the aim of removing as much precipitate as possible. After centrifugation, the supernatant was collected, placed in presoaked membrane dialysis tubing (MWCO 12 – 14 kDa) and dialyzed against nanopure water for three days. Following dialysis, the suspension of MHNs and the supernatant were combined (due to similar structures being observed by TEM) and lyophilized to afford 16 mg of a light brown powder in 69% yield. IR: ν = 3685 – 2545, 3110 – 3010, 3010 – 2835, 2385 – 2300, 1960 – 1850, 1720, 1640, 1600, 1550, 1490, 1450, 1390, 1365, 1350, 1260, 1210, 1180, 1140, 1095, 1070, 1030, 965, 905, 800, 755, 700 cm^{-1}. TGA: T_{onset} = 30 °C. $T_{decomposition}$: (30 – 100 °C) 4% mass loss; (100 – 210 °C) 5% mass loss, (210 – 250 °C) 9% mass loss; (290 – 375 °C) 48% mass loss, (410 – 470 °C) 16% mass loss, 18% mass remaining.

Recovery of MHNs *via* Magnetic Separation. A known amount of MHNs was added to a pre-weighed 10 mL vial and resuspended in nanopure water (2 mL). After gentle shaking, the MHNs were subjected to an external magnetic field for *ca*. 2 min followed by decanting of the water. This process was repeated twice, with collection of

the supernatant after every wash. The deployed MHNs were allowed to dry overnight and their weight was recorded five times for statistical analysis.

Oil Capture Experiments. Weathered crude oil from the Texas-Oklahoma pipeline (light sweet crude oil) was added to a vial containing nanopure water (3 mL) and the weight of the oil was recorded. Subsequently, powdered MHNs were added to the vial and they were allowed to rest with minimal movement. After *ca.* 1 h, the loaded material was separated *via* exposure to an external magnetic field for *ca*. 2 min, followed by decanting of the contaminated media for oil extraction. The original vial was washed twice with nanopure water (2 mL) in order to remove most of the water/oil mixture remaining. The vial was dried and its mass recorded in order to determine the mass of oil remaining in the original container. Subsequently, the oil present in the polluted environment was extracted using diethyl ether; the organic fractions were collected in order to evaporate the solvent and to record the mass of the extracted oil. Additionally, the water fraction was collected and lyophilized in order to determine the presence of any residual mass in the aqueous phase.

Oil Recovery Experiments. The loaded MHNs were transferred into a pre-weighed clean vial followed by addition of diethyl ether (2 mL). The sample was vortexed for *ca*. 30 s to wash the oil captured. The nanoparticles were separated from the mixture by exposure to an external magnetic field for *ca.* 1 min, followed by decanting of the solvent. This process was repeated twice, with a colorless solution

indicating extraction of the majority of the oil from the nanoparticles. The decanted mixture was allowed to dry and the mass of oil extracted from the nanoclusters was measured.

Recovery of Nanoparticles *via* Magnetic Separation after Diethyl Ether Wash. A known amount of MHNs was added to a pre-weighed 10 mL vial and resuspended in diethyl ether (2 mL). After vortexing for 30 s the MHNs were subjected to magnetic separation for *ca*. 1 min, followed by decanting of the solvent. This process was repeated twice, with collection of the supernatant after every wash. The deployed material was allowed to dry overnight and its weight was recorded five times for statistical analysis.

2.3 Results and Discussion

Synthesis and Characterization of Magnetically-active Hybrid Networks (MHNs). The MHNs were synthesized in a two-step manner as shown on Scheme 2.1.

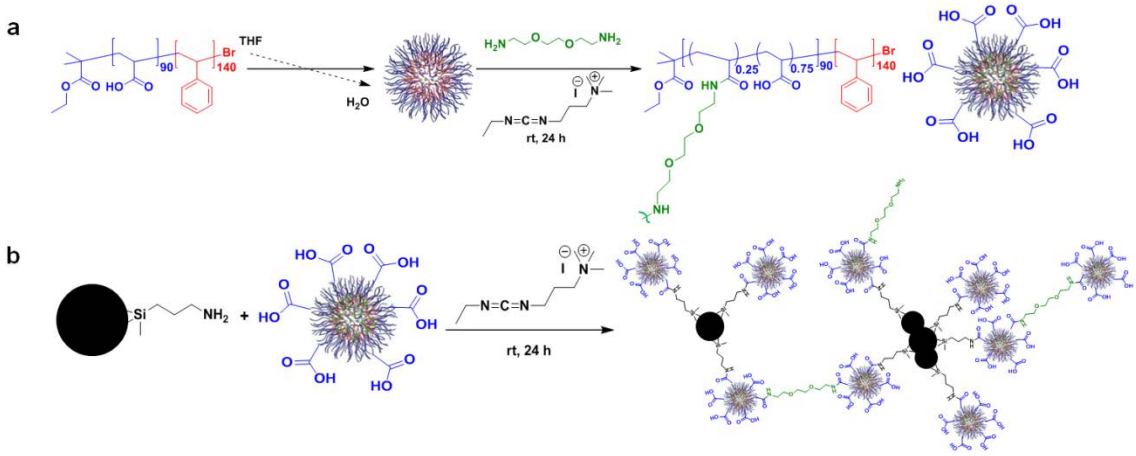

Scheme 2.1. Schematic representation of the synthesis of SCKs (a) and the covalent binding of SCKs to amine-functionalized IONs *via* amidation (b).

First, the preparation of the SCKs was performed from a modified literature procedure ($D_{h(n)}$ = 18 ± 5 nm as measured by dynamic light scattering (DLS), Figure 2.1),[23,26] followed by the covalent binding of these pre-established polymeric nanoparticles to amine-IONs ($D_{h(n)}$ = 50 ± 15 nm, Figure 2.2) *via* an amidation reaction between the acrylic acid functionalities of the hydrophilic shell of the SCKs and the amine moieties on the surface of the IONs in the presence of 1-[3'-(dimethylamino)propyl]-3-ethylcarbodiimide methiodide (EDCI).

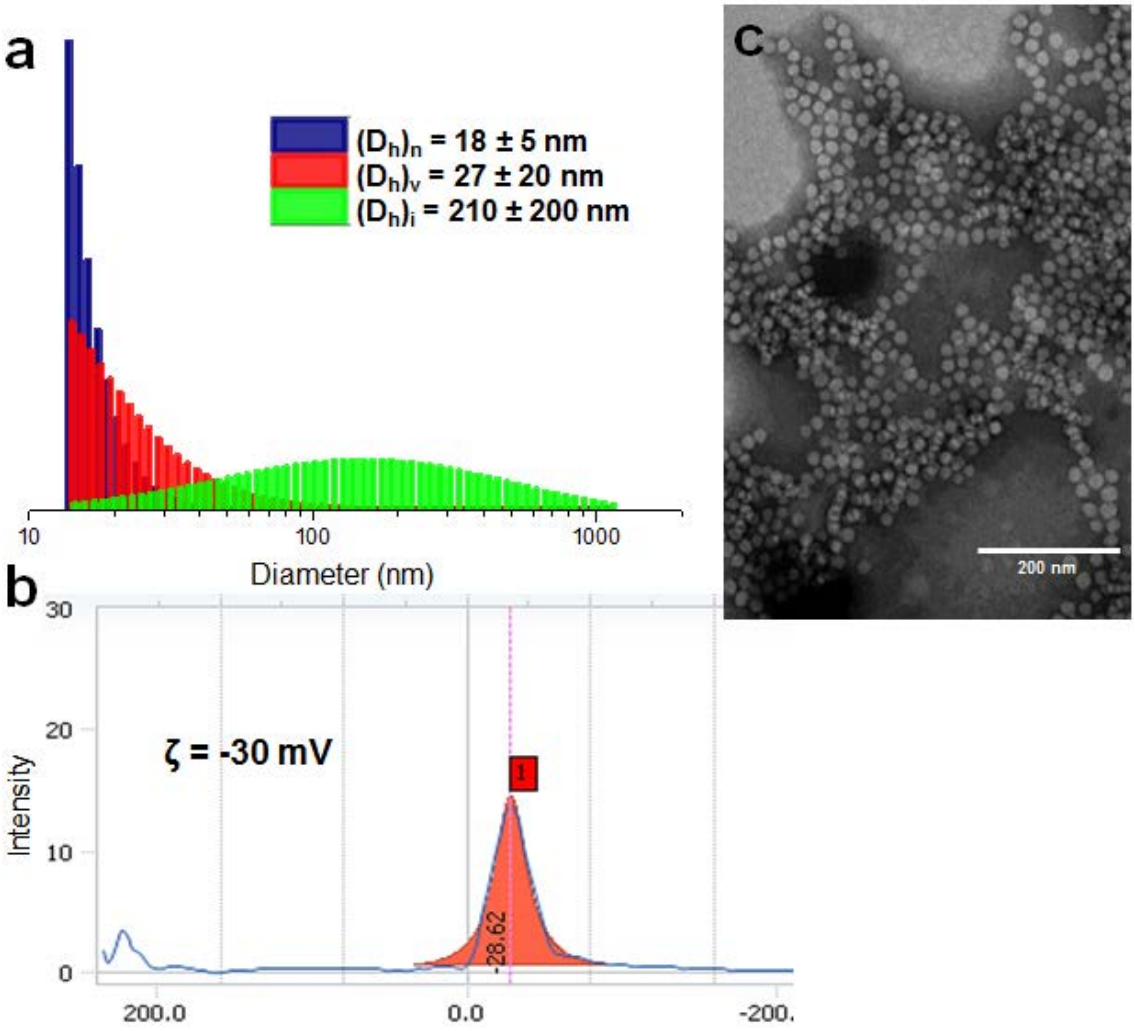

Figure 2.1. DLS (a), zeta potential (b) and TEM (c) of SCKs.

After purification by magnetic separation and dialysis of the supernatant, the composite material was characterized through transmission electron microscopy (TEM), infrared (IR) spectroscopy and thermogravimetric analysis (TGA). TEM imaging

revealed a hybrid network composed of agglomerated IONs coupled to multiple SCKs (Figure 2.3).

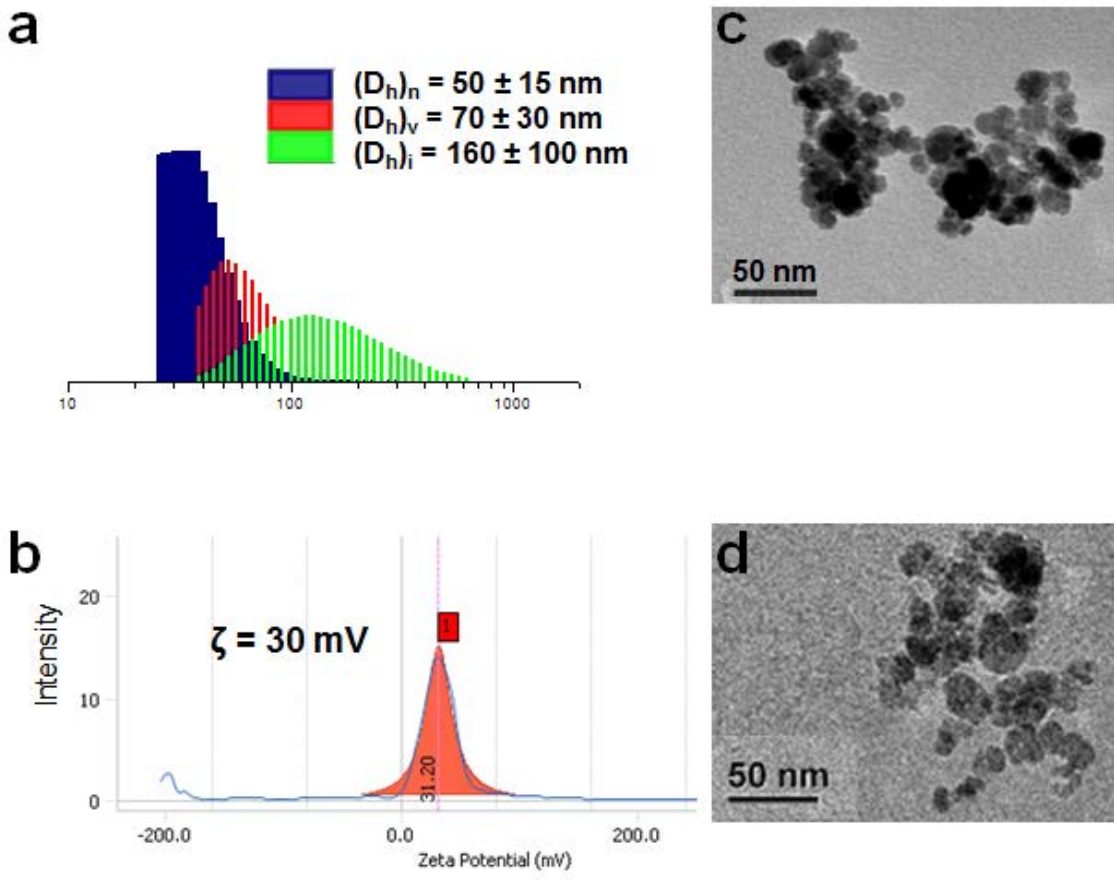

Figure 2.2. DLS (a), zeta potential (b), TEM (c) and cryogenic TEM (cryo-TEM, d) of amine-ION*s*.

The use of phosphotungstic acid (PTA) as a staining agent during TEM analysis improved the contrast to allow for the observation of the SCKs (light globular structures in Figure 2.3a) which would otherwise be difficult to visualize. However, staining also introduced artifacts[35] and provided ambiguity when determining whether the areas of high contrast (black areas in Figure 2.3a) corresponded to the transmission generated by amine-IONs or to areas of high concentrations of stain. In addition, the process of drying the sample on a TEM grid led to ambiguities of whether the SCK clusters were due to a drying pattern or were, in fact, representative of interconnections between SCK particles.

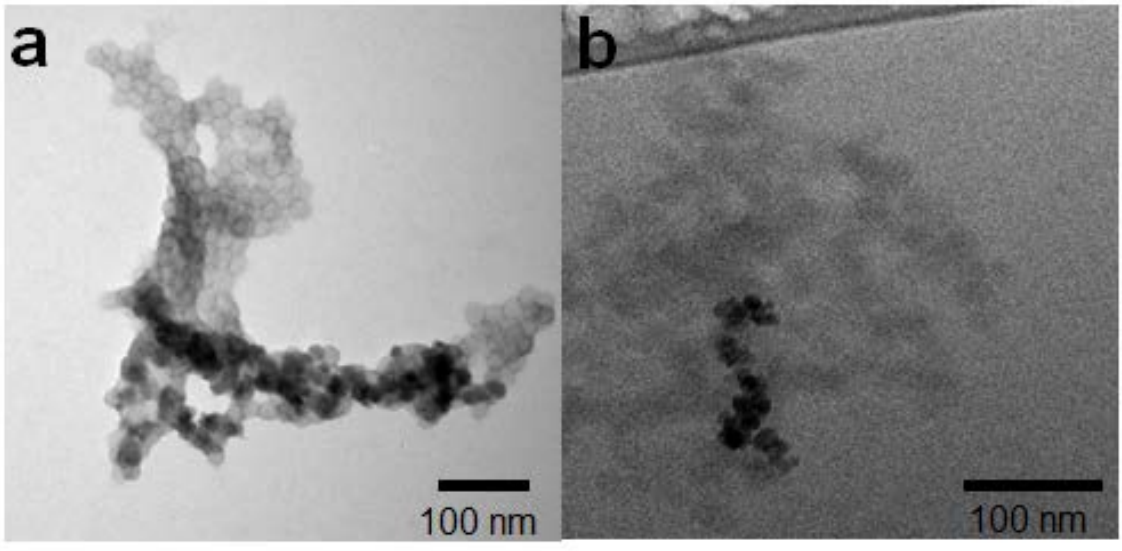

Figure 2.3. TEM image of MHNs after staining with phosphotungstic acid (PTA) (a) and cryo TEM image of MHNs (b).

Although the nanoparticles were composed of C, H, O, and N atoms, all of which have relatively low and similar atomic numbers (Z) and thus provide poor mass-thickness contrast by TEM,[36] cryogenic TEM (cryo-TEM) was able to confirm the presence of agglomerates of amine-IONs bound to several interconnected SCKs (Figure 2.3b). We hypothesized that the SCK-SCK interactions have a covalent character, facilitated by inter-particle amidation reactions between EDCI-activated carboxylic acids with residual amino groups in the shells of the nanoparticles, following the initial intra-particle shell crosslinking step. This hypothesis was corroborated by our control experiments, which were performed by adding EDCI to a solution of SCKs. TEM micrographs (Figure 2.4) revealed the formation of SCK clusters identical to those formed during the synthesis of the MHNs, which were not present before the second addition of EDCI, and which could have only formed if the residual amino groups in the shells of the SCKs reacted with residual carboxylic acid units, since no other source of amines was present in the system.

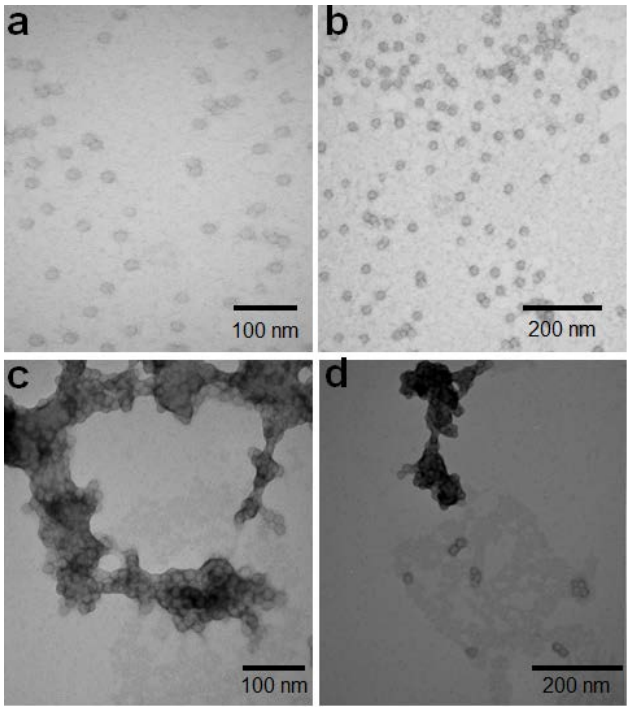

Figure 2.4. TEM images of SCKs (a – b) and SCKs after second addition of EDCI (c - d).

Moreover, to confirm the covalent nature of the MHNs throughout the inorganic and organic components, a series of control experiments was conducted (Figures 2.5 and 2.6) to compare the MHN structures collected from the precipitate and supernatant (Figures 2.5a, 2.5b and 2.6) following the addition of the EDCI coupling agent with analogous physical mixtures collected in the absence of the carbodiimide (Figures 2.5c, 2.5d and 2.6).

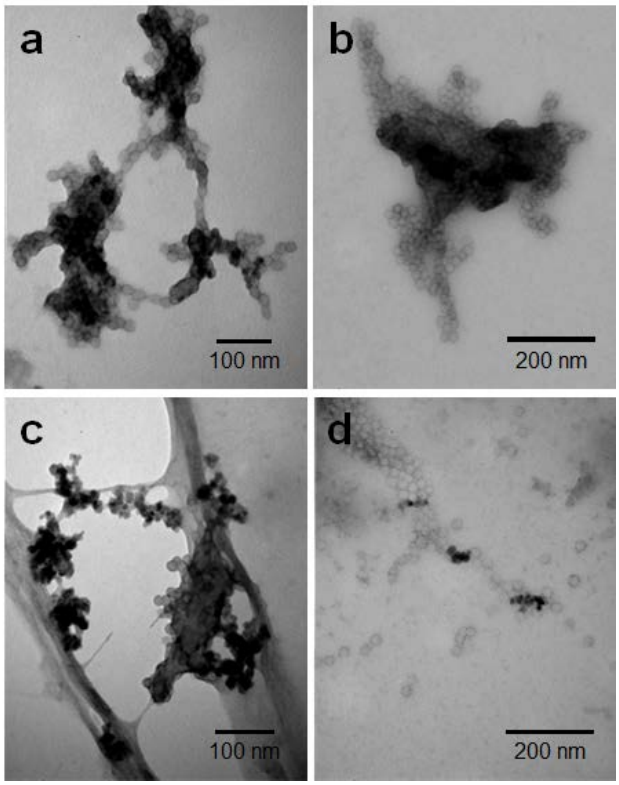

Figure 2.5. TEM images of the precipitate (a) and supernatant (b) of the MHNs, compared to the precipitate (c) and supernatant (d) of a physical mixture of SCKs and amine-IONs.

We cannot explain why SCK-SCK coupling proceeded during the amidation conditions employed for conjugation with the amine-IONs, but not during the intramicellar crosslinking reaction to establish the SCKs. Originally, the work-up and purification process involved separate treatments for the supernatant and precipitate obtained from centrifugation. With detailed TEM analyses, it was found that both the

precipitate and supernatant contained the same type of MHN structures, therefore, the samples were combined for further analyses and crude oil capture studies.

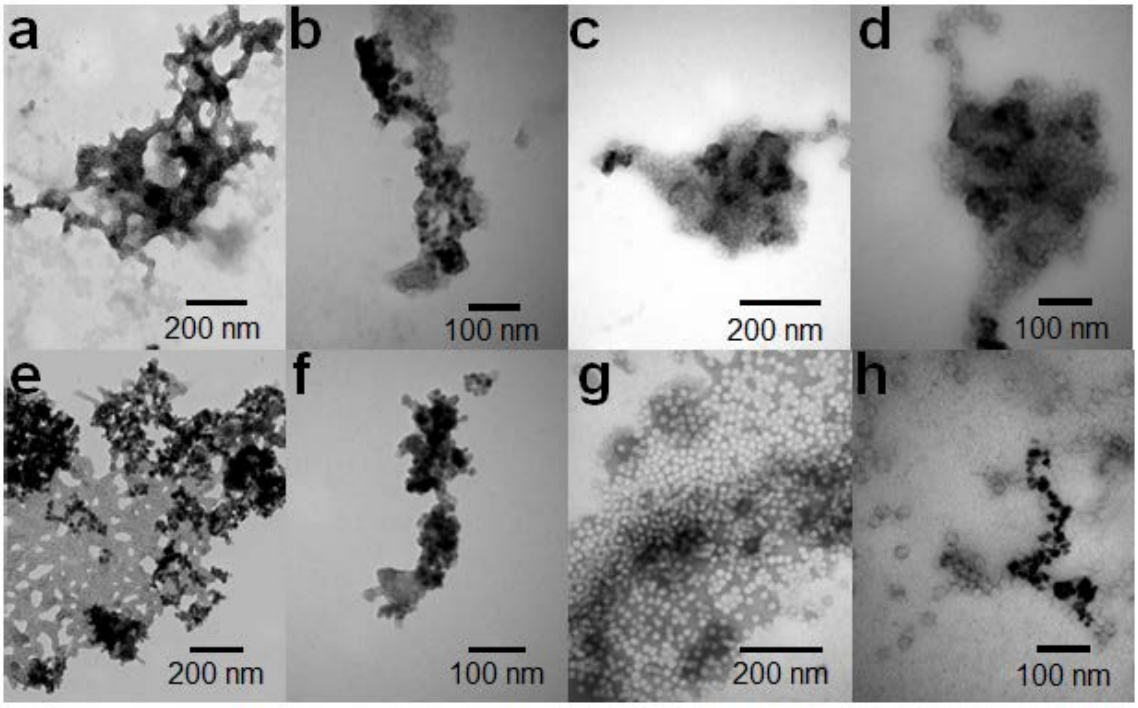

Figure 2.6. TEM images of the precipitate (a – b) and supernatant (c – d) of the MHNs, compared to the precipitate (e – f) and supernatant (g – h) of a physical mixture of SCKs and amine-IONs.

IR spectroscopy was used in addition to TEM to monitor structural changes in the composition of the SCKs (Figure 2.7a). The band at *ca.* 1710 cm^{-1} corresponds to the carbonyl stretch for the acrylic acid pendant groups of the SCKs, while the signals at

ca. 1640 cm^{-1} and *ca*. 1560 cm^{-1} are characteristic of the amide functional group and are an indication of the crosslinking of the shell which was performed to afford stability to the nanoparticles.[22] However, this second amidation reaction for the coupling of the inorganic and organic components revealed no significant changes to the IR absorbance bands between the SCKs and MHNs. This lack of measurable structural changes could be attributed to the use of amidation chemistries for both the crosslinking and coupling of the SCKs and amine-IONs.

TGA was also performed in order to gain a better understanding of the thermal stability and composition of the hybrid nanoconstructs. Comparison of the thermographs of amine-IONs, MHNs and SCKs (Figure 2.7b) revealed a lower decomposition temperature for the MHNs (*ca.* 190 °C) when compared to that of the SCKs (*ca.* 230 °C). This reduction of the stability of the hybrid networks could be due to the interconnection between the inorganic particles and the SCKs, which form an intricate network that can be affected by the thermal conductivity of the amine-IONs, or by metal-catalyzed oxidative degradation, typically observed in metal/polymer nanocomposites.[37-40] Moreover, the percentage of amine-IONs present in the MHNs was also assessed by TGA, which revealed an inorganic loading of *ca*. 16% by mass to the hybrid material, which is in agreement with the 15 ± 1 wt% feed ratio of amine-IONs : SCK used in the synthesis of the MHNs.

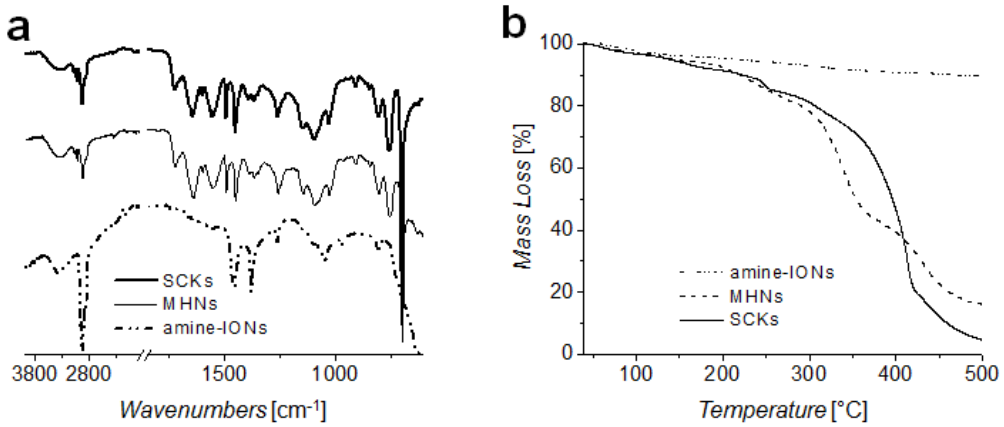

Figure 2.7. IR spectra of SCKs, MHNs and amine-IONs (a) and TGA thermographs of amine-IONs, MHNs and SCKs (b).

Qualitative and Quantitative Sequestration of Crude Oil by the MHNs. Following the complete characterization of the novel hybrid networks, the ability of the MHNs to sequester complex hydrophobic pollutants was assessed qualitatively. First, crude oil from the Texas-Oklahoma Enbridge pipeline was weathered according to a pre-established procedure,[41] and then added to nanopure water in order to mimic sheen contamination. Second, the lyophilized MHNs were deployed onto the polluted environment in a powder form at initial oil to MHN ratios (oil : MHN) of 2 : 1, 4 : 1, 6 : 1 and 8 : 1. Immediately after deployment, a color change from light tan to darker brown/black was observed for the MHNs, indicating that the particles had come into contact with the oil and had possibly taken-up the pollutant (Figure 2.8). After *ca.* 1 hour, the loaded nanoparticles were subjected to an external magnet (Neodymium

magnet, 90 lb pull). Due to the high magnetic response of the large conglomerates of oil and nanoparticles, these species were quickly, in a matter of seconds, attracted to the magnet. However, the smaller droplets of oil required longer time to be completely removed from the resting contaminated water; therefore magnetic separation was performed for a total of 2 minutes. The contaminants remaining in the polluted mixture were decanted and compared to control samples containing comparable amounts to the initial oil. Qualitatively, it could be observed that the MHNs were capable of sequestering most of the pollutants initially present in the water (Figure 2.8).

Figure 2.8. Pictographic representation of the oil capture procedure including deployment of MHNs (left), magnetically-induced separation from the polluted environment (center) and decanting of the remaining pollutant for extraction with diethyl ether and quantification (right).

The qualitative assessment of the sequestration of hydrophobic contaminants by the MHNs was followed by a quantitative determination of their loading capacity, which was achieved through a mass balance method. The mass of oil captured by the MHNs was calculated gravimetrically by measuring the initial mass of oil added into the pristine water, the mass of oil remaining in the vial after transfer of the polluted solution and oil containing MHNs, the mass of oil not captured from the polluted solution (analyzed after diethyl ether extraction from the water), and the mass of oil extracted with diethyl ether after MHNs deployment and recovery. The loading capacity of the materials was calculated as the ratio of the mass of oil sequestered in mg per mg of MHNs. For the initial ratio of 2.2 : 1 (oil : MHN), it was determined that 1.5 mg of oil were captured per 1 mg of MHNs. For the subsequent ratios of 4.4 : 1, 6.1 : 1 and 8.3 : 1, the loading capacities were found to be 2.1 : 1, 3.4 : 1 and 3.3 : 1, respectively (Figure 2.9a).

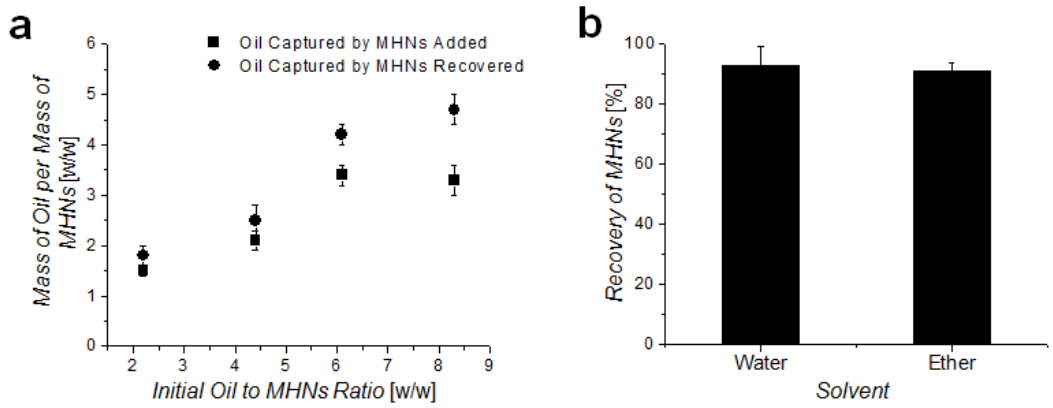

Figure 2.9. Loading capacity ratio of the MHNs, calculated as the mass of oil (mg) captured per mg of MHNs added (squares) and the mass of oil (mg) captured per mg of MHNs recovered (circles, a); and magnetic recovery of MHNs after deployment in water and diethyl ether (b).

Further, in order to address the concern that there may be populations of the interparticle crosslinked networks comprised only of SCKs, without having the composite structure together with amine-IONs, the magnetic recovery of MHNs was assessed. The experiments indicated that *ca*. 93% of the MHNs originally deployed in water could be recovered with the use of an external magnet (Figure 2.9b). Therefore, the loading capacity of the hybrid networks was also calculated as the ratio of the mass of oil sequestered in mg per mg of MHNs recovered. Through this approach, at the lower ratios of 2.2 : 1 and 4.4 : 1, quantitative recovery of the MHNs occurred, as observed by there being no significant difference in the captured oil values calculated by the two methods (Figure 2.9a). However, for higher loading ratios, significant

differences were observed. The effective amount of captured oil was higher, when taking into account the loss of fractions of the MHN samples during the procedures involving high proportions of oil (6.1 : 1 and 8.3 : 1), with a maximum oil sorption determined to be 4.7 mg of oil/mg of MHNs recovered. These differences can be attributed to an increase in the difficulty with which the pollutant-loaded networks were magnetically manipulated and recovered as the proportion of oil increased. As the concentration of oil in the polluted water was increased, it became more cumbersome to remove the oil-loaded networks and thus, to accurately calculate the loading capacity. In fact, attempts to further challenge the system with an initial loading ratio of 10 : 1 were unsuccessful, as it was not possible to remove the loaded MHNs from the resting polluted environment without leaching oil back into the system. Thus, by taking these observations into consideration, it can be determined that the maximum loading capacity falls in a range of *ca.* 3.5 to 4.5 mg of oil/mg of MHNs.

Oil Cargo Removal and Recyclability of MHNs. The recyclability of the MHNs was first addressed by removing the loaded pollutants through a wash with an organic solvent. Diethyl ether was selected as the organic solvent, since preliminary data indicated that it could remove the oil without solubilizing the MHNs. Moreover, control experiments were conducted to determine the magnetic recovery of the networks after the organic wash, which revealed that *ca*. 90% of the MHNs could be successfully retrieved (Figure 2.9b). The washing of the loaded nanoparticles was performed by re-dispersion in diethyl ether, followed by 30 seconds of vortexing. A change in the color

of the solvent from colorless to light yellow/brown indicated the removal of oil from the MHNs. Further confirmation of the removal of oil was provided by the change in the color of the nanoparticles from black (pollutant-loaded) to brown (similar color to the pristine system). The MHNs were removed magnetically from the diethyl ether/oil mixture followed by evaporation of the solvent, which allowed for the calculation of the amount of oil recovered from the networks; this amount was determined to be *ca* 90% of the amount of oil initially sequestered (Figure 2.10a).

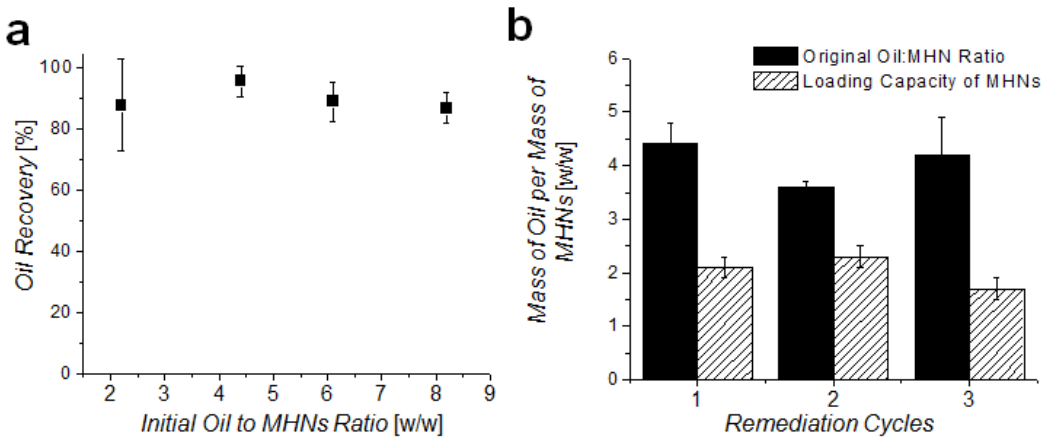

Figure 2.10. Percent oil recovery as a result of the washing of pollutant-loaded nanoparticles (a), and recyclability of the MHNs assessed as a comparison between the loading capacity of the MHNs after multiple remediation cycles, and the original oil : MHNs ratio (b).

The extraction of the loaded pollutants was followed by the re-utilization of MHNs for the sequestration of oil. The washed nanoparticles were re-deployed into contaminated media and were exposed to the same procedure as previously stated for the sequestration and quantification of oil removal. The loading capacity of the reused MHNs was assessed for three cycles at an initial oil : MHNs of 4 : 1 (Figure 2.10b). The ratio calculated across all cycles was determined to be *ca.* 2 : 1, which suggests little to no reduction of the efficiency of the MHNs following three cycles of deployment and organic washing. These data indicate that the MHNs system could be effective and viable for the sequestration and recovery of crude oil from water.

Interfacial Tension Measurements. In addition to synthesizing novel complex materials capable of removing hydrophobic pollutants from aqueous environments, we were also interested in understanding the mechanism of interaction between the pollutants and the MHNs. Our first step in this direction has been the determination of the interfacial tension (γ) between the oil and a suspension of MHNs *via* a pendant drop method. The interfacial tension of a drop of oil (density = 0.8234 mg/mL) in a 0.25 mg/mL aqueous suspension of MHNs was measured to be 19.4 ± 0.6 mN/m (see Table 2.1), which represents a 23.3% reduction in the interfacial tension of the oil when compared to its value in water (25.3 ± 0.2 mN/m). These results indicate an increased affinity of the oil for the suspension of MHNs, and are indicative of the possible formation of an emulsion between the oil and the water phases, stabilized by the MHN particles, as seen in the process of Pickering emulsification.[9] Although more data are

required in order to support this hypothesis, the formation of Pickering emulsions could indicate that the mechanism of loading is not limited to oil sorption into the hydrophobic core of the SCKs composing the magnetically-active networks, but includes the formation of magnetically-active droplets in water.[10,42-44] Moreover, we also measured γ for model aromatic and aliphatic contaminants in a suspension of MHNs, in order to determine if there is an increased affinity for one of the components of oil. The surface tension of toluene (model aromatic contaminant) was reduced from 35.2 ± 0.4 mN/m (water) to 19.1 ± 0.2 mN/m (MHNs), while the interfacial tension of decane (model aliphatic pollutant) was decreased from 52.3 ± 0.5 mN/m (water) to 37.7 ± 0.8 mN/m (MHNs). Analysis of these data showed that γ for toluene was reduced by 45.5% while that of decane was reduced by 27.9%, which could indicate an increased affinity for the aromatic components of the oil, or for smaller molecules over long chain aliphatic hydrocarbons. Even though these data are not conclusive, ongoing experiments are focused on determining any preferential sequestration of oil components by MHNs.

Table 2.1. Interfacial tension values for hydrophobic organic pollutants in water and MHNs.

	Media		
Drop Solvent	Water (mN/m)	MHNs (mN/m)	% Difference
Toluene	35.2 ± 0.4	19.1 ± 0.2	45.7
Decane	52.3 ± 0.5	37.7 ± 0.8	27.9
Crude Oil	25.3 ± 0.2	19.4 ± 0.6	23.3

2.4 Conclusions

The construction of magnetically-active hybrid networks for the removal of complex hydrophobic pollutants from water provided an exciting addition to the morphologies currently available for remediation. The maximum loading capacity calculated lies in the range of *ca* 3.5 – 4.5 mg of oil per mg of MHNs used, which is comparable to the capacity of existing nanotechnology. The high percent of recovery of the sequestered oil, as well as the re-utilization of the MHNs with quantitative efficiency are two factors that could lower the cost associated with production and use of the MHNs in environmental remediation. These characteristics, coupled with the MHNs' capabilities for water compatibility, magnetic manipulation and easy recovery of the cargo, also expand their possible applications to new challenges encountered by the constant search for energy sources, such as enhanced oil recovery. Although this novel

system demonstrated a lower oil uptake when compared to the MSCK system,[21] we have found unique insights into the mechanism of interaction between the MHNs and hydrophobic pollutants that significantly improve our understanding of these materials. Moreover, their uncomplicated assembly method provides unlimited opportunities to expand the scope of these materials, notably, through the tailoring of the SCK component for specific pollutants and applications. Ongoing studies are focused on altering the polymeric domains prior to assembly onto the inorganic component, to afford finely-tuned SCKs that could sequester particular pollutants encountered in diverse scenarios. In addition, multiple SCKs of different compositions could be coupled onto the inorganic magnetically-active vehicles, thus providing highly diverse materials with minimal synthetic modifications.

CHAPTER III

SEQUESTRATION CAPABILITIES OF MAGNETICALLY-ACTIVE HYBRID NETWORKS (MHNs) IN SALINE ENVIRONMENTS, AND THEIR MECHANISMS OF INTERACTION WITH POLLUTANTS OF LIMITED COMPLEXITY

3.1 Introduction

The contamination of fresh and marine aqueous environments by oil spills is a severe consequence of the exploration, extraction and transport of crude and refined oils. The extent of the spills and their severity often varies, however their impact on wildlife is significant.[45,46] Among the most affected are marine mammals and seabirds that often suffer from hypothermia, smothering and/or drowning due to the oiling of their fur or feathers, which takes place shortly after the spill occurs.[47,48] However, chronic exposure to oil remaining in the ecosystem can increase the mortality rate of animals born after the spills;[45,46] therefore the remediation of the areas affected is important for current and future generations.

Several types of materials have been designed to separate oil/water mixtures,[49-52] or to sequester hydrophobic contaminants.[53-56] However, because the materials intended for remediation can also have a toxic effect on wildlife, it is important to incorporate a mechanism for recovery of the loaded materials that can help diminish their impact on the environment. One approach that has been adopted is the incorporation of magnetically-active iron oxide nanoparticles (IONs) to yield composites capable of

sequestering hydrophobic pollutants, while exhibiting a response to an external magnetic field that allows for recovery once loaded.[21,57-62] Some research groups that have synthesized these magnetically active materials have evaluated the sequestration of pollutants of limited complexity, such as mineral or lubricant oil;[59-61,63-67] while others have recognized the complexity of crude oil and investigated the performance of their technologies with respect to this convoluted pollutant.[21,34,62,66-68]

Despite the interest of the scientific community in developing technologies capable of diminishing the negative effects of oil spills, the complexity in the composition of crude and refined oils remains a challenge. The main components of crude oil can be categorized into saturates, aromatics, resins and asphaltenes. However, the proportion of each of these components in each type of oil depends on different factors, including the raw source (crude oil *vs.* shale oil), degree of chemical modification after extraction[69] and geographical origin of the oil.[70,71] Consequently, there are many types of crude and refined oils encountered around the globe, which once spilled, experience the "weathering" effect of the elements changing the chemical composition and physical characteristics of the oil over time.[72-74] For these reasons it is cumbersome to analyze the performance of the materials against this diverse pollutant; however, attention must also be paid to the fraction of the oil that dissolves in water, known as the water-soluble fraction (WSF), which can also vary in composition and ranges from aliphatic *n*-alkanes to polycyclic aromatic hydrocarbons (PAHs). [69,70,72,75]

Due to the complexity of the composition of crude and refined oil, and the corresponding WSFs, a remediation approach that employs materials tailored to specific

types of crude and refined oils would allow for more targeted, and perhaps more efficient, remediation strategies. Our group has previously reported the design and synthesis of magnetically active hybrid networks (MHNs), which are hybrid inorganic/organic composite materials originally designed to sequester crude oil sheen from aquatic environments.[62] The MHNs were capable of sequestering *ca.* 4x their mass in crude oil, and maintained their loading capacity over multiple cycles of remediation. In this report, we expand on our previous work by investigating the ability of the MHNs to sequester specific aliphatic (dodecane) and aromatic (toluene) model components of crude oil, with the intent of determining whether preferential sequestration of the different components of crude oil takes place. Notably, we aim to discover whether the chemical composition of the polymeric materials capable of sequestering the components of crude oil has an effect on performance. This understanding will allow for the design and synthesis of materials tailored to specific pollutants encountered in various aqueous environments to afford highly efficient pollutant recovery. Moreover, given that oil spills can occur in both fresh water and marine environments, the capability of the MHNs to sequester dodecane and toluene from fresh water, as well as a 10% w/w NaCl aqueous solution (brine) has been investigated. These studies allowed us to further understand the mechanism of interaction of the MHNs with the pollutants, and demonstrate that the MHNs are capable of sequestering hydrocarbon pollutants *via* the dual mechanisms of absorption and emulsification. Furthermore, no preferential sequestration of either aromatic or aliphatic pollutants was observed when sequestering from fresh environments; however, a preference for the aromatic model contaminant was

observed when sequestering from brine. Our results provide evidence that tailoring the chemical composition of the polymeric components of the MHNs to the specific pollutants allows targeted remediation, which is anticipated to lead to more efficient removal of hydrophobic contaminants from aquatic environments.

3.2 Materials and Methods

Materials. All chemicals were purchased from Aldrich Chemical Co. or VWR and used without further purification unless otherwise noted. Amine-IONs were purchased from Chemicell GmbH. Nanopure water (18 MΩ•cm) was obtained from a Milli-Q water filtration system, Millipore Corp. (Bedford, MA). The neodymium magnet (90 lbs. pull) was purchased from magnets4less.com.

Characterization Techniques. IR spectra were recorded on an IR Prestige 21 system (Shimadzu Corp., Japan). Data were analyzed using IRsolution software. Thermogravimetric analysis was performed under Ar atmosphere using a Mettler Toledo model TGA/DSC1 with a heating rate of 10 °C/min. Measurements were analyzed using Mettler Toledo *STAR*^{e} software v 10.00.

Transmission electron microscopy (TEM) was performed on a JEOL 1200 EX operating at 100 kV and micrographs were recorded at calibrated magnifications using a SLA-15C CCD camera. Samples for TEM were prepared as follows: 5 μL of a solution was deposited onto a formvar-coated copper grid, and after 30 s, the excess solution was quickly wicked away using a piece of filter paper. The samples were negatively stained

with 1% phosphotungstic acid (PTA) aqueous solution. After 30 s, the excess staining solution was quickly wicked away using a piece of filter paper and the samples were left to dry overnight. Atomic force microscopy (AFM) was performed on a Bruker Multimode 8 atomic force microscope (Billerica, MA). TEM and AFM analyses where performed on MHN solutions prepared before and after deployment in a 10% w/w NaCl aqueous solution (brine) by resuspending the solid samples in nanopure water and sonicating for 5 min. Samples were prepared by spin coating 50 μL of solution onto freshly cleaved mica. Samples were dried overnight over a flow of N_2 and imaged with a Bruker ScanAsyst-Air AFM probe (silicon nitride, k = 0.4 N/m, f = 70 kHz). The system was operated in 'ScanAsyst' mode. Mass balance was performed through the use of a Citizen Scale micro balance (Mumbai, India) with a readability of 1 μg and repeatability of 1 μg.

Gas chromatography- mass spectrometry (GC-MS) was performed on a DSQ II single quadrupole GC/MS, coupled with an electron ionization mass spectrometer, a TRACE GC Ultra and a TriPLus autosampler (Thermo Scientific, Waltham, MA). Data analysis was performed using Xcalibur software. Confocal fluorescence microscopy experiments were conducted on a FV1000 confocal fluorescence microscope with an IX-81 inverted base (Olympus, Center Valley, PA) and photomultiplier tube (PMT) detectors. Samples were prepared by adding 1 mL of nanopure water to a glass-bottomed petri dish (MatTek, Ashland, MA), followed by addition of 26.6 μL of the dodecane/Nile red solution (30 $\mu g \cdot mL^{-1}$) to generate the contaminated environment (Dodecane : MHNs = 20 : 1 (w/w)). MHNs (1 mg) were added as a powder and the

mixture was imaged by confocal microscopy. A second set of samples was prepared in a 5 mL vial, where upon deployment of the MHNs, the sample was hand shaken to generate emulsion droplets which were transferred to a glass-bottomed petri dish with a Pasteur pipet, and diluted with nanopure water for imaging. Images were acquired upon excitation of the sample with a 488 or 543 nm laser source.

Synthesis of MHNs. The synthesis of the MHNs was performed according to a published procedure.[62] Briefly, a 250 mL vial was charged with a stir bar and an aqueous solution of SCKs (12 equiv., 70 mL, 0.27 mg/mL, 20 mg, 62 μmol of available acrylic acid units). A solution of amine-IONs in nanopure water (1 equiv., 22.6 mL, 0.15 mg/mL, 3.4 mg, 5.2 μmol of ligand) was added dropwise to the reaction mixture and it was allowed to stir for *ca*. 5 min, after which a solution of 1-[3'-(dimethylamino)propyl]-3-ethylcarbodiimide methiodide (EDCI, 8.8 equiv., 7.5 mL, 1.8 mg/mL, 13.5 mg, 45.4 μmol) was added *via* a syringe pump at a rate of 0.25 mL/min. The reaction was allowed to stir for 24 hours, followed by centrifugation at 10000 rpm for 5 min. The brown precipitate was resuspended in 15 mL of nanopure water with the aid of sonication and vortexing, and this process was repeated twice. The supernatant was collected and centrifuged 2 more times with the aim of removing as much precipitate as possible. After centrifugation, the supernatant was collected, placed in presoaked membrane dialysis tubing (MWCO 12 – 14 kDa) and dialyzed against nanopure water for three days. Following dialysis, the suspension of MHNs and the

supernatant were combined and lyophilized to afford 16 mg of a light brown powder in 69% yield.

Recovery of MHNs *via* Magnetic Action. A known amount of pristine MHNs and a physical mixture of amine-IONs and SCKs were added to pre-weighed 5 mL vials and resuspended in 10% w/w NaCl (brine) solution at a particle concentration of 1 mg/mL. The mixtures were vortexed for 30 s to facilitate resuspension and then subjected to an external magnetic field for 4 min prior to decanting the supernatant. This process was repeated three times, and the supernatant collected after each wash. The deployed MHNs were dried in a vacuum oven at 90 °C for 2 days and their weight was recorded as an average of five measurements for statistical analysis. A control sample was prepared by resuspending pristine MHNs into nanopure water and subjecting them to the procedure previously described.

Sequestration of Pollutants by the MHNs. Test and control samples were utilized for this experiment and subjected to the same conditions unless otherwise stated. Oil (toluene or dodecane) was added to vials containing nanopure water or a 10% w/w NaCl solution (brine, 3 mL) and the weight of the oil was recorded for both the test and the control samples. Subsequently, powdered MHNs were added to the test vials and they were allowed to rest for *ca.* 10 min after deployment of the MHNs. During this time, the vials were first gently shaken to maximize contact between the oil and the MHNs, and then vigorously shaken to sequester as much oil as possible. After

sequestration of the pollutants, the loaded MHNs were separated *via* exposure to an external magnetic field for *ca.* 2 min, followed by decanting of the contaminated media for extraction. The vial was washed twice with 2 mL of nanopure water (or brine) in order to remove most of the remaining water/oil mixture. Given that not all of the MHNs were recovered by the magnet during the first attempt, the separation process was repeated once more after the washing steps had been performed. An internal standard (IS, benzene-d_6 for toluene samples, and decane for dodecane samples) was added in the same amount (by weight) as the added oil, to the contaminated media of both test and control samples and mixed thoroughly. The remaining pollutant was extracted with 2 mL of hexanes 3 times, and the organic fractions were collected and dried over Na_2SO_4. The dry organic fractions of all samples were subjected to GC-MS analysis. The integration of the oil and internal standard peaks for each set of control and test samples was calculated and reported as the oil-to-internal standard (oil : IS) ratio. The mass of oil remaining in the test sample was determined according to equation 2. This procedure was performed for all three sets of control and test samples, and the oil sequestered was determined by subtracting the mass of oil remaining from the mass of oil originally added to the test sample.

$$[Oil_{test}] = \frac{(oil{:}IS)_{test}}{(oil{:}IS)_{control}} \times \frac{[IS_{test}]}{[IS_{control}]} \times [oil_{control}] \qquad (2)$$

3.3 Results and Discussions

Characterization of the Composition of Magnetically-active Hybrid Networks upon Deployment in a 10% w/w NaCl Solution. Magnetically-active Hybrid Networks (MHNs) are complex inorganic and organic composite materials that were initially synthesized to remove oil sheen from water following an oil spill.[62] The MHNs are comprised of two main components: polymeric shell crosslinked knedel-like (SCK) nanoparticles and iron oxide nanoparticles (IONs) functionalized with aminopropylsilane to afford amine moieties on the surface of the nanoparticles (amine-IONs). The SCKs were prepared by self-assembly of the amphiphilic block copolymer poly (acrylic acid)$_{90}$-*b*-polystyrene$_{140}$ (PAA$_{90}$-*b*-PS$_{140}$) into micellar structures with a hydrophobic polystyrene (PS) core and a hydrophilic poly (acrylic acid) (PAA) shell. These micellar structures underwent further crosslinking of the PAA shell with the diamine crosslinker 2,2'-(ethylenedioxy)bis(ethylamine) in the presence of 1-[3'-(dimethylamino)propyl]-3-ethylcarbodiimide methiodide (EDCI) to avoid disassembly upon dilution or deployment in challenging ionic environments. A similar amidation chemistry facilitated by EDCI was re-employed to create a covalent linkage between the amine-IONs and the SCKs, which led to the formation of interparticle crosslinks, not only between the amine-IONs and the SCKs, but also between SCK particles. These consecutive amidation reactions yielded complex and robust network-like structures with different compositions and morphologies capable of capturing crude oil from water with efficiencies between 350% and 450% (Scheme 3.1).

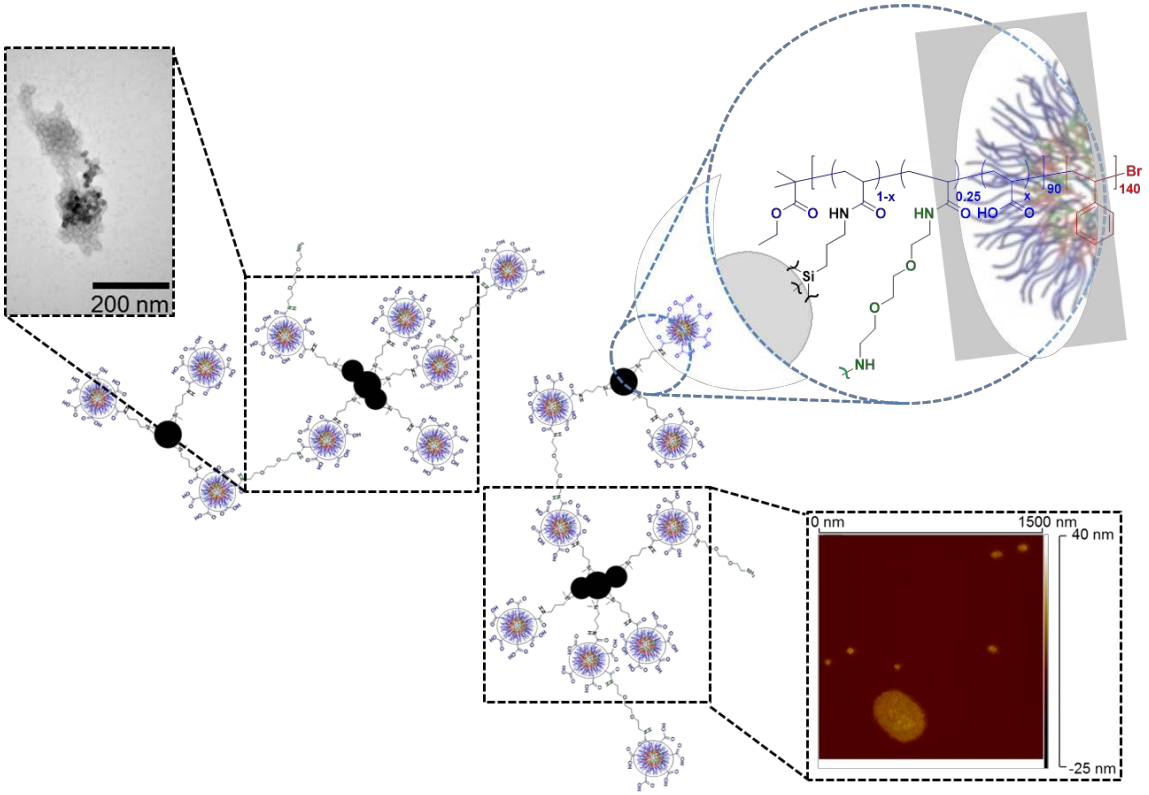

Scheme 3.1. Schematic representation of the MHNs, including their characterization *via* TEM (top left) and AFM (bottom right), and the composition of the polymeric SCKs.

Although the MHNs achieved highly efficient capture of crude oil from water, it remained unclear how the performance of the materials would be affected in saline environments; which is of significant importance given that oil spills take place in both fresh water and marine environments. We began by investigating the morphological and compositional changes to the MHNs upon exposure to environments resembling seawater. A simple 10% w/w NaCl aqueous solution (brine) was employed to characterize the morphology and composition of the materials as well as to study their

sequestration of specific components of crude oil. Complexation of the MHNs with the salt ions in the brine solution was expected because of the overall anionic character of the MHNs imparted by the acrylic acid moieties present on the shell of the SCKs, which are deprotonated under the slight acidic conditions of nanopure water (pH range 5-6).[62] Additionally, salt complexation could also occur with any free amine groups present in the network structures. Therefore, employing this simple brine solution allowed us to control the deployment environment to determine the extent of the complexation of NaCl by the composites, and to obtain a better understanding of the interactions taking place between the materials and the contaminants in the presence or absence of salt.

Compositional analysis of the MHNs before and after deployment in brine was performed in order to understand the effect that NaCl can have on the materials. Analysis of the MHNs before and after deployment in brine *via* infrared (IR) spectroscopy revealed no significant changes between the two samples (Figure 3.1a). The expected bands corresponding to the carbonyl stretch for the acrylic acid pendant groups of the SCKs (*ca.* 1710 cm^{-1}), and the amide functional groups (*ca*. 1640 cm^{-1} and *ca*. 1560 cm^{-1}) formed after crosslinking of the SCKs and covalent binding of the SCKs to amine-IONs, were observed before and after exposure to the brine solution. These results indicated that the crosslinking of the SCKs and the covalent bonds between the SCKs and amine-IONs did not suffer measurable changes upon exposure to a saline environment.

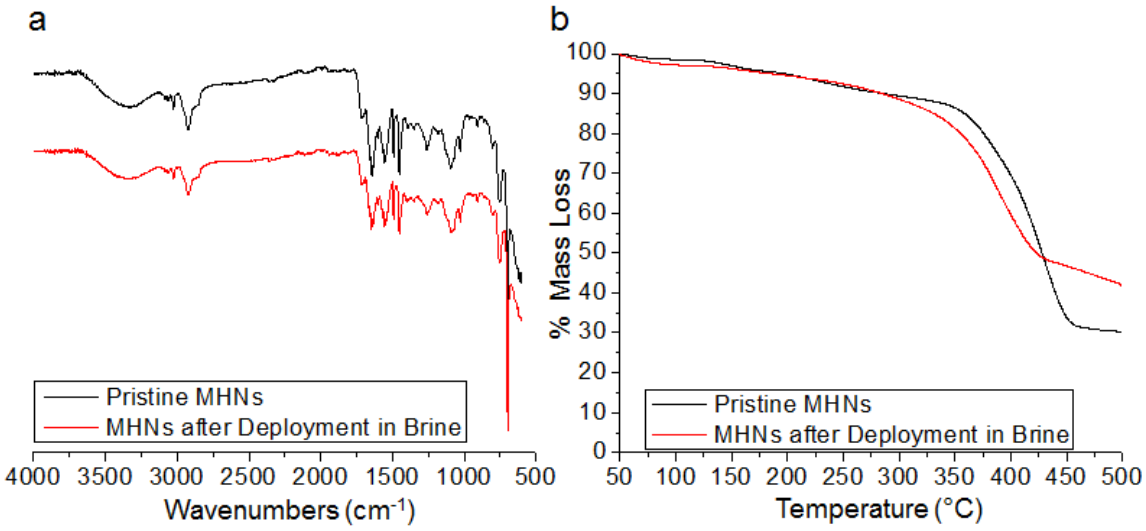

Figure 3.1. IR spectra (a) and TGA thermographs (b) of MHNs before and after deployment in brine.

Moreover, thermogravimetric analysis revealed a reduction in the decomposition temperature of the MHNs after deployment in brine of *ca.* 40 ℃ when compared to that of the pristine MHNs (Figure 3.1b). Deployment of the MHNs in brine also led to an increase in the mass remaining at 500 ℃ of *ca.* 15%, and indicated a higher percentage of thermally stable components remaining in the sample pan. The increase of the percentage of thermally-stable materials could be due to the loss of polymeric components upon deployment in brine caused by the disruption of the electrostatic interactions between the anionic SCKs and the cationic amine-IONs. This would lead to an overall higher percentage of amine-IONs in the MHNs which are thermally stable at

temperatures lower or equal to 500 °C. This observation may also be explained by complexation of the salt ions with the components of the MHNs, which would increase the percentage of inorganic content in the network structures that would not undergo thermolysis below 500 °C. Alternatively, the increased mass remaining could also be due to a combination of both the loss of polymeric materials and ionic complexation with the components of the MHNs; however these causes could not be identified *via* TGA alone.

Recovery of the MHNs *via* Magnetic Action upon Deployment in a 10% w/w NaCl Solution. To better understand the effect of NaCl on the network structure of the MHNs and to elucidate possible complexation of sodium and chloride ions, the recovery of the MHNs *via* magnetic action after deployment in brine was evaluated. An MHN recovery of over 90% upon deployment in nanopure water has been previously reported,[62] and indicated that strong interactions, either covalent or electrostatic, hold the network structure together and allow for the removal of most of the organic and inorganic components from nanopure water *via* magnetic action. After resuspension of the MHNs in brine, a reduction in the recovery efficiency of the MHNs was expected, as the SCKs that were electrostatically associated to amine-IONs may not be completely recovered. Additionally, to emphasize the need for covalent interactions to hold the network structure together, particularly for their utilization in salt water environments, the recovery of MHNs was compared to the recovery of a physical mixture (PM) of SCKs and amine-IONs. The PM was prepared following the same procedure utilized for

the synthesis of the MHNs, but without addition of EDCI. Hypothetically, this material would have the same ability to sequester pollutants as the MHNs; however, its recovery upon deployment in saline environments may be lower than that of covalently-linked MHNs, as the organic and inorganic components of the PM are linked only by electrostatic interactions, which may be screened upon exposure to high ionic strength environments.

The recovery of the particles from brine was first assessed qualitatively. The particles were resuspended in brine at a concentration of 1 mg/mL, vortexed to facilitate resuspension and exposed to an external magnetic field for 4 min following removal of the supernatant. Comparison of the color of the supernatants (Figure 3.2) suggested a higher recovery for the MHNs than for the PM. The light brown color of the PM supernatant indicated that a higher concentration of amine-IONs and/or SCKs remained suspended in brine. In contrast, the MHN supernatant was practically colorless, similar to that of the supernatant following MHN recovery from nanopure water, which was performed as a control experiment. These data suggested that the recovery of the MHNs from brine was relatively similar to that of the MHNs from water.

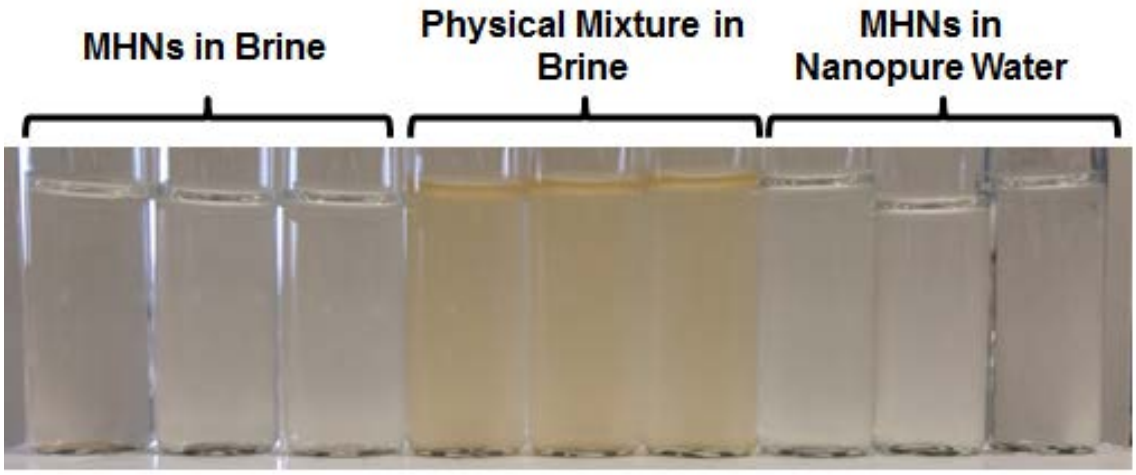

Figure 3.2. Optical images of the supernatant of the MHNs (left) and a physical mixture of SCKs and amine-IONs (center) after deployment in brine, and supernatant of the MHNs after deployment in nanopure water (right).

The recovery of the particles was also assessed quantitatively. Originally, the weight of the particles recovered was recorded once all the remaining water was evaporated, and the percent recovery was calculated. The recovery of the MHNs from nanopure water was calculated to be *ca.* 95%, while the recovery of the MHNs from brine was greater than 100%, even after ensuring the particles were dry. These results can be explained by the complexation of ions with the MHNs. To corroborate this hypothesis, inductively coupled plasma–atomic emission spectroscopy (ICP-AES) and ion chromatography experiments were performed, which determined that upon deployment in brine *ca.* 30% of the recovered mass corresponded to NaCl complexed

with the MHNs, and *ca.* 40% of the mass corresponded to NaCl complexed with the PM (Table 3.1).

Table 3.1. Content of NaCl found on samples of MHNs and a physical mixture of SCKs and amine-IONs (PM) upon deployment in brine at a concentration of 1 mg/mL, followed by aqueous wash to remove excess salt and separation from solution *via* magnetic action.

Sample	Wt% NaCl
MHN	29.1 ± 1.8
PM	40.7 ± 10.2

Once the mass of the complexed NaCl was taken into consideration, the recovery of the hybrid materials from brine was recalculated to be *ca.* 84%, a *ca.* 10% reduction in the recovery efficiency of the MHNs following deployment in brine compared to that achieved in nanopure water (Figure 3.3). The high percent mass recoveries of MHNs from both nanopure water and brine suggest that the interactions between the SCKs and the amine-IONs have a covalent character, yielding robust structures that can retain their composition in high salinity environments. In contrast, the recovery efficiency of the PM upon deployment in brine was determined to be 54 ± 10%. These data revealed a

ca. 40% reduction in the recovery efficiency of the PMs compared to the MHN recovery from nanopure water, and a *ca.* 30% reduction compared to the MHN recovery from brine. Initially, the lower recovery efficiency of the PM was attributed to disruption of the electrostatic interactions between the SCKs and the amine-ION*s* by NaCl. However, analysis of the recovery efficiency of the PM upon deployment in nanopure water showed that 60 ± 2.0% of the mass of the PM was recovered, indicating that the reduction in the recovery efficiency of the PM was not caused by the introduction of salts into the system. Nevertheless, these data corroborate the importance of the covalent linkages employed in the MHNs, since the absence of these covalent interactions led to lower recoveries that contribute to contamination of fresh water and marine environments.

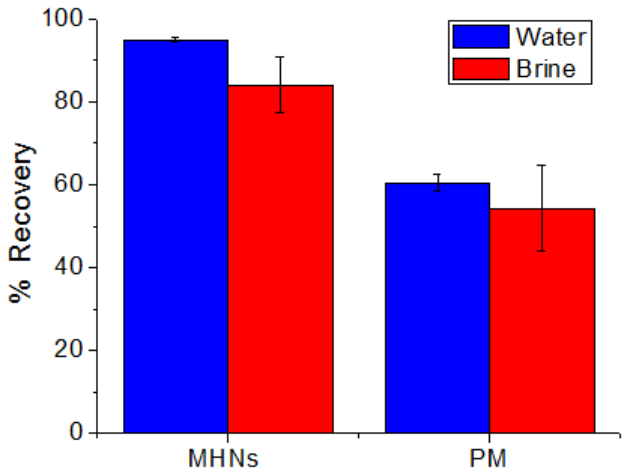

Figure 3.3. Percent recovery of MHNs and Physical Mixture (PM) from water and brine upon magnetic action.

Morphological Characterization of Magnetically-active Hybrid Networks upon Deployment in a 10% w/w NaCl Solution. To investigate the morphological changes experienced by the network structure of the MHNs, or by the individual SCKs composing the networks, TEM of the MHNs was performed before and after deployment in brine. The light globular structures observed in the micrographs (Figure 3.4) correspond to the SCK nanoparticles which exhibited a globular shape, while the areas of high contrast may be agglomerated amine-IONs or high concentrations of the staining agent employed during sample preparation. The MHNs were previously imaged *via* cryogenic TEM (cryo-TEM) without the use of a staining agent,[62] and both components of the MHNs were identified without the ambiguity usually caused by staining TEM samples.[35] The micrographs of the MHNs before resuspension in brine (Figure 3.4a) showed the typical network structure composed of multiple SCKs interconnected among themselves, and to amine-IONs. The size of the particles observed ranged from *ca.* 20 nm, corresponding to individual SCKs, to several hundreds of nanometers. Since the morphology of the MHNs is difficult to control, the size of the networks varied significantly; however, the dimensions of these networks did not typically exceed the nanometer range. On the other hand, large agglomerates with dimensions in the micrometer range were observed once the MHNs were deployed in brine (Figure 3.4b). Although typical networks were still observed, the majority of the structures identified resembled the agglomeration of networks into large macrostructures. The formation of these macrostructures or "flocs" can be caused by the interaction of the sodium and chloride ions with the electrical double layer of the MHNs that contributes to their

resuspension in water,[76] leading to flocculation of the network structures and the formation of the macrostructures observed by TEM.[77]

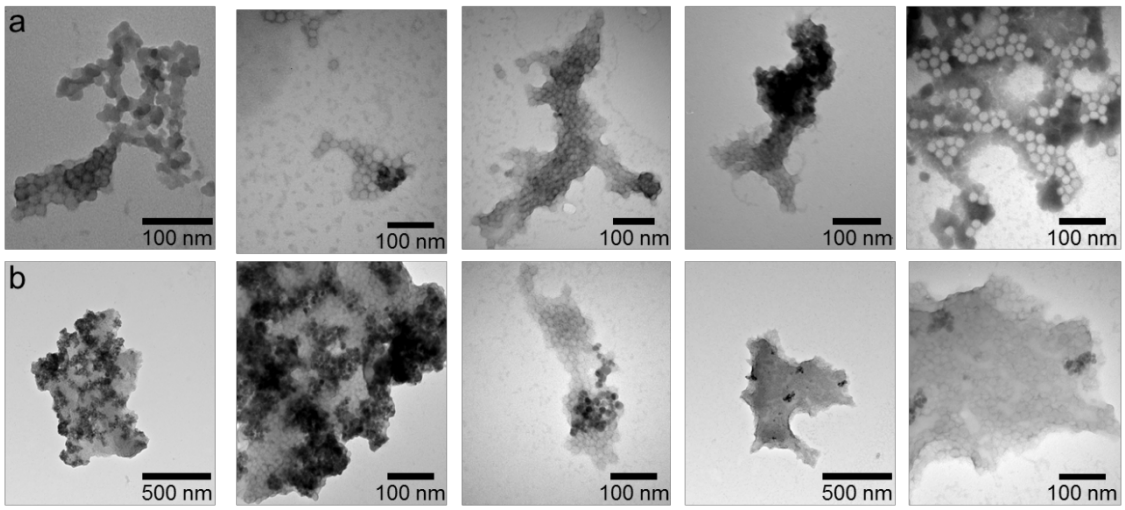

Figure 3.4. TEM of MHNs before (a) and after (b) deployment in brine.

In addition to TEM, AFM was performed in order to analyze the structure of the networks and their individual components in greater depth. The 3D representation of the height image for the MHNs before and after deployment in brine, showed the presence of structures of different sizes composed of individual particles (Figures 3.5a and 3.5c), which were similar to those observed by TEM. A closer inspection of the MHNs (Figures 3.5b and 3.5d) revealed several round nanoparticles confined together to form a

larger structure, regardless of the medium in which they were deployed. The diameter of the individual nanoparticles was determined *via* the cross-sectional analysis performed on the height image of the MHNs (white lines drawn on Figures 3.5b and 3.5d), and showed nanoparticles of *ca.* 15 nm in diameter; which corresponded in size and shape to the morphology of the SCKs as determined by TEM and dynamic light scattering (DLS).[62] Moreover, the height profile derived from the cross-sectional analysis of the pristine MHNs (black trace on Figure 3.5e) revealed the arrangement of individual particles in a single layer. However, multiple layers of nanoparticles were observed when the same analysis was performed on the MHNs upon deployment in brine (red trace on Figure 3.5e). These data complement the information obtained *via* TEM, and provide evidence of the hierarchical assembly of individual nanoparticles, which lead to the formation of networks with sizes in the micrometer range, possibly caused by flocculation of the MHNs in the presence of NaCl.

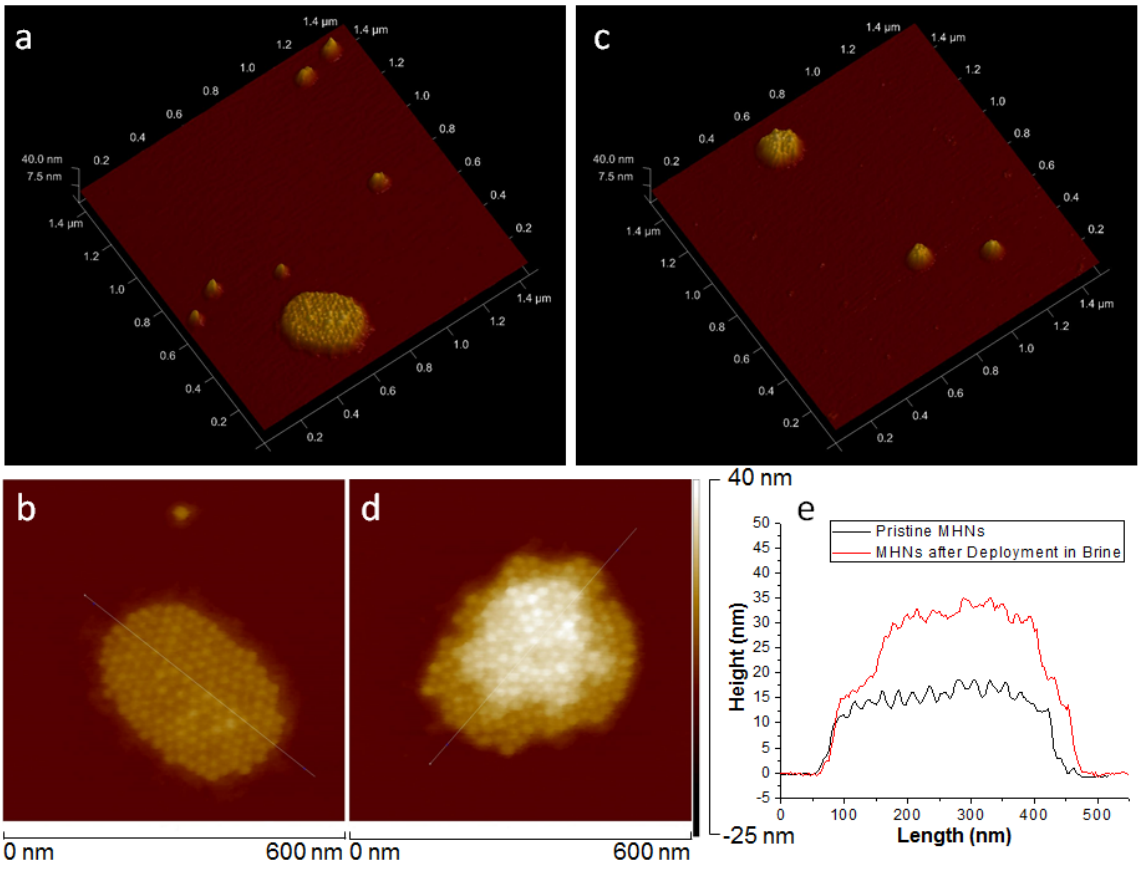

Figure 3.5. 3D representation (top) of AFM height images (bottom) of the MHNs before (a-b) and after (c-d) deployment in brine. Section analysis (e) of the cross section white lines seen on b and d, depicting the individual nanoparticles that compose the larger structure.

Sequestration of Model Aliphatic Components of Crude Oil: Performance in fresh water *vs.* saline environments. Due to the inherent variability in the composition of crude oil and refined oil, it is of interest to determine if the MHNs exhibit preferential sequestration for some of the components of oil. However, the complex composition of crude oil makes it difficult to quantify the amount of oil sequestered by the MHNs, and

even more difficult to determine and quantitate the sequestration of individual components. To facilitate these studies, dodecane was selected as a model for the aliphatic components of crude oil, which are typically known as "saturates" and account for the majority of the components of the crude oil.[71]

The maximum loading capacity of the MHNs towards dodecane was determined following deployment and recovery of MHNs at various mass ratios of dodecane-to-MHNs (oil:MHN) present in a fixed volume of nanopure water or brine. In these experiments, the MHNs were deployed as a powder and allowed to equilibrate with minimal movement on the surface of the contaminated environment for *ca.* 10 min. Resuspension of the MHNs was observed when they made direct contact with the aqueous phase. On the other hand, a change in color from light brown to dark was observed upon contact of the MHNs with the dodecane resting on the surface of the water; which was attributed to absorption of the hydrophobic contaminant by the MHNs, and was more evident as the concentration of dodecane in the water was increased. After equilibration, the system was hand-shaken in order to maximize contact between the pollutants and the MHNs, followed by separation of the loaded MHNs from water *via* magnetic action. The remaining contaminated environment was decanted, and the vial was washed three times with water to remove any remaining pollutants. Upon combination of the aqueous washes with the remaining contaminated environment, decane was added as an internal standard in order to monitor the efficiency of the extraction of the organic components from water, as well as for the quantification of the remaining dodecane *via* GC-MS. Once the dodecane remaining in the water had been

quantified, the amount of pollutant sequestered by the MHNs was determined, and the loading capacity was calculated as the mass of dodecane (mg) captured per mg of MHNs deployed. For the initial oil : MHN ratios of 10 : 1, 15 : 1, 20 : 1 and 25 : 1, the loading capacity of the MHNs in nanopure water was calculated to be 8.7, 11.6, 17.0 and 17.9, respectively (Figure 3.6). An initial plateau was observed at oil : MHN = 25 : 1, however; further challenging of the system at higher oil : MHN ratios revealed that the MHNs were capable of sequestering much higher amounts of oil. In fact, as much as 33 ± 3 mg of dodecane per mg of MHNs used were sequestered at an oil : MHN = 45 : 1.

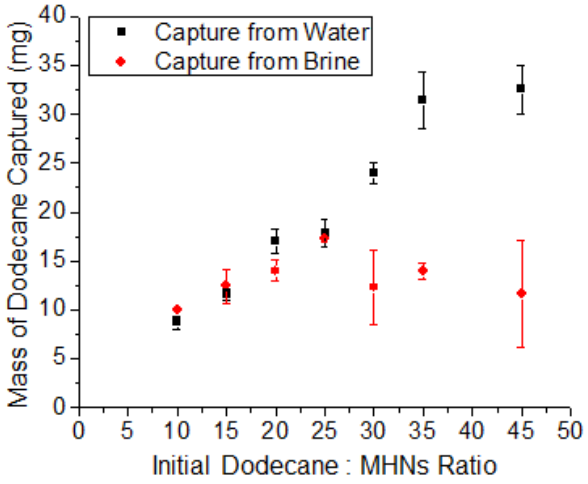

Figure 3.6. Comparison of the loading capacity ratio of the MHNs towards dodecane when captured from water and brine.

On the other hand, the performance of the MHNs was significantly affected when the remediation routine was performed in brine. Up to an oil : MHN = 25 : 1 no significant differences were observed in the performance of the MHNs in water or brine as a function of oil:MHN ratio. However, analysis of the sequestration of dodecane from nanopure water at oil : MHN above 25 : 1 greatly differed from the results obtained in brine. In water, a significant increase in the loading capacity of dodecane was observed at an oil : MHN = 30 : 1, with a calculated loading capacity of 24 ± 1 : 1 compared to the 18 ± 1 : 1 calculated at an oil : MHN = 25 : 1. On the contrary, the calculated loading capacity in brine at an oil : MHN = 30 : 1 was 12 ± 4 : 1, significantly lower than the 17 ± 0.5 : 1 ratio calculated at an oil : MHN = 25 : 1. Overall, the maximum loading capacity of the MHNs for dodecane when sequestering from brine was determined to be 17.3 mg of dodecane per mg of MHNs, which represented a *ca.* 47% reduction in the loading capacity observed in nanopure water.

Although the performance of the MHNs was affected by the presence of salts, there was a remarkable increase in the loading capacity of the MHNs in water when compared to their efficiency towards the capture of crude oil. Up to a ratio of 45:1 the amount of dodecane captured was *ca.* 9 times higher than the maximum amount of crude oil sequestered. However, the remediation routine employed to capture dodecane involved hand-shaking of the samples to maximize contact between the pollutants and the MHNs, which led to the formation of emulsion droplets visible to the naked eye (Figure 3.7). This phenomenon was not previously observed during the sequestration of crude oil, since the high viscosity of the pollutant, and the gravimetric method employed

for quantification, prevented us from applying a mechanical stimulus to maximize contact between the MHNs and the crude oil. Thus, the increase in the sequestration efficiency of the MHNs towards dodecane is attributed to the formation of emulsion droplets, which coupled with the absorption that takes place upon contact of the MHNs with the pollutants, increases the amount of contaminants that can be removed from the water with the use of an external magnet.

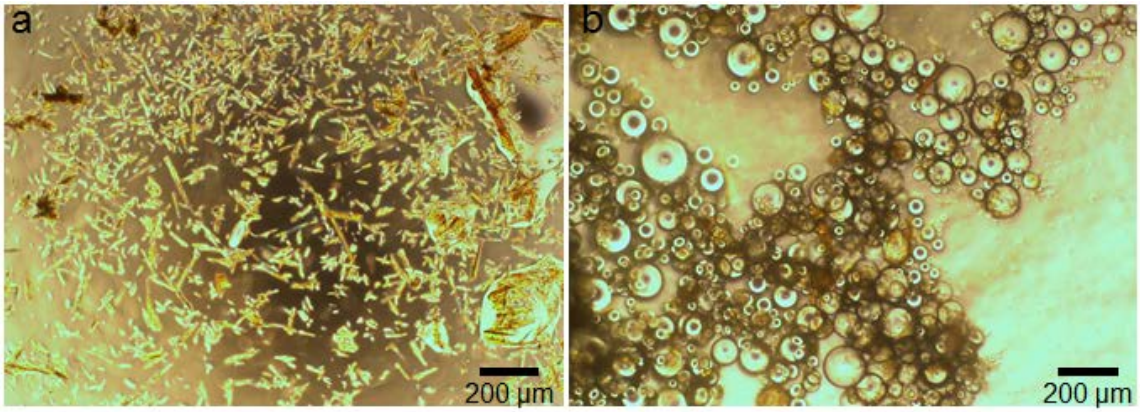

Figure 3.7. Optical microscopy images of MHNs deployed onto a dodecane-polluted environment at a dodecane : MHN = 30 : 1 before (a) and after (b) agitation to induce emulsion formation.

These results are supported by the IR spectroscopy experiments performed to determine if the MHNs undergo compositional changes after pollutant entrapment. The spectra of dodecane and the pristine MHNs were compared to those of the MHNs

recovered *via* magnetic action after sequestering dodecane from water at three oil : MHN ratios: 10 : 1, 20 : 1 and 30 : 1 (Figure 3.8). Overall, no major changes were detected in the structure of the MHNs upon capturing the contaminant, as the characteristic vibrations of the carbonyl and amide functional groups remained unaltered. A strong vibration at *ca.* 2920 cm^{-1} was observed in the spectrum of dodecane, and corresponds to the C-H stretch in the alkane molecule. This same vibration was observed in the spectra of the MHNs before and after contact with dodecane, and a *ca.* 2-fold increase in the signal intensity was observed at an oil:MHN = 10:1, with no further increase in the signal detected at the higher oil:MHN ratios of 20:1 and 30:1. These data indicate that saturation of the system is achieved at an oil:MHN ratio = 10:1, and further support our claims that emulsification contributes to the highly efficient removal of dodecane from water.

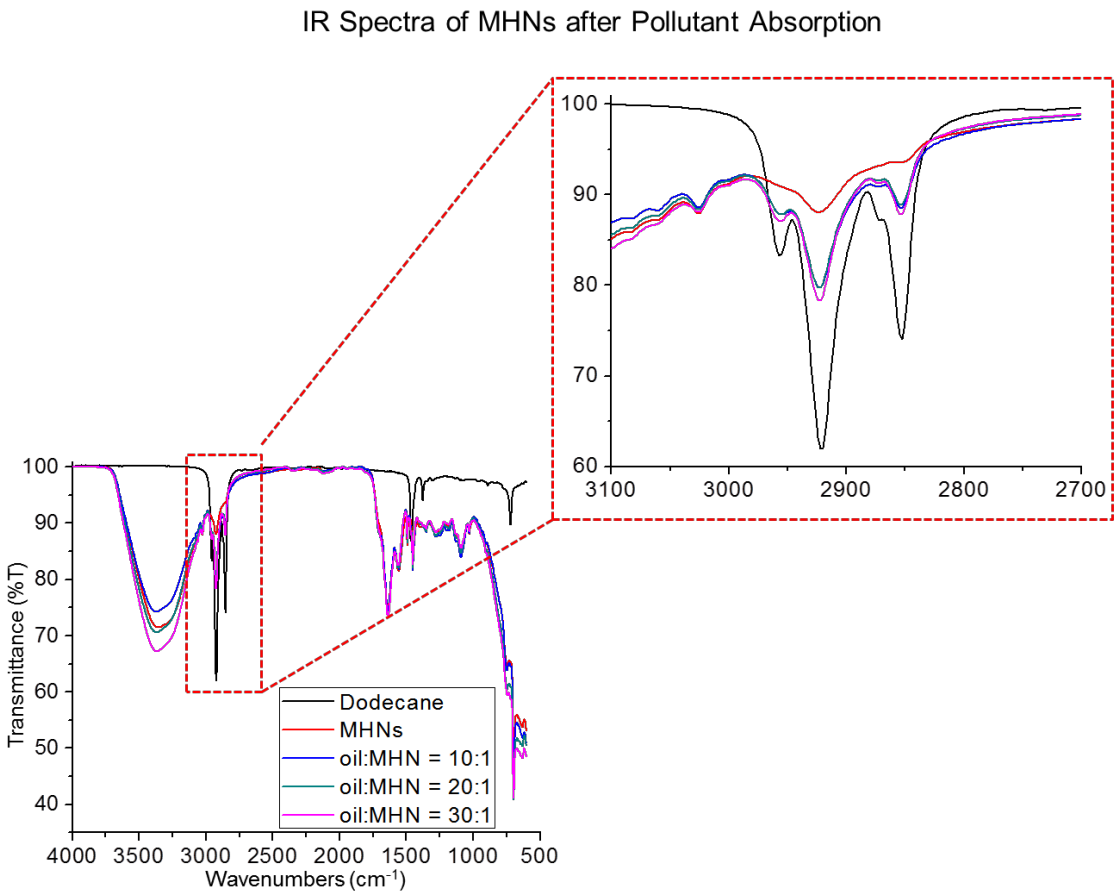

Figure 3.8. IR spectra of dodecane, MHNs and MHNs deployed onto a dodecane/water mixture at various oil : MHN ratios.

The ability of the MHNs to stabilize emulsion droplets can be explained by the phenomenon known as Pickering emulsification.[8] In Pickering emulsions, solid particles assemble at the oil-water interface creating a barrier that inhibits droplet coalescence.[9] Previous reports regarding Pickering emulsions stabilized in saline environments have noted that the stability of an emulsion is typically reduced in the presence of salts.[8,78,79] This behavior has been attributed to the interference of the salt ions with the electrical

double layer associated with charged particles, which leads to particle flocculation and to an increase in the diameter of the droplets formed, producing less stable emulsions.[78-80] Furthermore, the increase in the droplet diameter is due to an attempt to accommodate a larger volume of oil within the droplet; however, limitations to this expansion builds up pressure and eventually leads to the expulsion of excess oil from the droplet.[78] These observations help to explain the reduction of the emulsification ability of the MHNs in the presence of salts, which could be a consequence of a disruption in the electrical double layer of the MHNs that can cause the formation of the flocs previously observed *via* TEM and AFM. Overall, these observations indicate that emulsification plays a significant role in the packaging of dodecane by the MHNs, and it is a factor that must be carefully considered when determining the viability of the MHNs as materials for remediation.

Sequestration of Model Aromatic Components of Crude Oil: Performance in fresh water *vs.* saline environments. Although aliphatic organic compounds constitute the majority of the components of crude oil, asphaltenes and other aromatic components are also significant constituents of crude oil and the associated WSFs. Therefore, it is important to determine whether there is preferential sequestration by the MHNs of the aromatic components of crude oil. Toluene was selected as a model compound given its significant presence in crude oil samples; it is typically found in crude oil as part of the BTEX group, *i.e.,* volatile organic compounds containing benzene, toluene, ethylbenzene and xylenes.[75]

Similarly to the dodecane experiments, the loading capacity of the MHNs was calculated as the ratio of the mass of toluene sequestered (mg) per mg of MHNs deployed (Figure 3.9). For a 5 : 1 oil : MHN ratio, it was determined that 4.1 mg of toluene were captured by 1 mg of MHNs. The performance of the MHNs for toluene capture was very similar to that of the dodecane capture. In water, it was determined that 4.1 mg of toluene were captured by 1 mg of MHNs at an oil : MHN = 5 : 1. For the higher oil : MHN ratios of 10 : 1, 15 : 1 and 20 : 1, the loading capacities ratios were found to be 7.9, 13.1 and 14.5, respectively. A plateau was reached at an oil : MHN = 30 : 1; however, further challenging of the system with higher oil : MHN ratios revealed that as much as 34 ± 3 mg of toluene can be captured per 1 mg of MHN at an oil : MHN = 45 : 1.

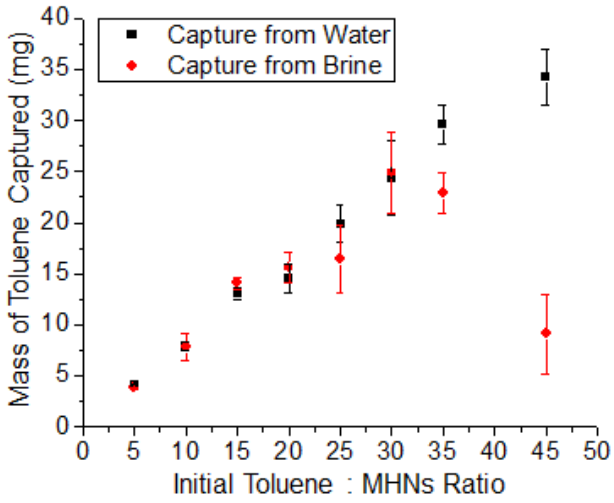

Figure 3.9. Comparison of the loading capacity ratio of the MHNs towards toluene when captured from water and brine.

The performance of the MHNs towards toluene in brine followed a similar trend to that observed towards dodecane, although some differences were identified. In general, the loading capacity towards toluene was lower in brine *vs.* water, with a maximum loading capacity from brine of 25 ± 4 mg of toluene per mg of MHNs achieved at an oil : MHN ratio of 30 : 1. This represented a *ca.* 27% reduction in the loading capacity compared to that of the MHNs in water, and is attributed to a reduction in the emulsification ability of surfactant-like particles in the presence of salts.[78-80] However, the toluene loading capacity when sequestering from brine (25 ± 4 : 1) was *ca.* 30% higher than the dodecane loading capacity (17 ± 0.3 : 1), which indicates a preference for the packaging of toluene in saline environments. These results suggest that although emulsification plays a role in the capture of toluene and dodecane, when

the emulsion stability is challenged by the presence of salts, absorption dominates the interactions between pollutants and MHNs. In the case of toluene, the π-π interactions between the PS core of the SCKs and toluene may be responsible for the *ca.* 30% increase in the toluene loading capacity compared to that of dodecane. Overall, these results are promising in that by carefully selecting the polymeric components of the SCKs to target specific pollutants, a more tailored and efficient remediation approach can be achieved. Such targeted approaches can lead to the development of a plethora of materials that effectively remove various types of pollutants from aqueous and saline environments.

Investigation of the Mechanisms of Interaction Between the Hydrophobic Pollutants and the MHNs. Confocal fluorescence microscopy was performed to investigate the mechanisms of interaction taking place between the MHNs and the hydrophobic pollutants. The experiments were designed with the goal of obtaining evidence of the absorption of the pollutants by the MHNs, which we hypothesized to be the main mechanism of interaction. However, given the formation of the emulsions observed during the sequestration of the pollutants, and the possible capability of the MHNs to act as Pickering emulsifiers, these experiments were also aimed at obtaining evidence of the assembly of the MHNs at the interface of the emulsion droplets. Initially, the organic dye Nile red was dissolved in either toluene or dodecane at a concentration of 30 μg/mL and added to 1 mL of water or brine to mimic a contaminated aqueous environment. The MHNs were deployed onto these polluted environments

containing the Nile red/toluene solution at an oil : MHN = 20 : 1, and as observed previously, optical microscopy revealed needle-like structures of multiple shapes and lengths in the solution (Figure 3.10a). Evidence of the absorption mechanism was obtained upon excitation of the sample with a 543 nm laser. The fluorescence image showed heterogeneous needle-like structures exhibiting red fluorescence (Figure 3.10b), which was made possible by the absorption of the Nile red/toluene solution by the MHNs.

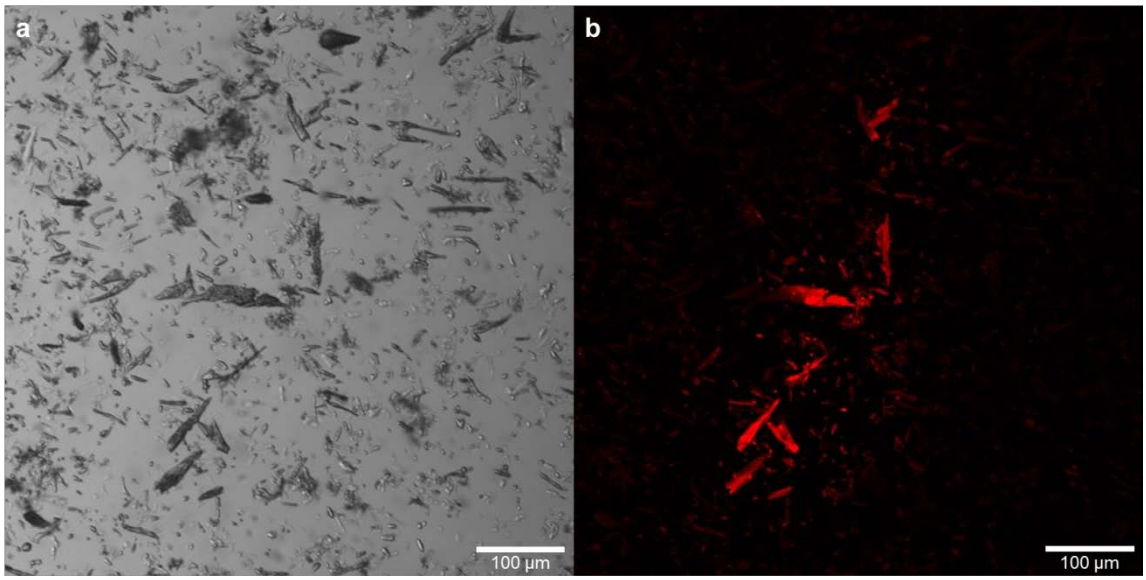

Figure 3.10. Optical microscopy image (a) and confocal microscopy image (b) of MHNs deployed onto a water/toluene/Nile red mixture at a toluene : MHN = 20 : 1, obtained upon excitation with the 543 nm laser, depicting the fluorescently-active MHNs.

Similar results were obtained when the solution of dodecane and Nile red was employed to mimic the contaminated environment at the same oil : MHN ratio of 20 : 1 (Figure 3.11). Upon hand-shaking of the system, optical microscopy showed the formation of emulsion droplets covered by heterogeneous structures of different shapes and sizes, which we have attributed to the MHNs (Figure 3.11a). Excitation of the sample with the 543 nm laser revealed that the MHNs arranged themselves on the surface of the droplets, outlining the circumference of the droplet, and like in the toluene case, displaying red fluorescence (Figure 3.11b). Given that the MHNs employed in these experiments were not fluorescently tagged, the observance of fluorescently active MHNs can be attributed to the absorption of hydrophobic pollutants.

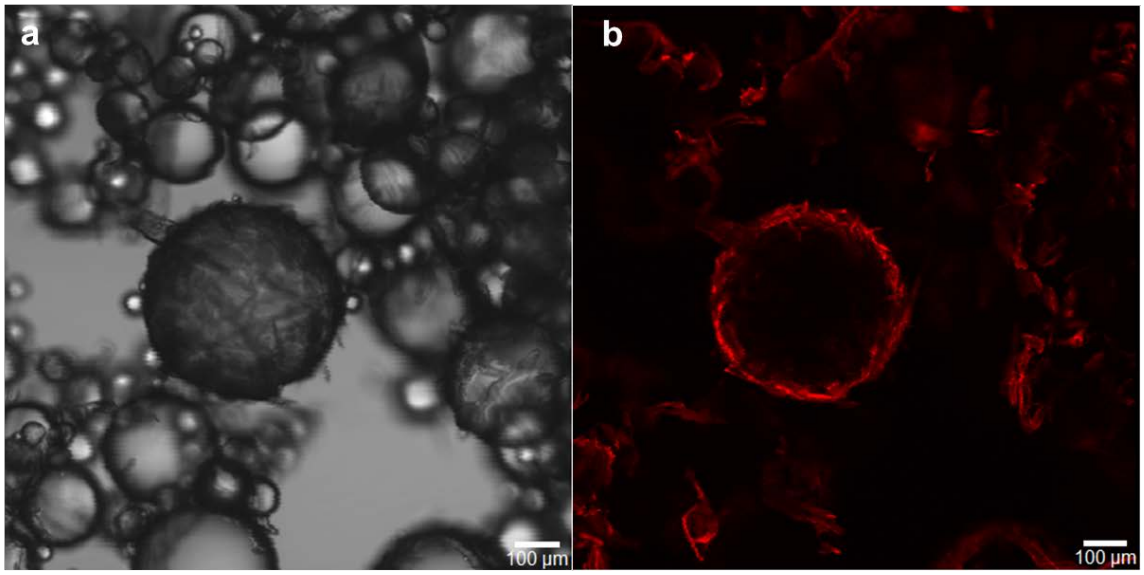

Figure 3.11. Optical microscopy image (a) and confocal microscopy image of a dodecane/water/MHN mixture upon hand shaking and irradiation with a 543 nm laser (b).

Confocal fluorescence microscopy also provided evidence of the occurrence of a second mechanism of interaction between the MHNs and the contaminants, and of the ability of the MHNs to act as Pickering emulsifiers. The arrangement of the MHNs at the surface of the droplets was observed *via* confocal microscopy, and the confinement of the MHNs to the surface of the droplets was visualized by obtaining multiple images of the sample at different points along the z axis (See video in Figure 3.12). In general, these data revealed the stabilization of the droplets by the MHNs; however, the composition of the droplets remained unknown.

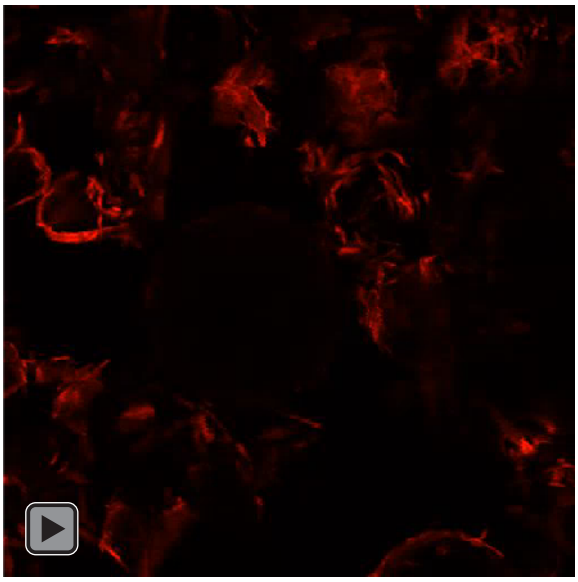

Figure 3.12. By clicking the .avi file above see a video of the MHNs arranged at the droplet interface after absorption of the Nile red/dodecane solution and hand-shaking of the system to induce emulsion formation.

Additional analyses of the Nile red/dodecane solution by fluorescence spectroscopy showed that when dissolved in dodecane, Nile red exhibited fluorescence upon excitation at 543 nm as well as at 488 nm (Figure 3.13). Consequently, the emission signal from Nile red was detected in two different wavelength ranges: between 500 nm and 530 nm for the emission produced by the excitation at 488 nm, and between 555 nm and 655 nm for that produced by excitation at 543 nm. These settings were then employed to the above mentioned experiment, where the emulsion droplets formed by hand-shaking of the dodecane/water/MHN mixture containing Nile red dissolved in dodecane were excited with the 543 nm and 488 nm lasers and analyzed *via* confocal microscopy (Figure 3.14).

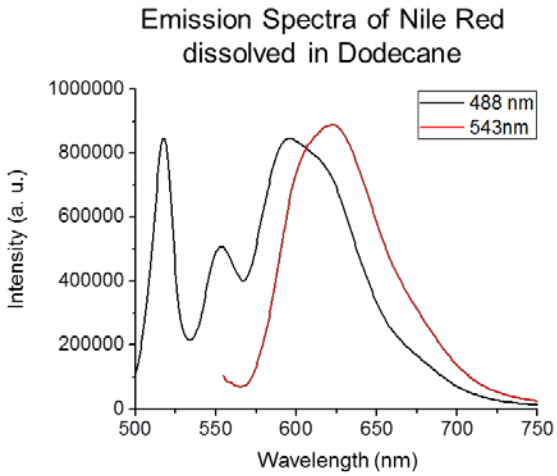

Figure 3.13. Emission spectra of a Nile red/dodecane solution (30 μg/mL) excited at two different wavelengths, 488 nm (black trace) and 543 nm (red trace).

As previously observed, the excitation of the sample at λ = 543 nm revealed the MHNs loaded with the Nile red/dodecane solution assembled at the droplet interface (Figure 3.14a). However, upon excitation with the 488 nm laser, the emission signal detected between 500 nm and 530 nm allowed us to determine that the MHNs were capable of stabilizing oil droplets in a continuous aqueous phase (Figure 3.14b). The green fluorescence observed inside of the droplets was due to the excitation of the Nile red dissolved in dodecane, and indicated that the droplets stabilized were composed of oil.

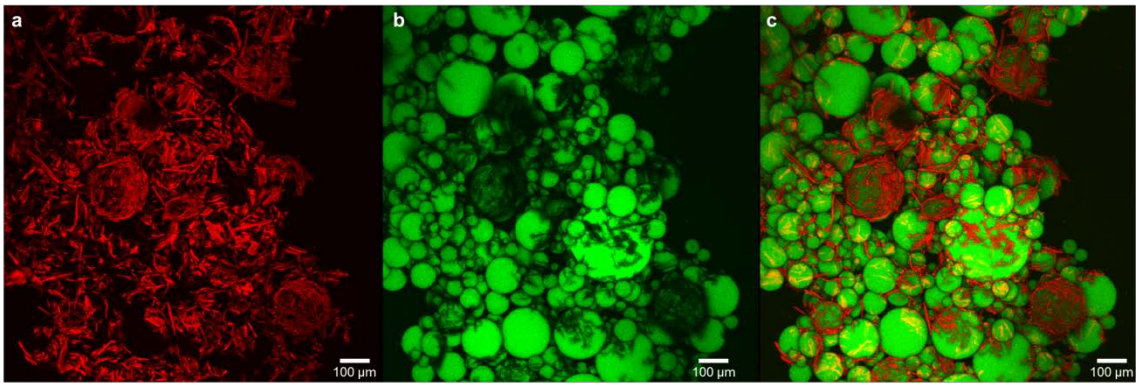

Figure 3.14. Confocal microscopy image upon excitation with a 543 nm laser (a), depicting the MHNs arranged on the surface of some droplets and exhibiting red fluorescence after absorption of the Nile red/dodecane solution; and upon excitation with a 488 nm laser (b) showing green emulsion droplets due to the emission produced by the Nile red dissolved in dodecane. Overlay (c) of the confocal microscopy images a and b, depicting the dual mechanism of absorption and emulsification that act simultaneously to sequester pollutants from aqueous environments.

It is important to note that based on the emission spectra of Nile red dissolved in dodecane (Figure 3.13) one would expect to observe red fluorescence inside the droplets, but it was difficult to determine fluorescence signal inside the droplets shown in Figure 3.11b and in the video presented in Figure 3.12. Therefore, the various micrographs obtained by scanning the emulsified sample along the Z axis at an excitation $\lambda = 543$ nm were analyzed individually. The results displayed red fluorescence both inside the MHNs and inside the droplets; however, a reduction in the intensity of the emission signal detected inside the droplets was observed (Figure 3.15).

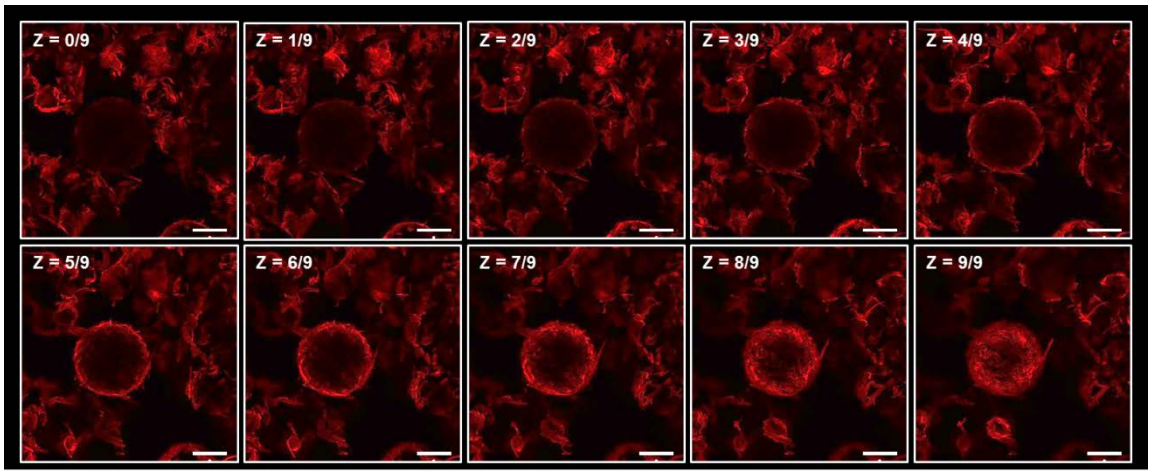

Figure 3.15. Confocal laser micrographs of a Nile red/dodecane/water/MHN mixture upon hand shaking and irradiation with a 543 nm laser. Images were taken at various positions along the z axis, beginning from the bottom and progressively moving to the top. Scale = 100 µm.

This phenomenon was also observed when the emission signal produced by an excitation λ = 488 nm was detected (Figure 3.16). In general, the emission signal could be detected inside the droplets in both emission ranges (between 500 nm to 530 nm and between 555 nm to 655 nm), but a decrease in the intensity of the signal detected at the higher wavelength range was observed both in the single image (Figures 3.16a and 3.16c), as well as in the image produced from a compilation of scans along the Z axis (Figures 3.16b and 3.16d).

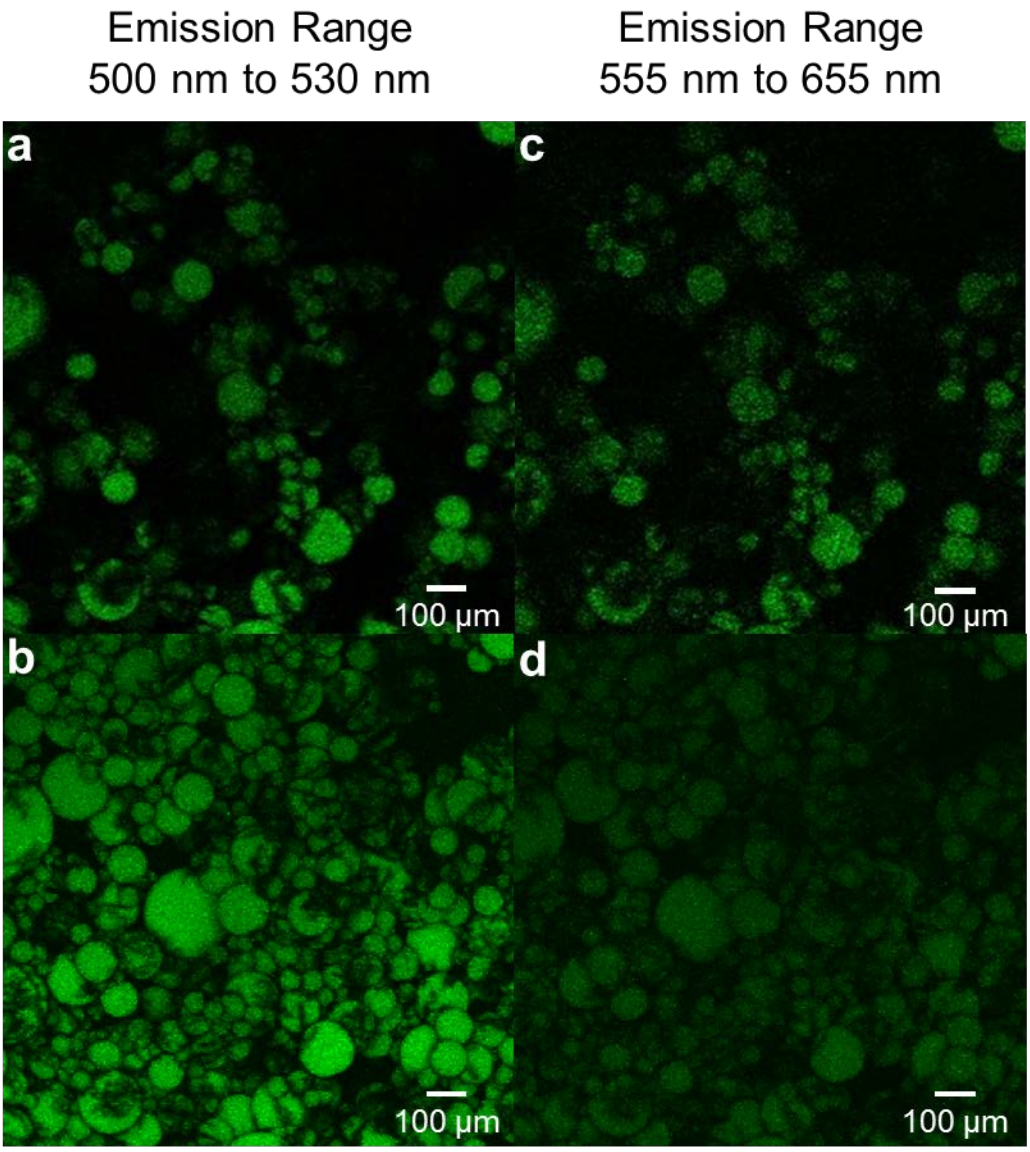

Figure 3.16. Confocal microscopy images of the same sample of a dodecane/water/MHN mixture upon hand shaking and irradiation with a 488 nm laser with emission detected at two different wavelength ranges: 500 nm – 530 nm (a-b) and 555 nm – 655 nm (c-d). The top row displays images of a single focal point of the same sample, while the bottom row displays an image produced from the combination of 49 images collected along the Z axis.

The decrease in the emission intensity of Nile red, as well as the difference in the emission spectra of the same Nile red/dodecane solution upon excitation at different wavelengths is not surprising, as the dye is known to exhibit solvatochromism.[81] Additionally, Nile red has been employed as a molecular probe to determine the microenvironment surrounding the dye, given that depending on the solvent, Nile red exhibits changes in the absorption and emission spectra, quantum yields, and fluorescence intensity.[82,83] These characteristic changes are attributed to the formation of the twisted intramolecular charge transfer (TICT) state, which is caused by the transfer of an electron from the electron-donating diethylamino group to the electron-accepting quinoid part of the molecule. The electron transfer is enabled by the free rotation around the single bond connecting these two groups, that leaves the molecule in a twisted configuration in which the diethylamino and quinoid groups are almost perpendicular to each other. During this twisting process, the Nile red molecule goes from a fairly non-polar state to a polar product that is more easily stabilized in the presence of polar solvents.[82-84] In general, blue shifts in the emission and excitation spectra are observed as the hydrophobicity of the solvent is increased.[81] We observed this trend when measuring the emission spectra of Nile red dissolved either in toluene or dodecane (Figure 3.17). Although both solvents are hydrophobic, dodecane has an octanol-water partition coefficient (Log P) of 6.80 compared to that of 2.73 for toluene,[85] which indicates increased hydrophobicity for dodecane and is consistent with the blue shifts previously reported for Nile red in hydrophobic solvents.

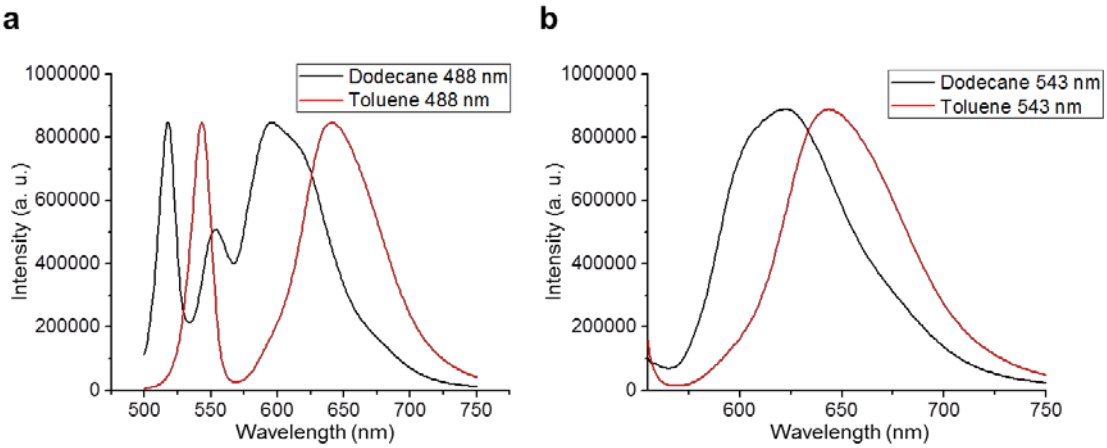

Figure 3.17. Emission spectra of Nile red dissolved in toluene or dodecane at a concentration of 30 µg/mL upon excitation at λ = 488 nm (a) and λ = 543 nm (b).

In summary, these experiments revealed that the dual mechanisms of absorption and emulsification dominate the interactions between the pollutants and the MHNs, and can be observed by the overlay of the images obtained upon excitation with the 488 and 543 nm light sources. The overlay of the two images in Figure 3.14c showed how the MHNs turned fluorescently-active after absorption of the fluorescently-labelled pollutant, and arranged themselves at the interface of droplets that were composed of the hydrophobic contaminant.

3.4 Conclusions

To improve our understanding of the performance of the MHNs in environments similar to seawater the sequestration of model components of crude oil (such as

dodecane and toluene) from water and brine was investigated, and the results showed a significant increase in recovery when compared with the performance of the MHNs for sequestration of crude oil. A maximum loading capacity of *ca.* 30 mg of oil (toluene or dodecane) per mg of MHN was determined when sequestration was performed in water, which represented an efficiency of *ca.* 3000%. Detailed examination *via* confocal microscopy revealed that the dual mechanisms of absorption of hydrophobic pollutants, as well as emulsification took place during the sequestration experiments, a phenomenon that had not been previously observed. Additionally, although the deployment of the MHNs in brine did not significantly affect the composition of the MHNs, it led to the flocculation of the networks into larger heterogeneous microstructures. These observations allowed us to explain the decrease in the performance of the MHNs observed when sequestration was performed in brine. In general, lower loading capacities were achieved when capturing both toluene and dodecane from brine compared to those in water. However, a higher maximum loading capacity of 25 : 1 (oil : MHNs) was determined for toluene, compared to the 17 : 1 maximum loading capacity calculated for dodecane. These results indicated that when the mechanism of emulsification is compromised by the presence of salts in the system, the mechanism of absorption dominates. In this case, it is possible to design the chemistry with a specific pollutant in mind, in such a way that common interactions such as π-π stacking, van der Waals and/or hydrogen bonding drive the sequestration of the contaminants to yield highly efficient remediation approaches. It may also be possible to incorporate further responsive characteristics into the MHN materials, for instance to combine photo-

thermal or other behaviors to drive the emulsification and de-emulsification processes.[86-88]

CHAPTER IV

MAGNETIC PICKERING EMULSIONS STABILIZED BY HYBRID INORGANIC/ORGANIC NETWORKS

4.1 Introduction

The stabilization of emulsions by solid particles is a phenomenon that has been developed since the beginning of the last century and has gained increasing interest over the past decade. These emulsions, whose discovery is often attributed to Spencer U. Pickering, but which was first described by Walter Ramsden in 1903,[7] are known as Pickering emulsions.[8] Most of the work performed on Pickering emulsions involves the stabilization of single droplets yielding oil-in-water (o/w) or water-in-oil (w/o) emulsions. However, recent work has also yielded the stabilization of double emulsions of the oil-in-water-in-oil (o/w/o) or water-in-oil-in-water (w/o/w) types.[89,90]

Traditionally, the stabilization of Pickering emulsions has been achieved through the use of discrete, individual particles that have varied significantly in their compositions and morphologies, including inorganic particles, such as laponite clay,[91,92] silicon oxide,[93,94] zirconium phosphate,[95] cadmium selenide,[96,97] gold,[98] and iron oxide,[99] as well as organic materials, such as bionanoparticles,[100] latex beads,[101] polymersomes,[102] Janus nanoparticles,[103,104] shell crosslinked micelles,[105]

---

* Jeniree A. Flores, Ashlee A. Jahnke, Adriana Pavia-Sanders, Zhengdong Cheng and Karen. L. Wooley, *Soft Matter*, **2016**, *12*, 9342-9354. Reproduced by permission of The Royal Society of Chemistry.

carbonaceous microspheres,[106] and polysiloxane microspheres.[107] In addition to these materials, starch-based[108] and fat-based[109] particles have been investigated, with particular interest for their utilization in the food industry.

More recently, applications of the Pickering effect have transcended the mere stabilization of emulsions to give rise to a novel approach towards the synthesis of materials. This technique has been widely utilized for the construction of membranes,[96,110] capsules,[111] colloidosomes;[101,112,113] latex beads,[91,92,103] and hybrid inorganic/organic latex beads.[93,114] For instance, Lin *et al* utilized tri-*n*-octylphosphine oxide (TOPO)-stabilized CdSe nanoparticles, capable of undergoing assembly at an oil-water interface, to yield ultra-thin (*ca.* 5 nm thickness) nanoparticle membranes upon assembly of the nanoparticles at a flat oil-water interface, and crosslinking of the TOPO ligands.[97] This process was extended to nanoparticle stabilization and crosslinking at water-in-oil emulsion interfaces to yield globular membranes capable of encapsulating oil-soluble or water-soluble compounds. The nanoparticle-crosslinked membranes displayed stability after removal from the interface, as well as elasticity and permeability, which are characteristics that could be advantageous in controlled diffusion and release applications. Additionally, an example that applied organic particles for colloidosome formation was developed by Thompson and co-workers, who utilized poly(glycerol monomethacrylate)-based polystyrene latex beads to stabilize oil-in-water emulsions.[115] Once assembled at the interface, the latex beads were crosslinked within the oil droplets with tolylene 2,4-diisocyanate-terminated poly(propylene glycol), which yielded permeable colloidosomes that were stable upon removal of the internal oil

phase. The colloidosomes were loaded with a fluorescein cargo and its release was measured over time to assess the permeability of the membranes. It was found that complete release was achieved within 24 hours; therefore, the permeability of the colloidosomes was tuned by coating them with a thin layer of polypyrrole that led to improved control over the cargo release. Moreover, in the field of emulsion polymerization, Colver *et al.* employed inorganic SiO_2 nanoparticles of *ca.* 25 nm in diameter to stabilize an emulsion composed of styrene or methyl methacrylate (MMA) in water.[93] Following the stabilization of the emulsion, potassium persulfate (KPS) was added to initiate the polymerization at 65 °C, and yield highly dispersed polystyrene (PS) or poly (methyl methacrylate) (PMMA) particles armored with a layer of SiO_2 nanoparticles on the surface of the polymeric beads.

In addition to allowing for the synthesis of unique materials, Pickering emulsions can also be used to stabilize droplets while incorporating responsiveness to an external stimulus, thereby providing a means to control the stability of the emulsion. For instance, Fujii and co-workers prepared pH-responsive emulsions, whereby shell crosslinked micelles composed of the triblock terpolymer poly(ethylene oxide)-*block*-poly(glycerol monomethacrylate)-*block*-poly(2-(diethylaminoethyl)ethyl methacrylate)) were synthesized and used to stabilize 1-undecanol-in-water emulsions at pH 8-9.[105] The droplets could be easily destabilized upon addition of 1 drop of a 1 M HCl solution, and readily re-stabilized after re-homogenization at pH 8-9; thus, providing control over the demulsification procedure. Additionally, magnetically-active emulsion droplets that are responsive to an external magnetic field have also been achieved.[10,42,43] Of particular

importance is the work of Melle and co-workers, whereby carbonyl iron particles were used to stabilize millimeter-sized droplets in decane-water emulsions.[10] Alteration of an external magnetic field allowed for the manipulation of the droplets, making it possible to transverse the water-oil interface. Complete phase separation was obtained by further increasing the magnetic field; providing a means to reversibly destabilize the emulsion, as the emulsified phase was easily reproduced upon hand shaking of the sample.

Despite the variety of materials available, and in some cases the variety of shapes of the particle stabilizers, the majority of the work performed on Pickering emulsions involves the stabilization of the droplets by single, dispersed particles. However, one of the few reports in the literature that used multi-particulate macrostructures is the work of Shen *et al.*[116] Single-walled carbon nanotube/silica (SWNT/silica) nanohybrids, whose unique structure was composed of silica particles of *ca.* 50 nm, fused to bundles of SWNTs of *ca.* 10 nm in diameter, were demonstrated to be capable of stabilizing water-in-oil emulsions, and after functionalization with palladium on the surface of either silica or the SWNT, their application was expanded from the stabilization of droplets to the catalysis of biofuel upgrade reactions at the oil/water interface.[117]

In this contribution, we expand on the progress made involving the stabilization of emulsions by nanohybrids of complex morphologies and the inclusion of responsivity, by reporting the use of magnetically-active hybrid inorganic/organic networks (MHNs) for the stabilization of emulsion droplets at the oil/water interface. The MHNs were obtained by covalently linking a mixture of polymeric shell crosslinked knedel-like (SCK) nanoparticles, composed of poly(acrylic acid)$_{90}$-*block*-polystyrene$_{140}$ (PAA$_{90}$-*b*-

PS_{140}) block copolymers, and amine-functionalized IONs (amine-IONs). To the best of our knowledge, this is the first report in which a network of covalently bound organic and inorganic particles is able to stabilize oil-water emulsions. It is demonstrated that emulsions can be formed *via* different methods of emulsification, with different types of oil, and a minimal concentration of particle stabilizers. The assembly of the MHNs at the oil/water interface has been analyzed, and as is commonly observed in the synthesis of materials *via* the Pickering polymerization technique, it leads to the formation of surface-decorated materials. Additionally, the incorporated amine-IONs within the network structure provide magnetic responsivity to the stabilized droplets, possibly making them suitable for various applications, in particular, the extraction of hydrocarbons and the water purification activities performed daily in the oil and gas field.

4.2 Materials and Methods

Materials. All chemicals were purchased from Aldrich Chemical Co. or VWR and used without further purification unless otherwise noted. Amine-IONs were purchased from Chemicell GmbH. Dextran-functionalized FITC (dex-FITC, 3000 – 5000 Da) and Nile red were purchased from Sigma Aldrich. Nanopure water (18 MΩ•cm) was acquired by means of a Milli-Q water filtration system, Millipore Corp. (Bedford, MA). A neodymium magnet (90 lbs. pull) was purchased from magnets4less.com.

Characterization Techniques. The emulsions were homogenized *via* vortexing with a G-560 Vortex Genie 2 (120 V, 0.65 A, 60 Hz, speed 6-7, Scientific Industries, Bohemia, NY) for 1 min, or probe sonication with a 150VT ultrasonic homogenizer (Biologics, Inc.,150 W, 20 kHz, 3.9 mm probe) at 30% power, 50% pulse, for 1 min. Optical microscopy was performed through a 4x or 10x objective on an Olympus IX-70 inverted microscope, equipped with a mercury arc lamp and an Olympus DP72 digital camera (Olympus, Center Valley, PA). A representative sample from the emulsified phase was transferred with a Pasteur pipette and placed on a glass-bottom, 6 well plate and further diluted with a couple of drops of nanopure water. Images were collected from various areas of the sample and the diameter of the droplets observed was measured with a CellSense software and reported in the form of a histogram analyzed with Origin 8.0 Pro (Origin Lab, Northampton, MA). The stability of the emulsions was assessed by measuring the emulsified fraction as well as the organic solvent and water fractions, when applicable. The samples were maintained at 4°C to prevent evaporation of the organic solvents, and monitored until the fractions were too small to measure accurately.

The type of emulsion stabilized was determined *via* confocal microscopy carried out on a FV1000 confocal microscope with an IX-81 inverted base (Olympus, Center Valley, PA) and PMT detectors. Nile red was dissolved in toluene or dodecane at a concentration of 10 μg/mL, while dex-FITC was utilized as a water-soluble dye at a concentration of 30 μg/mL. The samples were analyzed at an excitation wavelength = 488 nm, and emission was detected between 580 nm and 650 nm for Nile red and

between 495 nm and 545 nm for dex-FITC. The emulsions were prepared at various water-to-oil (W : O) ratios and an MHN concentration of 1 mg/mL. The MHNs were resuspended in the dex-FITC solution and further utilized in the preparation of emulsions as previously described.

Transmission electron microscopy (TEM) analysis was performed on a JEOL 1200 EX operating at 100 kV and micrographs were recorded at calibrated magnifications using a SLA-15C CCD camera. Samples for TEM were prepared as follows: 5 μL of a solution were deposited onto a formvar-coated copper grid, and after 30 s, the excess of the solution was quickly wicked away by a piece of filter paper. The samples were negatively stained with 1% phosphotungstic acid (PTA) aqueous solution. After 30 s, the excess staining solution was quickly wicked away by a piece of filter paper and the samples were left to dry overnight. Scanning Electron Microscopy (SEM) analysis was performed on a JEOL JSM-7500F operating at an acceleration voltage of 2 kV or 5 kV, and a working distance (WD) of 14.7 mm. Prior to analysis, the samples were coated with 5 nm of Platinum/Palladium (80%/20%).

Interfacial tension (ITF) measurements were performed with an Attension Theta optical tensiometer (Biolin Scientific, Stockholm, Sweden), and analysis was performed by fitting drops with a Young-Laplace formula using the Theta Software. First, the ITF between water and toluene or dodecane was measured as a control. Water was utilized as the drop phase and it was immersed in *ca*. 5 mL of toluene or dodecane, while five high speed images of the water drop were obtained in a period of 20 s. The ITF was calculated for each image and the process was repeated at least three times with three

different water droplets. The same procedure was followed to determine the effect of the MHNs on the ITF between water and the organic solvents, at a concentration of 0.5 mg/mL.

Synthesis of MHNs. The synthesis of the MHNs was performed according to a published procedure.[62] Briefly, a 250 mL vial was charged with a stir bar and an aqueous solution of SCKs (12 equiv., 70 mL, 0.27 mg/mL, 20 mg, 62 μmol of available acrylic acid units). A solution of amine-IONs in nanopure water (1 equiv., 22.6 mL, 0.15 mg/mL, 3.4 mg, 5.2 μmol of ligand) was added dropwise to the reaction mixture and it was allowed to stir for *ca*. 5 min, after which a solution of 1-[3'-(dimethylamino)propyl]-3-ethylcarbodiimide methiodide (EDCI, 8.8 equiv., 7.5 mL, 1.8 mg/mL, 13.5 mg, 45.4 μmol) was added *via* a syringe pump at a rate of 0.25 mL/min. The reaction was allowed to stir for 24 hours, followed by centrifugation at 10000 rpm for 5 min. The brown precipitate was resuspended in 15 mL of nanopure water with the aid of sonication and vortexing, and this process was repeated twice. The supernatant was collected and centrifuged 2 more times with the aim of removing as much precipitate as possible. After centrifugation, the supernatant was collected, placed in presoaked membrane dialysis tubing (MWCO 12 – 14 kDa) and dialyzed against nanopure water for three days. Following dialysis, the suspension of MHNs and the supernatant were combined and lyophilized to afford 16 mg of a light brown powder in 69% yield.

Preparation of Fluorescein-labelled Micelles. A 100 mL round bottom flask was charged with a stir bar, and PAA_{90}-*b*-PS_{140} (1 equiv, 60 mg, 3.3 μmol) was dissolved in 60 mL of THF and allowed to stir for *ca.* 15 min. Nanopure water (60 mL) was added with the aid of a syringe pump at a rate of 20 mL/h, the resulting solution was placed in presoaked dialysis membrane tubing (MWCO 12 – 14 kDa) and dialyzed against nanopure water for 2 days. Following characterization, the micelles were fluorescently labelled by adding fluorescein-5-thiosemicarbazide (0.05 equiv, 6.2 mg, 14.6 μmol, dissolved in 1 mL of *N*, *N*-Dimethylformamide) to the aqueous solution, followed by stirring for 2 h. A stock solution of 1-[3'-(dimethylamino)propyl]-3-ethylcarbodiimide methiodide (EDCI, 0.05 equiv, 4.8 mg, 16.1 μmol) was prepared in 100 μL of nanopure water and added dropwise to the vessel. The reaction mixture was allowed to stir overnight, and placed in presoaked membrane dialysis tubing (MWCO 12 – 14 kDa) for 3 days. The resulting micelles were crosslinked as previously described,[62] purified and further employed in the synthesis of MHNs to yield FITC-functionalized MHNs. IR: ν = 3490 – 2460, 3095 – 2985, 2980 – 2790, 1655, 1625 - 1525, 1510, 1490, 1470 – 1420, 1415, 1370, 1350, 1310, 1300 – 1260, 1260 – 1230, 1215, 1190, 1160, 1140, 1120, 1045 – 975, 950, 910, 880, 845, 820, 800, 785, 765, 760 – 740, 730, 700, 650, 625 cm^{-1}. $Dh_{(N)}$ (DLS) = 50 ± 10 nm.

Preparation of Emulsions. Toluene-water emulsions were prepared by resuspending the MHNs in nanopure water at the desired concentration and alternating between vortex and sonication as agitation methods to obtain fully suspended particles.

The W : O ratio was varied while maintaining a total emulsion volume of 2.5 mL. The biphasic systems were emulsified *via* vortex for 1 min, or by utilizing a probe sonicator at 30% power, and 50% pulse for 1 min. Dodecane-water emulsions were prepared by following the same preparation method but utilizing probe sonication as the method of emulsification.

Synthesis of Polystyrene Beads. A stock solution of azobisisobutyronitrile (AIBN) in styrene was prepared by dissolution of 1.2 mg of AIBN in 300 µL of styrene. The Styrene-water emulsions were prepared at a W : O = 10 : 1, by utilizing 1 mL of either an MHN or amine-ION aqueous suspension (0.5 mg/mL in nanopure water) and 100 µL of the styrene stock solution. Homogenization was achieved *via* vortexing, and then the reaction mixture was immersed in an oil bath at 80 °C and was allowed to react for 24 hours. The brown solid layer formed after polymerization was washed with nanopure water, dried and resuspended in tetrahydrofuran (THF). Samples were drop-cast onto TEM grids and placed on carbon tape for further SEM analysis.

4.3 Results and Discussion

Preparation of Oil-water Emulsions. Magnetically-active hybrid networks (MHNs) are inorganic/organic composite materials that are composed of polymeric SCK nanoparticles covalently bound to amine-IONs, which have remarkable abilities to interact with both hydrophobic and hydrophilic species.[62] The SCKs were synthesized from poly (acrylic acid)$_{90}$-*block*-polystyrene$_{140}$ block copolymers upon self-assembly in

water and crosslinking reactions to afford nanostructures composed of polystyrene hydrophobic cores and crosslinked poly (acrylic acid) hydrophilic shells (Scheme 4.1). These MHNs were originally synthesized for the remediation of aqueous environments contaminated with crude oil sheen, which would be facilitated by the hydrophobic-hydrophobic interaction that could take place between the crude oil molecules and the cores of the SCKs. However, our investigation into the mechanism of interaction between the MHNs and the crude oil suggested that these hybrid networks could stabilize oil-water emulsions, as they were capable of reducing the interfacial tension between toluene and water, as well as decane and water. These discoveries led us to hypothesize that the mechanism of interaction between the crude oil and the MHNs was not limited to sequestration of the hydrophobic pollutant into the core of the SCKs, but included the stabilization of oil-water emulsions *via* Pickering emulsification (Scheme 4.1).

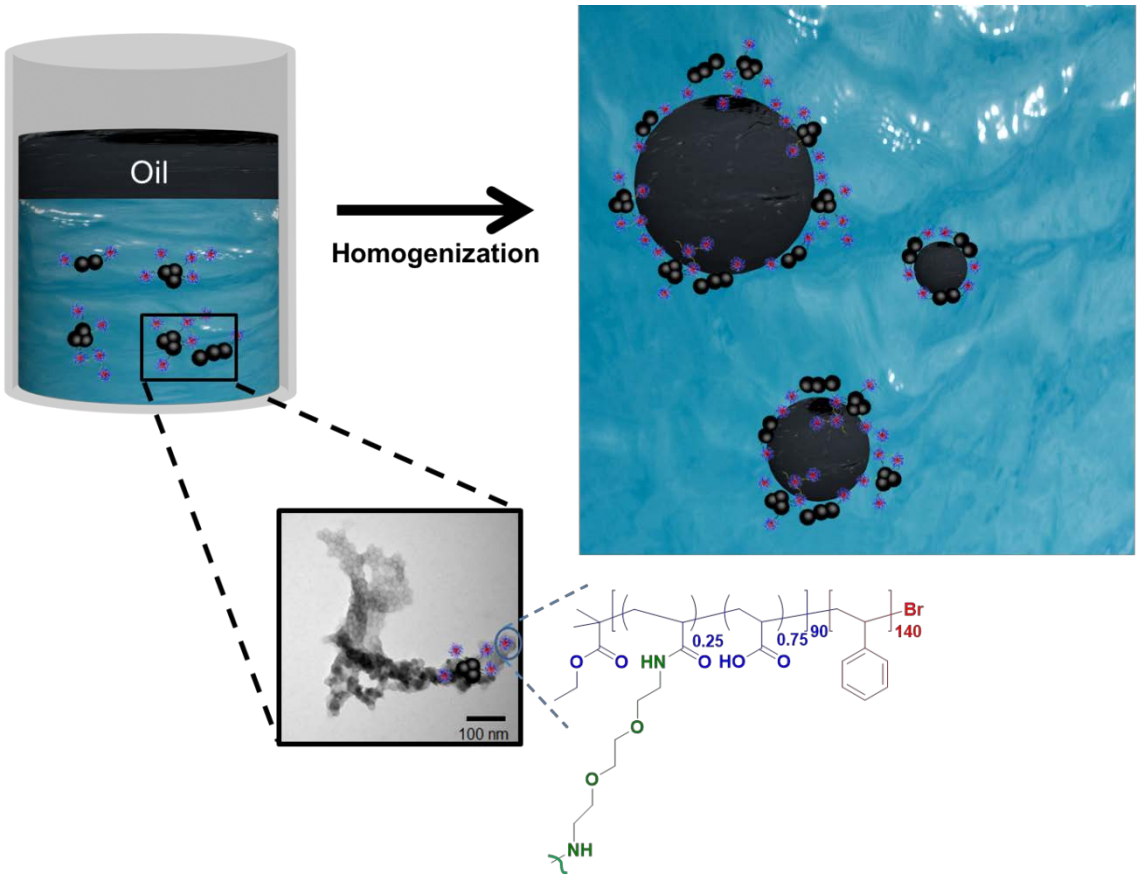

Scheme 4.1. Schematic representation of the MHNs suspended in the water phase with the inset depicting their TEM characterization (left), and their assembly at the interface between oil and water to stabilize oil-in-water emulsions (right).

In order to test this hypothesis and based on our preliminary results, two different types of organic solvents, toluene and dodecane, were selected to prepare oil-water emulsions. Dodecane has been employed in multiple literature procedures to simulate crude oil,[118-122] therefore, it was selected as a mimic for the aliphatic components of crude oil. Additionally, toluene was selected to mimic the aromatic components of

crude oil, given its lower health repercussions compared to other commonly-used solvents, such as benzene. Although the amphiphilic character of the MHNs allowed for their resuspension in nanopure water, toluene and dodecane; the suspensions of the MHNs in these organic solvents displayed inferior stability than the suspension in nanopure water (Figure 4.1). Consequently, the emulsions were prepared at the desired concentration of MHNs, by resuspending lyophilized networks in nanopure water, yielding a light-brown solution that created a significant contrast with the colorless organic solvents (Figure 4.1). Initially, the emulsions were prepared at different W : O volume ratios, while maintaining a total volume of 2.5 mL and a [MHN] = 0.5 mg/mL (with respect to the nanopure water used as solvent). Additionally, two methods of emulsification were studied—vortexing and the commonly-used and mechanically-demanding homogenization through probe sonication.[42,107,123-126] The former was selected because it provided a more consistent approach to the preparation of emulsions than the commonly used "hand shake method",[111,127-130] while requiring less mechanical power than homogenization through probe sonication.

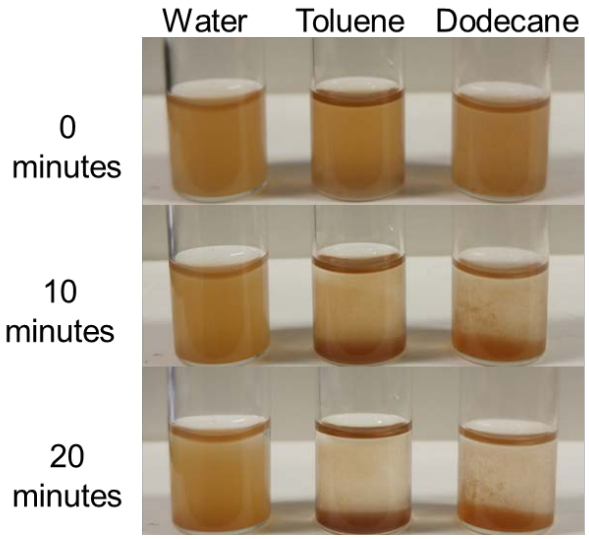

Figure 4.1. Pictographic representation of a suspension of MHNs in water (left), toluene (center) and dodecane (right) immediately after resuspension, and the stability of the resuspension over a period of 20 minutes.

Initial studies showed that toluene-water emulsions could be formed *via* both vortexing and probe sonication, and after emulsification, it was evident that the MHNs played a role in stabilizing the emulsions (Figure 4.2). The formation of large, light-brown droplets at the interface was observed with the naked eye, and the water fraction that was previously light-brown due to the presence of the MHNs, turned colorless. In contrast to the vortex method, probe sonication resulted in emulsions that were initially cloudy through the water fraction, which could indicate the formation of a secondary emulsion. However, after *ca*. 24 hours, the cloudiness dissipated and the water fraction turned colorless as observed in the vortex case.

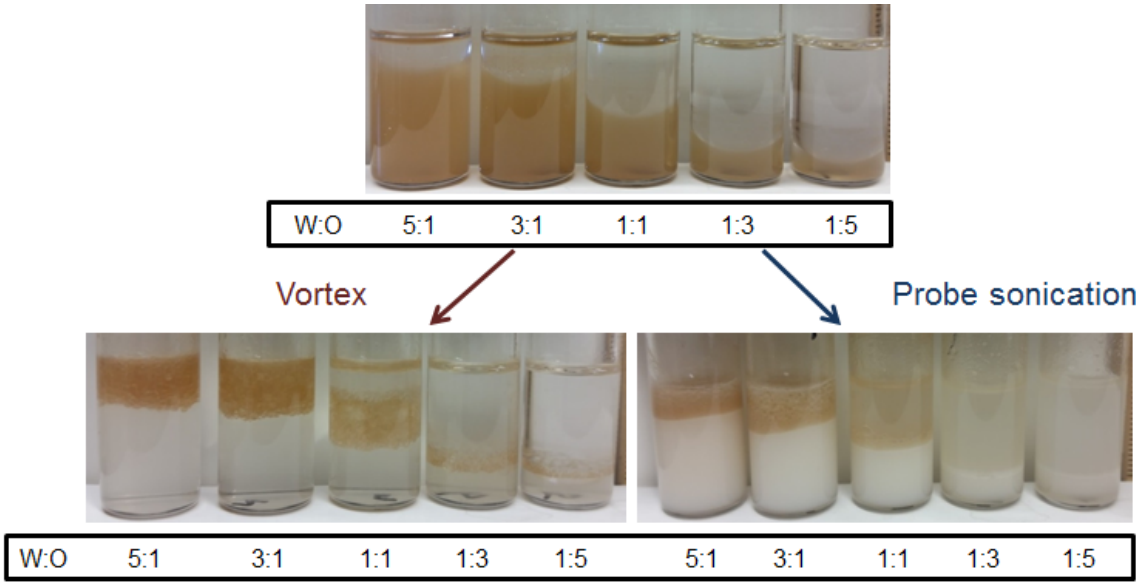

Figure 4.2. Toluene-water emulsions prepared at different W : O ratios before (top) and after (bottom) emulsification *via* two different methods: Vortex (left) and probe sonication (right).

The formation of dodecane-water emulsions was different to the emulsification of toluene and water, as the dodecane-water emulsions formed *via* vortexing were unstable, and coalesced into the two original oil and water phases after a few seconds (Figure 4.3). These results were surprising initially, however; interfacial tension (γ) measurements (Table 4.1) revealed that the MHNs (concentration = 0.5 mg/mL) caused no significant reduction of the γ between dodecane and water, while the γ between toluene and water was reduced by *ca.* 32%. These results could explain why toluene-water emulsions can be formed by the two methods, but dodecane-water emulsions required the higher energy probe sonication method to be formed.

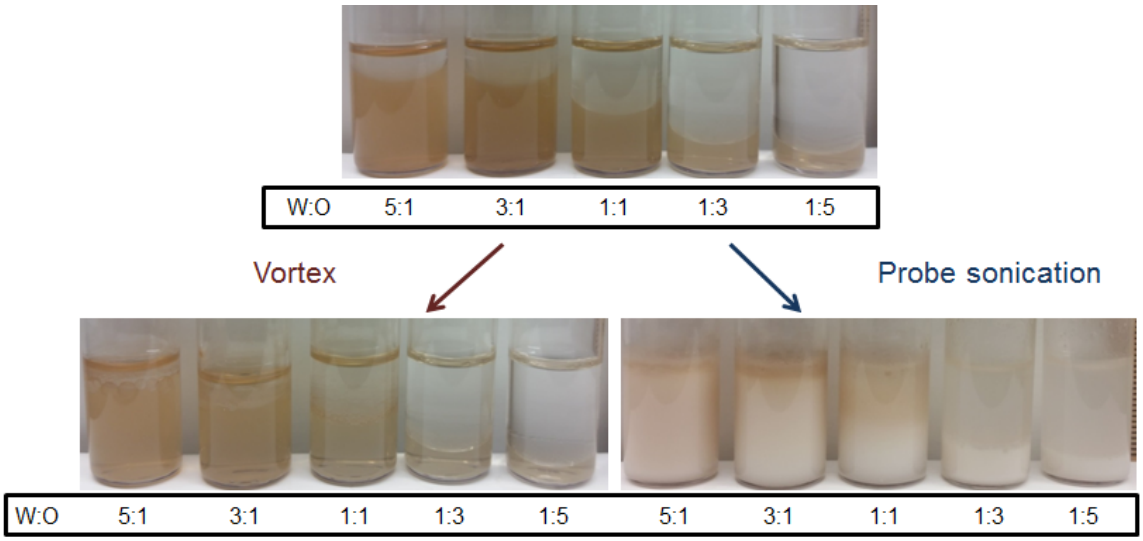

Figure 4.3. Dodecane-water emulsions prepared at different W : O ratios before (top) and after (bottom) emulsification *via* two different methods: Vortex (left) and probe sonication (right).

Table 4.1. Interfacial tension (γ) values between toluene or dodecane and water, and toluene or dodecane and an MHN solution [0.5 mg/mL].

Interfacial Tension (γ)		
	Media	
Drop Solvent	Toluene (mN/m)	Dodecane mN/m)
Water	31 ± 5	44 ± 5
MHNs	21 ± 2	42 ± 3
% Difference	31	0

Stability of Emulsions. The stability of the emulsions was studied following the preparation of samples utilizing both toluene and dodecane as the oil phases, as well as vortex and probe sonication as the methods for emulsification. For this study (Figure 4.4), the W : O volume ratio was gradually varied, and an analysis was performed on samples containing higher ratios of water (W : O = 5 : 1, 3 : 1), equal ratios of water-to-oil (W : O = 1 : 1), and lower ratios of water-to-oil (W : O = 1 : 3, 1 : 5). Originally, the emulsions (toluene-water prepared *via* vortex or probe sonication, and dodecane-water prepared *via* probe sonication only) were formed at equal and higher ratios of water to oil; however it was noticed that the toluene-water emulsions were only stable for a couple of weeks if the samples were stored under ambient conditions. This effect was attributed to the evaporation of toluene, since precipitation of the MHNs was observed after a couple of weeks, along with the disappearance of the toluene phase. Therefore, in order to prevent the evaporation of the oil phase, the samples were emulsified, stored at 4°C and analyzed for their formation and stability over a period of time.

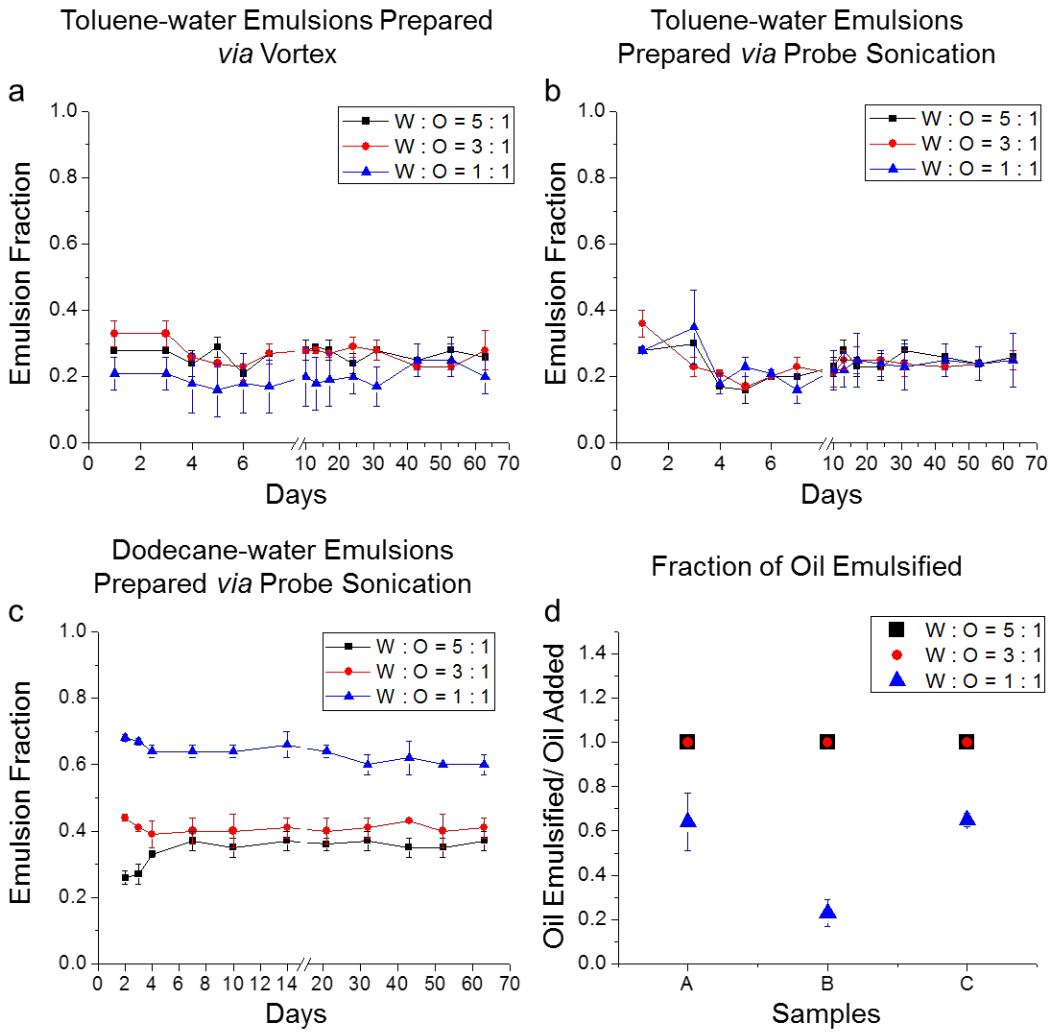

Figure 4.4. Stability of toluene-water emulsions prepared *via* vortex (a) and probe sonication (b), and dodecane-water emulsions prepared *via* probe sonication (c) at different W : O ratios. Fraction of the oil emulsified at different W : O ratios (d), for toluene-water emulsions prepared *via* vortex (A) and probe sonication (B), and dodecane-water emulsions prepared *via* probe sonication (C).

As mentioned before, formation of stable emulsions was observed at equal and higher ratios of water-to-oil (W : O = 1 : 1, 3 : 1 and 5 : 1), regardless of the type of oil

or the method of emulsification employed. However, although no appreciable emulsion formation was observed at the lower ratios of water-to-oil (W : O = 1 : 3 and 1 : 5); it is worth noting that possible emulsion formation could take place upon addition of oil volume fractions ranging from 50 vol.% to 75 vol.%. Initially, the stability of the emulsions was assessed by monitoring the oil released due to droplet coalescence immediately after emulsion formation (Figure 4.4d). The length of the oil emulsified was compared to the initial length of the volume of oil added to the samples, and the emulsified oil fraction was determined. For all samples prepared at W : O = 5 : 1 and 3 : 1, 100% of the oil added was incorporated into the emulsion. Furthermore, for the toluene-water samples prepared *via* vortex, *ca.* 60% of the oil added was emulsified; while for the same emulsions prepared *via* probe sonication *ca*. 20% of the oil was emulsified. It is important to highlight that the difference observed between these two samples can be due to the less clear oil/emulsion boundary observed immediately after probe sonication (Figure 4.2), which typically becomes more evident after the cloudiness dissipates *ca.* 24 h after homogenization. Moreover, a similar phenomenon was observed for the dodecane-water emulsions, where *ca.* 60% of the oil added was incorporated into the emulsion, but the same blurry oil/emulsion boundary was observed (Figure 4.3).

In addition to monitoring the fraction of the oil emulsified immediately after emulsion formation, the stability of the emulsions was also determined by monitoring the length of the emulsion fraction over a period of time. All samples were monitored for approximately 60 days, during which no significant reduction of the emulsified

fractions was observed (Figures 4.4a-c). All in all, these data confirmed that the MHNs are capable of stabilizing oil-water emulsions which display stability for prolonged periods of time.

Characterization of Emulsions *via* Optical Microscopy. A preliminary assessment of the emulsified samples under the initial homogenization conditions ([MHN] = 0.5 mg/mL, W : O = 3 : 1) revealed the formation of droplets of varying sizes, including large droplets that could even be observed with the naked eye. Therefore, in order to avoid the bias for large particles commonly associated with dynamic light scattering measurements of polydispersed samples,[131,132] and following previously established procedures,[90,94,133,134] the emulsions were characterized by optical microscopy. Analysis of the dilute samples showed that highly dispersed emulsions were obtained regardless of the organic solvent or method of preparation used (Figure 4.5). In fact, the difference between the droplets was so large that determining an average droplet size did not provide meaningful information. Consequently, the distribution of the droplet size for all samples was determined, and revealed highly dispersed emulsion samples, with droplets ranging from just a few micrometers to hundreds of micrometers in diameter. These results led us to focus our efforts on investigating certain parameters that could have an effect on the droplet size distribution, such as the MHN concentration and W : O ratio; with the general understanding that smaller droplets lead to the formation of more stable emulsions.[135]

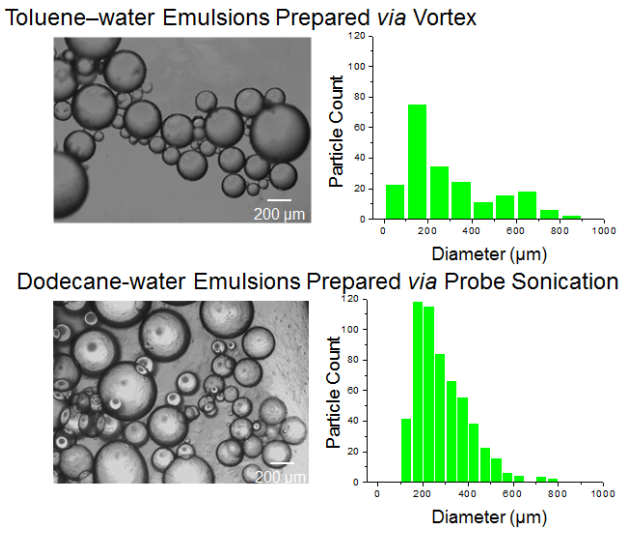

Figure 4.5. Optical microscopy images and droplet size distribution of toluene-water emulsions prepared *via* vortex, and dodecane-water emulsions prepared *via* probe sonication.

Evaluation of the Effect of the Water-to-Oil (W : O) Ratio. One of the parameters that can have a significant effect on the stability of emulsions is the water-to-oil (W : O) ratio. Several reports have indicated that the W : O ratio could determine the type of emulsion stabilized, and could even induce inversion of the emulsified phase.[94,128,133,136] In order to study the effect of the W : O ratio on the droplet size distribution of the emulsions, the MHN concentration and total emulsion volume were held constant (0.5 mg/mL and 2.5 mL, respectively), while the W : O ratio was varied. In the case of the dodecane-water emulsions (Figure 4.6a), a shift towards a smaller and narrower droplet size distribution was observed as the W : O ratio was changed from 1 :

1 to 3 : 1; however, further increasing the water ratio (W : O = 5 : 1) produced emulsions with droplets of larger diameters than the 3 : 1 emulsions.

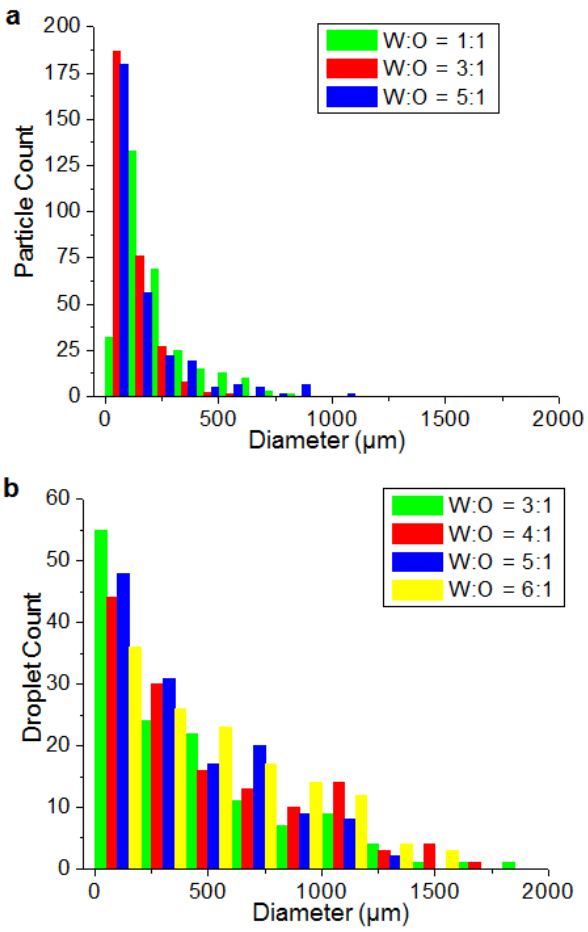

Figure 4.6. Histograms of the droplet size distribution of dodecane-water emulsions prepared *via* probe sonication (a), and toluene-water emulsions prepared *via* vortex (b) at different W : O ratios.

On the other hand, the toluene-water emulsions were less sensitive to the W : O ratio than were the dodecane-water emulsions. Even though formation of the emulsions was observed at a W : O = 1 : 1 for samples prepared *via* vortex and probe sonication (Figure 4.7), the size of the droplets at this W : O ratio made the characterization of these samples *via* optical microscopy difficult.

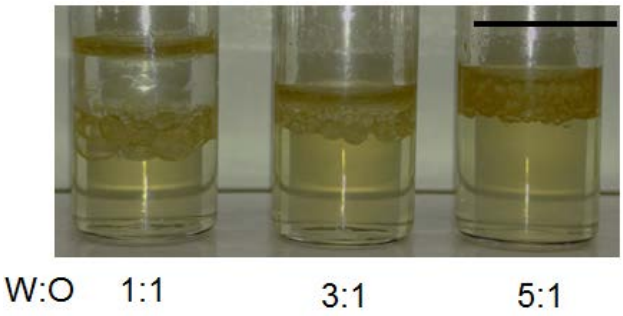

Figure 4.7. Pictographic representation of toluene-water emulsions prepared *via* vortex at three different W : O ratios. Scale bar = 1 inch.

The droplets formed were visibly large and had diameters on the order of millimeters, making them too large and unstable to image under the microscope. Therefore, only the samples prepared at W : O = 3 : 1, 4 : 1, 5 : 1 and 6 : 1 were analyzed (Figures 4.6b and 4.8). Visually, there was a significant difference between the droplet size of the emulsions prepared at W : O = 1 : 1 and 3 : 1, with droplets of smaller

diameter observed for the emulsion with the higher water fraction. However, further increasing the W : O ratio had no significant effect on the droplet size distribution of samples prepared either *via* vortex or probe sonication. All together, these data indicate that a W : O = 3 : 1 might provide ideal conditions for the formation of stable dodecane-water and toluene-water emulsions, regardless of the method of emulsification.

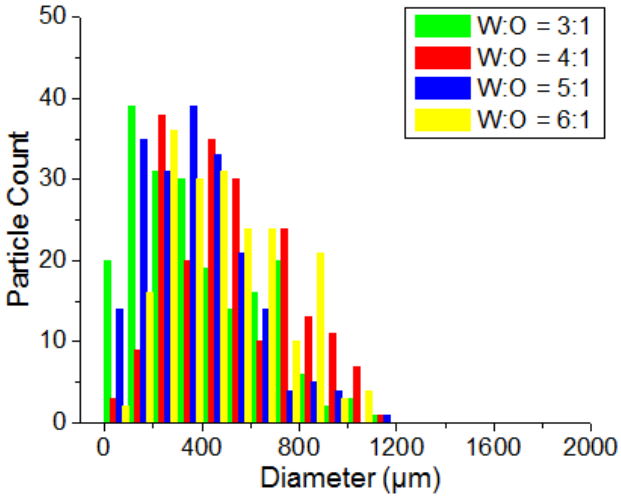

Figure 4.8. Histogram of the droplet size distribution of toluene-water emulsions prepared *via* probe sonication at various W : O ratios.

Evaluation of the Effect of the MHN Concentration. Another significant parameter in the stabilization of emulsions is the concentration of the solid particles

acting as stabilizers. In order to focus our studies, and based on the knowledge learned regarding the effect of the W : O ratio on the size of the droplets, a W : O ratio of 3 : 1 was selected to perform these experiments while the concentration of the MHNs suspended in nanopure water was varied until no significant changes were observed for the systems studied. In the case of the dodecane-water emulsions, a broad distribution was obtained at a concentration = 0.5 mg/mL (Figure 4.9a), and a significant shift towards smaller, less dispersed droplets was observed by increasing the concentration to 1 mg/mL, and even more so at 1.5 mg/mL. However, further increasing the concentration to 2 mg/mL shifted the distribution towards larger droplets, indicating a possible saturation of the system. A more in-depth analysis was performed to determine the percentage of the droplets that fell within three size ranges: a small range from 0 to 200 µm, a medium range from 200 µm to 600 µm, and a large range from 600 µm to 1200 µm (Table 4.2). The results indicated that at a concentration of 0.5 mg/mL *ca.* 28% of the droplets lay in the small range, with a significant increase to *ca.* 95% observed in this size range at 1 mg/mL. Once the concentration was increased to 1.5 mg/mL, 100% of the droplets were found in the smaller range; however, increasing the concentration to 2 mg/mL lowered the percentage of droplets present in this range to *ca.* 96%. Although these percentages of particles within the 0-200 µm range are similar, the histograms reveal differences in the particle sizes and size distributions.

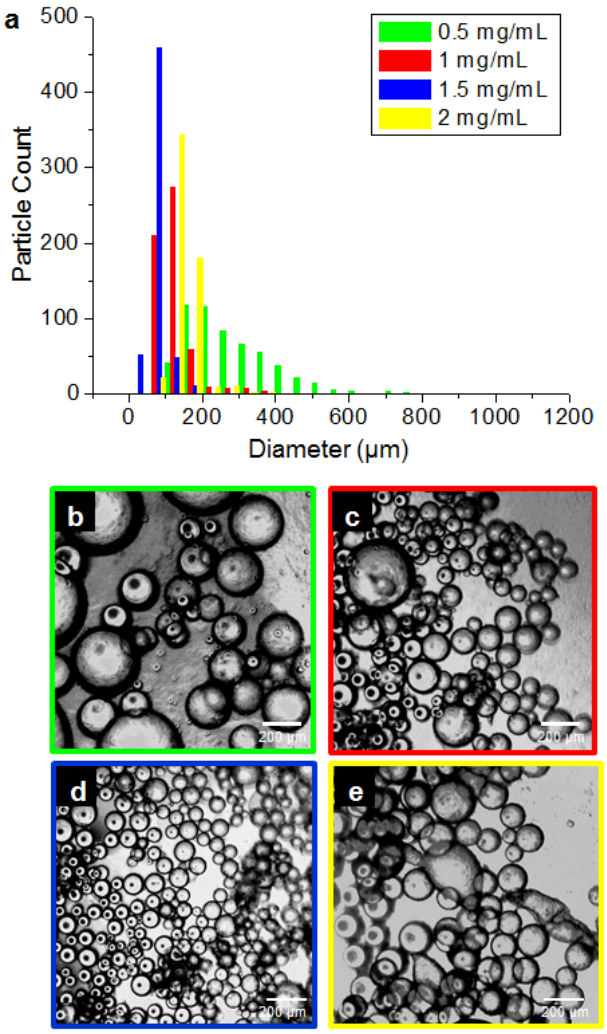

Figure 4.9. Histograms of the droplet size distribution (a) and optical microscopy images (b - e) of dodecane-water emulsions prepared at a W : O = 3 : 1, and varying concentrations of MHNs (optical microscopy images are color coded on the borders following the legend on Figure 4.9a).

A similar phenomenon was observed for the toluene-water emulsions prepared *via* probe sonication, but the effect was less prominent (Figure 4.10b). Increasing the

concentration from 0.5 to 1 to 1.5 mg/mL shifted the distribution towards smaller droplets, and further increasing the concentration to 2 mg/mL reverted the trend, yielding emulsions of larger droplets than those formed at 1.5 mg/mL. Moreover, the quantitation of the droplet distribution showed that at a concentration of 0.5 mg/mL *ca.* 33% of the droplets lay in the small range, with an observed increase to *ca.* 38% at 1 mg/mL, and *ca.* 45% at 1.5 mg/mL; while only *ca.* 24% of the droplets lay within this range at a concentration of 2 mg/mL.

Table 4.2. Distribution of the droplet size of emulsions stabilized at different MHNs concentrations and methods of emulsification.

			Concentration of MHNs (mg/mL)			
Organic Solvent	Method	Size Range (μm)	0.5	1	1.5	2
Toluene	Vortex	0 – 200	47%	69%	40%	28%
		200 – 600	40%	22%	59%	69%
		600 – 1200	13%	9%	1%	3 %
	Probe Sonication	0 – 200	33%	38%	45%	24%
		200 – 600	57%	59%	55%	73%
		600 – 1200	10%	3%	0%	3%
Dodecane	Probe Sonication	0 – 200	28%	95%	100%	96%
		200 – 600	70%	5%	0%	4%
		600 – 1200	2%	0.0%	0%	0.0%

These results were slightly different to those observed for toluene-water emulsions prepared *via* vortex. A shift in the distribution towards a lower size range was observed after increasing the concentration from 0.5 mg/mL to 1 mg/mL, while further increasing the concentration to 1.5 mg/mL and 2 mg/mL yielded distributions similar to those obtained at 0.5 mg/mL (Figure 4.10a). Additionally, at a concentration of 0.5 mg/mL *ca.* 47% of the droplets lay in the small size range discussed previously; while at a concentration of 1 mg/mL *ca.* 69% of the droplets lay in this range. Additionally, a

reduction of the percentage of droplets present in the small range was observed as the concentration of MHNs was further increased, while the percentage of the droplets present in the middle range increased.

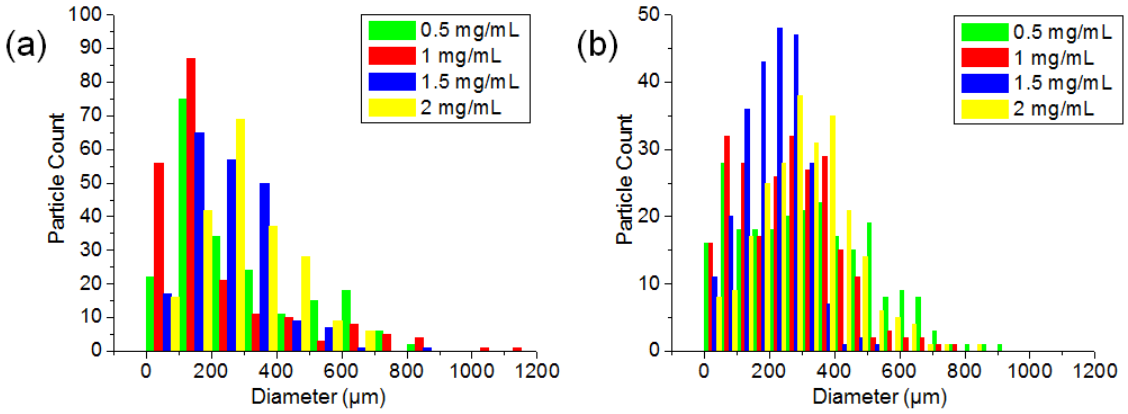

Figure 4.10. Histograms of the droplet size distribution of toluene-water emulsions prepared *via* vortex (a) and probe sonication (b), at a W : O = 3 : 1 and varying concentrations of MHNs.

In order to understand the discrepancy of these results, a detailed TEM study of the MHNs before and after probe sonication was performed. This study was done with the aim of analyzing the effect of probe sonication on the morphology of the MHNs. As described before, the MHN system was originally designed for the sequestration of hydrophobic pollutants from aqueous environments, and exhibited a network-like

morphology composed of multiple SCKs bound to amine-IONs.[62] The configuration and arrangement of the two components of the networks cannot be controlled; therefore the synthesis of the MHNs yields structures of different sizes, compositions and topologies. The TEM micrographs of the MHNs before probe sonication exhibited similar structures (Figure 4.11 a-d), where most of the SCKs appeared to be linked to clusters of SCKs and amine-IONs or to other SCKs, with few singular SCK nanoparticles observed in the samples. In addition, the TEM analysis after probe sonication also revealed network-like structures of various sizes and compositions, which are characteristic of the MHNs (Figure 4.11 e-h). However, we also observed smaller MHN clusters that appeared to be composed of fewer SCKs and amine-IONs than those observed prior to probe sonication. Moreover, fiber-like structures and singular SCKs surrounded by what appeared to be polymeric residue (Figures 4.11g and 4.11h) were also observed. It is hypothesized that these structures correspond to loose strands of block copolymer resulting from the break-down of some of the SCK nanoparticles; however, it is difficult to determine with certainty whether the strands are in fact block copolymers, or artifacts commonly present in stained TEM grids.[35] Nevertheless, the micrographs also showed the presence of well-defined network structures, indicating that the MHN morphology is retained, even if some fragmentation of the structures occurred.

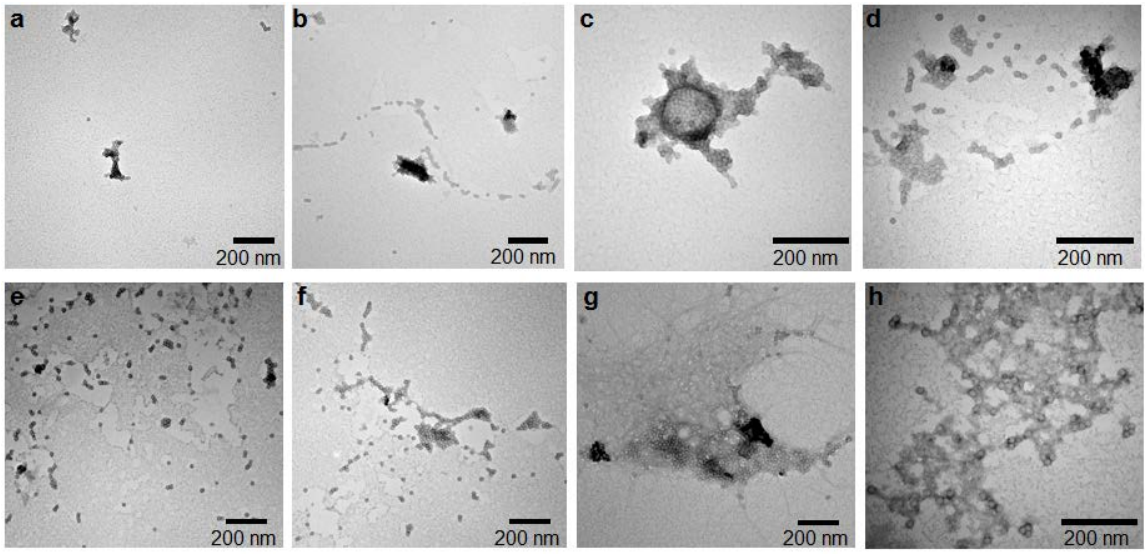

Figure 4.11. Transmission electron micrographs of a suspension of MHNs (0.5 mg/mL) before (a - d) and after (e - h) probe sonication.

To corroborate the previously stated hypothesis that the MHNs underwent fragmentation under probe sonication, recovery of the MHNs *via* magnetic action before and after probe sonication was performed. The results indicated (Figure 4.12) that only *ca.* 51% of the MHNs could be recovered from the water *via* magnetic action after probe sonication, compared to the *ca.* 84% recovery of a control sample of MHNs that was not subjected to probe sonication. This difference corresponded to *ca.* 33% decrease in the recovery efficiency of the MHNs, and indicated that the method of probe sonication led to the disconnection of some of the MHN network structure into either individual SCKs or polymer fibers, which were no longer covalently bound to the amine-IONs and, thus, remained in the water upon separation *via* magnetic action. The effects of probe

sonication on the morphologies of the MHNs and SCKs are not surprising, since scission of covalent bonds in polymer fibers,[137] and molecular bottlebrushes[138] has been widely reported in the field of mechanochemistry. Additionally, the fractionation of non-crosslinked and crosslinked polymer micelles as a consequence of sonication has also been previously observed by our group, as well as others.[139-143]

In general, these observations could explain why a slightly higher MHN concentration is required to produce less dispersed emulsions *via* probe sonication than *via* vortex. The dissociation of the SCK nanoparticles into polymer strands would reduce the concentration of particles present in the solution, and thereby reduce the concentration of particle stabilizers capable of yielding stable emulsions. As a consequence, larger concentrations of MHNs would be required to achieve the same results by probe sonication as were observed when emulsions were prepared *via* vortex.

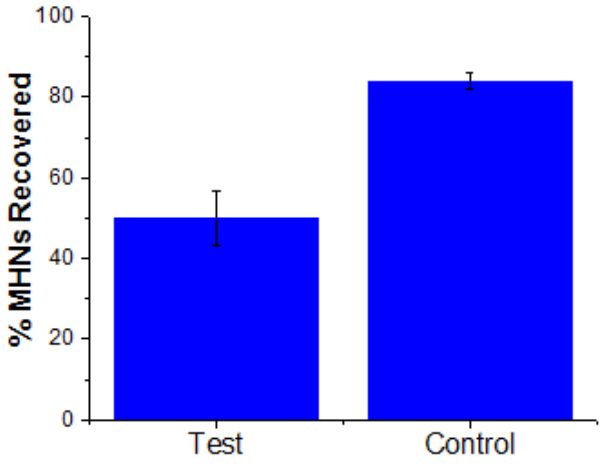

Figure 4.12. Recovery of MHNs after probe sonication *via* magnetic action, where the test sample was subjected to probe sonication, whereas the control sample was not.

Determination of the Type of Emulsions Stabilized by the MHNs *via* Confocal Microscopy. In order to determine whether oil-in-water (o/w) or water-in-oil (w/o) emulsions were stabilized by the MHNs, a series of control studies was performed *via* confocal microscopy. The organic dye Nile red was dissolved in either toluene or dodecane in order to identify the oil phase in the emulsion sample, while the water-soluble dye dex-FITC was incorporated to identify the water phase. In the case of the toluene-water emulsions prepared *via* vortex, three different emulsion samples were prepared at a [MHN] = 1 mg/mL and a W : O = 3 : 1, and analyzed (Figure 4.13). The first sample was prepared by utilizing an aqueous dex-FITC solution as the water fraction without dye being present in the toluene fraction. The confocal micrographs obtained showed green fluorescence in the background, indicating a continuous phase

composed of water. The second sample was prepared by utilizing a solution of Nile red in toluene as the oil fraction, with no fluorescent dye present in the water fraction. In this case, red fluorescence was identified within the emulsion droplets, while no fluorescence was observed in the background, indicating that the droplets were composed of toluene. Lastly, an emulsion sample containing both dex-FITC in the water phase, and Nile red in the oil phase was analyzed. As expected, the micrographs showed red droplets surrounded by a green background, corroborating the findings that toluene-in-water (o/w) emulsions were stabilized by the MHNs. Moreover, this same experiment was performed at the same MHN concentration and different W : O ratios (5 : 1 and 1 : 1, Figure 4.14), and no differences were observed, indicating the formation of o/w emulsions even at varying W : O ratios. The same results were observed for toluene-water emulsions and dodecane-water emulsions prepared *via* probe sonication, at the same concentration and different W : O ratios.

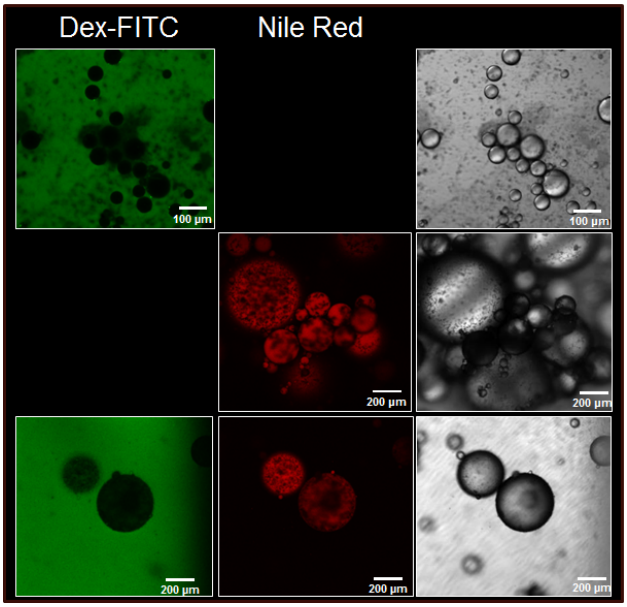

Figure 4.13. Confocal laser micrographs depicting the type of toluene-water emulsions formed *via* vortexing at a [MHN] = 1 mg/mL and a W : O = 3 : 1.

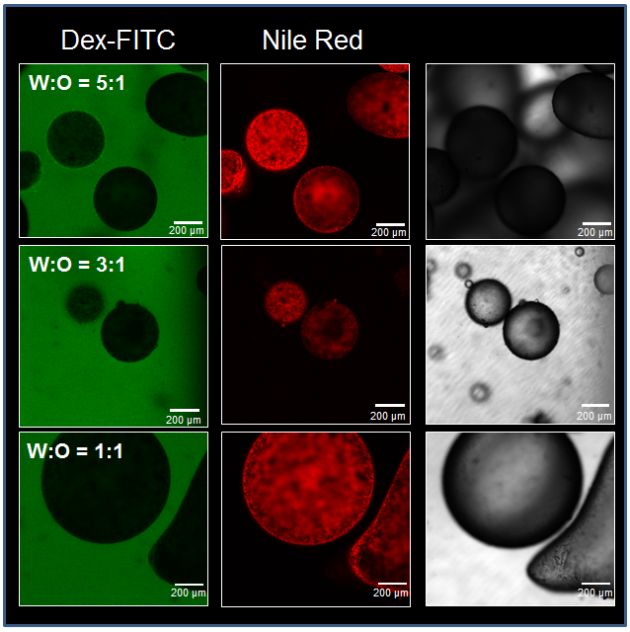

Figure 4.14. Confocal laser micrographs depicting the type of toluene-water emulsions formed *via* vortexing at a [MHN] = 1 mg/mL and varying W : O ratios.

Assembly of the Networks at the Oil/water Interface. To determine whether the MHNs assembled at the interface between oil and water, an emulsion of styrene and water was prepared *via* vortex at a W : O = 10 : 1, and AIBN was dissolved in styrene prior to emulsification to initiate the polymerization of styrene upon stabilization of the oil droplets by the MHNs. The solid sample obtained after polymerization was resuspended in THF and analyzed *via* scanning electron microscopy (SEM). The SEM results showed the formation of multiple PS beads of circular, as well as irregular shapes (Figure 4.15a and 4.15b); which corresponded to the shapes of the droplets observed *via* optical microscopy under all conditions studied. Additionally, inspection of the PS

beads at higher magnification revealed the presence of smaller nanostructures, which imparted texture to the surface of the beads. These nanostructures corresponded in size and shape to the SCKs that compose the network structure of the MHNs, and were not observed when PS beads were synthesized from the emulsion polymerization of styrene droplets stabilized solely by amine-IONs (Figures 4.15c and 4.16). In contrast, the amine-ION-stabilized beads showed a much smoother surface than those stabilized by the MHNs.

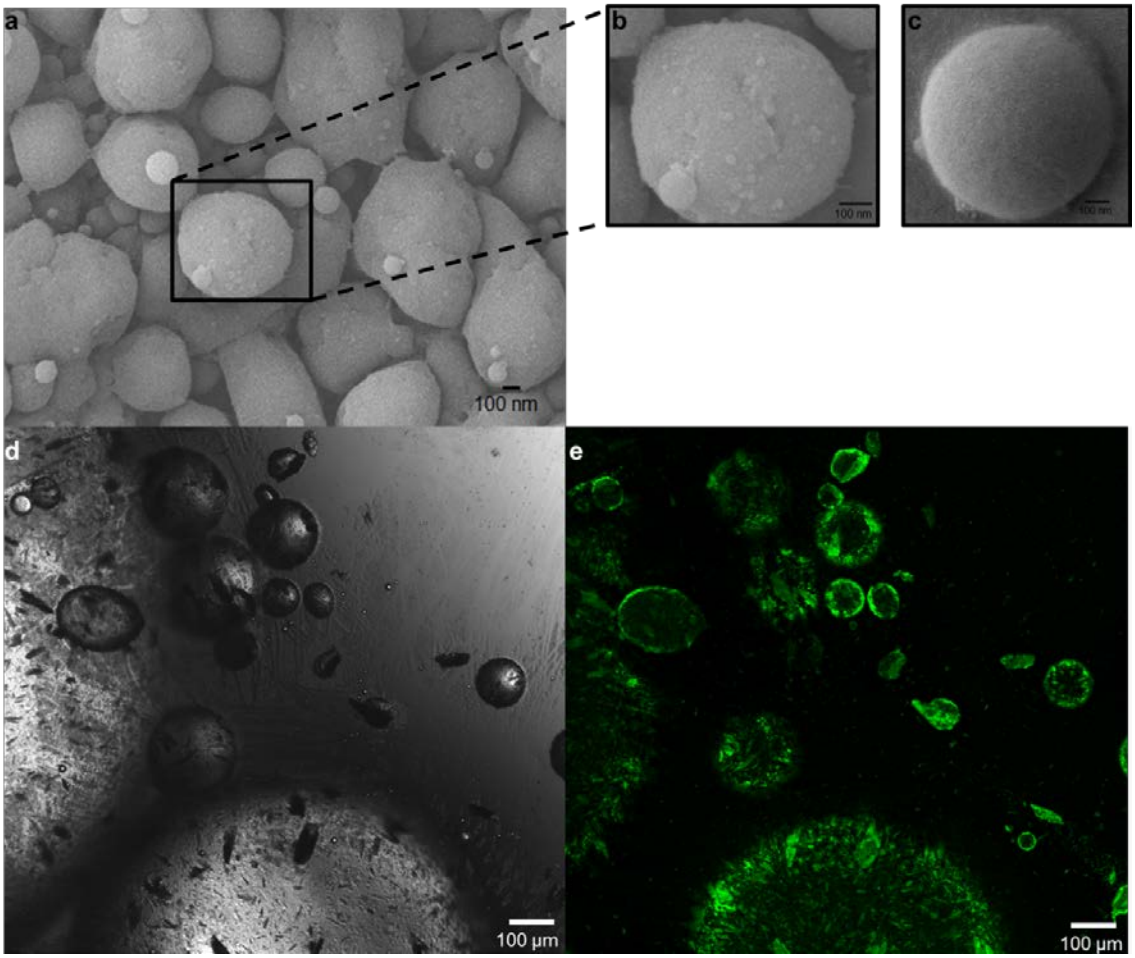

Figure 4.15. Scanning electron micrographs of polystyrene beads synthesized from the emulsion polymerization of styrene droplets stabilized in water by the MHNs (a - b), or by the amine-IONs (c). Optical micrograph (d) and confocal laser micrograph (e) of a toluene-water emulsion formed *via* vortex at a [FITC-MHN] = 1 mg/mL and W : O = 3 : 1, stabilized by FITC-MHNs.

Additionally, confocal microscopy was also employed to assess the surface coverage of the droplets by the hybrid networks. To do so, MHNs were prepared by utilizing micellar structures prepared from PAA_{90}-*b*-PS_{140} that were functionalized with

fluorescein-5-thiosemicarbazide (FITC), and which were crosslinked to generate FITC-functionalized SCKs. These fluorescently-labelled SCKs were further employed in the synthesis of the MHNs to yield FITC-functionalized MHNs (FITC-MHNs), which were utilized to prepare a toluene-water emulsion *via* vortex at a W : O = 3 : 1, and [FITC-MHN] = 1 mg/mL. The emulsion droplets were characterized both by optical microscopy (Figure 4.15d) and confocal microscopy (Figure 4.15e) upon excitation of the sample with a 488 nm laser. The data showed droplets of various sizes which are characteristic of the emulsions stabilized by the MHNs (Figure 4.15d). Moreover, the droplets appeared to be decorated with irregular species of different sizes and morphologies, which coincide with our previous characterization of the MHNs. Furthermore, the confocal image (Figure 4.15e) showed that the irregular structures present on the surface of the droplets exhibited green fluorescence, and covered the majority of the droplet's surface, although some areas of the surface remained uncovered.

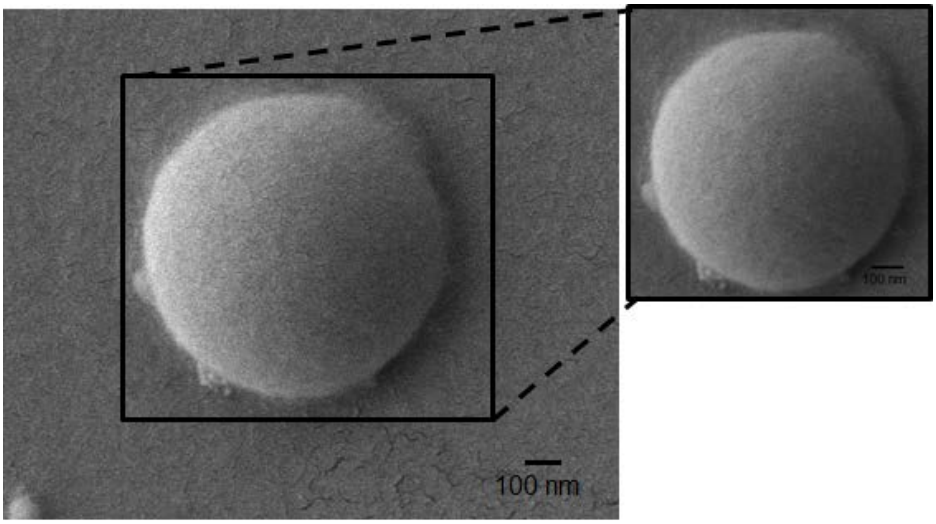

Figure 4.16. Scanning electron microscopy (SEM) image of polystyrene beads synthesized from the emulsion polymerization of styrene droplets stabilized by amine-IONs in water.

Additionally, given that the droplets appeared to be present at different positions along the Z axis, the sample was further analyzed by collecting multiple confocal images while progressively moving the focal point along the Z axis (Figure 4.17). The data showed the evolution of the surface coverage, which began from the bottom of the sample (Z = 0 μm - 16 μm) and displayed droplets covered with green fluorescence from the FITC-MHNs, to the formation of green "haloes" at higher Z coordinates (Z = 64 μm - 208 μm), which were a consequence of the arrangement of the FITC-MHNs at the oil/water interface. Unfortunately the large diameter of some of the droplets made it impossible to completely image the larger droplets from bottom to top; as the top of the droplet was out of the focal range of the instrument.

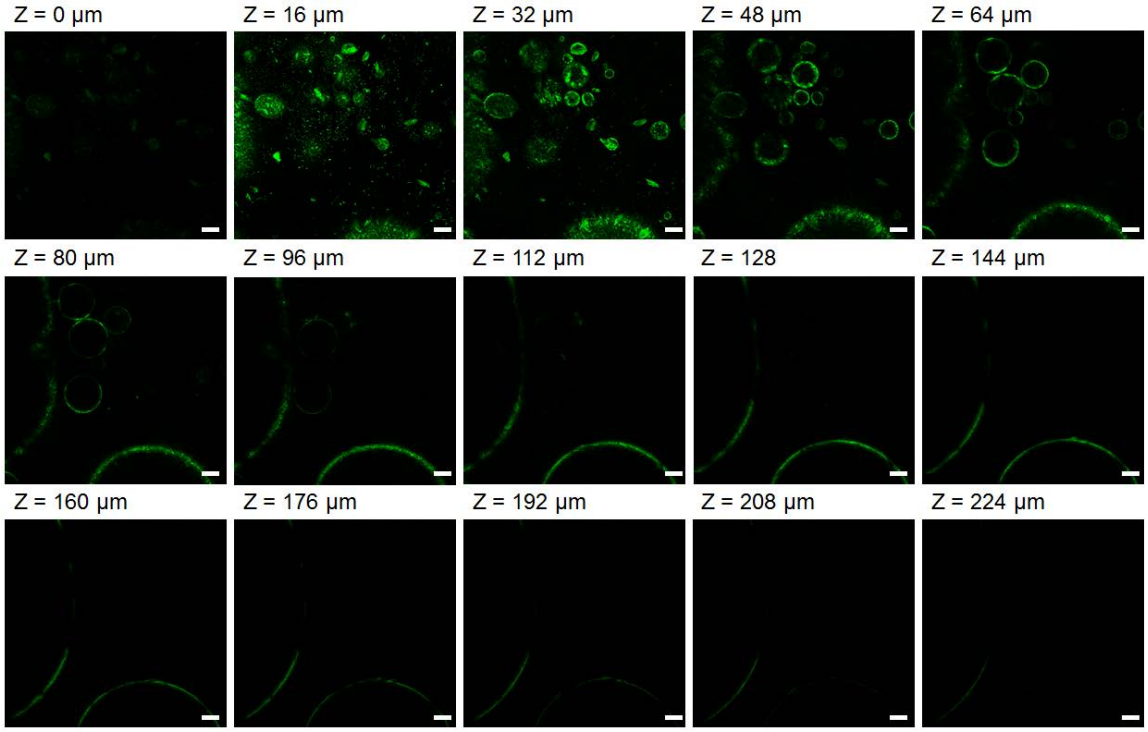

Figure 4.17. Confocal laser micrographs of a toluene-water emulsion formed *via* vortexing at a [FITC-MHN] = 1 mg/mL and W : O = 3 : 1, stabilized by FITC-MHNs. Images were taken at various positions along the z axis, beginning from the bottom (upper left image) and progressively moving to the top (bottom right). Scale bar = 100 µm.

Nevertheless, the combination of the SEM and confocal microscopy data showed that the MHNs can assemble at the oil/water interface to stabilize the emulsions, covering a significant portion of the droplets formed, despite the irregular size and shapes that are characteristic of the MHNs. Moreover, the unique capability of the MHNs to stabilize emulsion of hydrophobic monomers in water, and withstand polymerization, can give raise to the synthesis of materials with morphologies that may

be unattainable *via* the conventional methods employed for assembly of polymeric materials.

Magnetic Responsivity of Emulsions. One of the most interesting features of the emulsions stabilized by the MHNs is their responsivity to an applied magnetic field. This feature is attributed to the presence of magnetically-active IONs within the network structure of the MHNs, which in turn, stabilize the oil droplets formed. A qualitative assessment with a neodymium magnet (90 lbs. pull) allowed us to identify the magnetic response of the droplets, which were not only attracted to the magnet, but were also magnetically manipulated to transverse the interfacial barrier between the oil and water phases (See video of Figure 4.18). It was also noticed that upon removal of the applied magnetic field, the droplets returned to their original state, without disrupting the stability of the emulsion. Moreover, we have exploited this characteristic of the emulsions to separate the emulsified oil phase from the water phase *via* magnetic action (Figure 4.19). The toluene droplets were manipulated with a magnet while the water phase present in the sample was decanted, allowing the toluene droplets to remain inside the vial, thus separating the two phases. We have identified that the magnetic responsivity of these emulsions could be further exploited in applications related to the process of extraction of hydrocarbons, and the consequential water purification activities that are routinely performed in the oil and gas field.

Figure 4.18. By clicking the .mp4 file above see a video of magnetically active toluene-in-water emulsion droplets produced from MHNs in W : O at a ratio of 3 : 1.

Figure 4.19. Pictographic representation of a toluene-water emulsion before (left) and after (right) separation of the emulsion fraction *via* magnetic action.

4.4 Conclusions

We have explored the use of intricate, inorganic/organic composite networks, known as MHNs, as particle stabilizers for oil-water emulsions. Although the stabilization of Pickering emulsions has been traditionally achieved by the utilization of dispersed particles of different shapes and compositions, the use of network-like structures to stabilize emulsions has not been fully explored in the literature. The MHNs, which are composed of multiple polymeric nanoparticles bound to each other and to iron oxide nanoparticles, have displayed the ability to stabilize toluene-water and dodecane-water emulsions for at least 2 months. The emulsions stabilized can be homogenized by mechanical stimuli, such as vortexing or probe sonication; and in all cases oil droplets were stabilized in a continuous aqueous phase, yielding o/w emulsions.

To further understand the role of MHNs as particle stabilizers, the effects of the W : O ratio and MHN concentration on the droplet size distribution were analyzed. Although the emulsions displayed a high dispersity in the size of the droplets stabilized, the data showed that a W : O = 3 : 1 yielded the smallest droplets with the least dispersion observed, regardless of the type of oil and method of homogenization utilized. Moreover, the MHNs showed the remarkable ability to stabilize emulsions at extremely low concentrations. It was found that the emulsions homogenized *via* vortex at an MHN concentration of 1 mg/mL yielded the smallest droplets. These same results were observed for emulsions homogenized *via* probe sonication at a slightly higher concentration of 1.5 mg/mL.

Additionally, the magnetic character incorporated into the MHNs by the amine-IONs present within the network structure, led to the formation of magnetically-active emulsion droplets which were easily manipulated by an external magnetic field, providing a facile method of separation for the emulsified oil phase and the aqueous phase. This particular characteristic of the emulsions stabilized by such intricate network structures provides a pathway for their application not only towards the extraction of hydrocarbons *via* enhanced oil recovery, or after the implementation of the steam-assisted gravity drainage technology in oil sands, but also towards the remediation of the produced water that results from the constant efforts to provide clean and affordable energy to the growing global population. Each of these systems has the possibility for broad application in fields where emulsions are commonly employed, such as the beauty industry.

CHAPTER V

CONCLUSIONS

This dissertation has expanded on the design and synthesis of magnetically-active, hybrid inorganic/organic materials for the sequestration of hydrophobic contaminants present in aqueous environments; in particular, but not limited to, crude oil deposited in the water by oil spills. Progress has been made in the development of novel morphologies comprised of polymeric nanoparticles bound to magnetically-active iron oxide nanoparticles (IONs), which displayed the ability to sequester crude oil and other less complex pollutants, *via* the dual mechanisms of absorption and emulsification. These materials, now known as magnetically-active hybrid networks (MHNs), also displayed magnetic responsivity that allowed for their efficient removal from the contaminated environment once loaded, and for their possible utilization in multiple industrial applications thanks to the formation of emulsion droplets that can be easily manipulated with an external magnetic field.

Although it was not originally envisioned, the network-like structure of the MHNs allowed for the development of unique hierarchical structures, which displayed a remarkable ability to sequester pollutants with quantitative recyclability. The MHNs were originally designed to display a “raspberry-like” structure; however, the implementation of similar amidation chemistries for the crosslinking of the hydrophilic domain of the shell crosslinked knedel-like (SCK) nanoparticles, and for the covalent binding of the SCKs to amine-functionalized IONs (amine-IONs), yielded the formation

of network-like structures whose composition and morphology was uncontrolled. Their ability to sequester crude oil with an efficiency of up to 450%, coupled with the recovery of *ca.* 90% of the crude oil originally sequestered, and their recyclability for up to three cycles of remediation without compromising their loading capacity, allowed these complex nanostructures to compete with the remediation technologies available in the academic literature. Although the performance of the MHNs was remarkable, and some preliminary studies suggested that the MHNs could be capable of sequestering hydrophobic entities *via* the mechanism of emulsification, the performance of the MHNs in more complex saline environments remained unknown.

Chapter III addressed these unanswered questions by investigating the ability of the MHNs to sequester model aromatic and aliphatic components of crude oil, both in fresh water and saline environments. In order to facilitate the studies, toluene and dodecane were selected as model aromatic and aliphatic contaminants; respectively. Initially, no differences were found in the loading capacity of the MHNs towards both toluene and dodecane when sequestration was performed in water. However, the employment of less complicated pollutants allowed for the identification of emulsion formation during the sequestration experiments, and for the detailed investigation of the mechanism of interaction taking place between the MHNs and the pollutants. The results revealed that the MHNs were capable of absorbing hydrophobic contaminants from water, and of stabilizing emulsion droplets upon hand shaking of the MHNs/oil/water mixture. This latter mechanism of emulsion formation allowed us to explain the difference encountered in the loading capacity of the MHNs when

sequestration was performed in a saline environment. In general, a reduction in the loading capacity of the MHNs towards both pollutants was found, compared to the performance of the MHNs in water. The lower loadings were due to a reduction in the emulsification ability of the MHNs when salts were present in the system, and could be explained by the flocculation of particles in the presence of salts, and to an overall reduction in the concentration of MHNs capable of stabilizing the emulsion droplets.

Although the ability of the MHNs to stabilize emulsions was initially unexpected, this novel feature was further explored in Chapter IV. The studies revealed the formation of toluene-in-water and dodecane-in-water emulsions stabilized by these network-like structures, which had not been previously reported in the literature. Concentrations as low as 1 mg/mL were sufficient to generate toluene-water emulsions with a narrow droplet size distribution *via* vortexing; while a slightly higher concentration of 1.5 mg/mL was required to stabilize toluene-water and dodecane-water emulsions with similar characteristics, *via* probe sonication. The more mechanically-demanding homogenization method by probe sonication caused partial rupture of the network structure of the MHNs into smaller clusters of particles, and of the SCKs into individual polymer strands; however, some of the MHNs still exhibited the characteristic morphology after being subjected to the high shear and stress produced by probe sonication. These observations helped to explain why a somewhat higher concentration of MHNs was needed to obtain similar results *via* probe sonication. Moreover, studies performed *via* scanning electron microscopy (SEM) and fluorescence confocal microscopy revealed the assembly of the MHNs at the oil/water interface,

which yielded sufficient coverage of the oil droplets to prevent coalescence, thus generating emulsions stable for at least 2 months.

This dissertation has made significant contributions to the field of nanotechnology; specifically to the ramification of nanotechnology focused on the synthesis of remediating materials, as well as to the field of Pickering emulsions. The development of the complex MHNs, as well as their comparable loading capacity and efficient recyclability, are characteristics that make the MHNs a competitive system for the sequestration of hydrophobic pollutants. The highly efficient (> 90%) removal of the MHNs from water once loaded not only allows for the recovery and further reutilization of the oil spilled, but it significantly reduces the possibility of further contamination; an advantage that is not provided by the use of surfactants as a remediation approach. Nevertheless, the removal *via* magnetic action is not completely efficient, *ca.* 10% of the MHNs deployed cannot be removed from fresh water and *ca*. 20% cannot be recovered from saline environments. The amount of MHN that cannot be removed from the water, albeit small, can still pose significant threat to the flora and fauna of our planet; therefore, there exists the need to construct magnetically-active hybrid materials from biodegradable building blocks. The use of bio-based and degradable materials in the synthesis of MHN-type nanoconstructs, will allow for the breakdown of the fraction that remains in the water into less harmful components to the ecosystem, thereby diminishing the impact that these materials can have on the environment.

This piece of work has also led to an increased understanding of the performance and mechanistic operation of the MHNs in fresh water and saline environments; which has opened the door to the development of tailored nanomaterials capable of sequestering specific pollutants by exploiting the chemical composition of the polymeric component of the MHNs. Future studies should be focused on expanding the types of contaminants to be sequestered from aqueous environments, which could include polycyclic aromatic hydrocarbons (PAH) as well as heavy metal contaminants, such as arsenic and mercury. In addition, the ability of the MHNs to stabilize oil/water emulsions (specifically when the emulsion involves a hydrophobic monomer) and of withstanding conditions amenable to polymerization, could give rise to the development of materials capable of exhibiting morphologies that may be unattainable *via* the conventional methods employed for the assembly of nanoparticles.

REFERENCES

(1) Reports from the United States Coast Guard National Response Center, http://www.nrc.uscg.mil/Default.aspx, (accessed February, 2015).

(2) US Environmental Protection Agency: Oil Spill Response Techniques, http://www.epa.gov/emergencies/content/learning/oiltech.htm, (accessed September, 2013).

(3) Identification of Oil on Water: Aerial observation and identification guide, http://www.scribd.com/doc/220918003/AMSA-IDENTIFICATION-of-OIL-on-WATER-Aerial-Observation-and-Identification-Guide, (accessed November, 2014.).

(4) Gong, Y.; Zhao, X.; Cai, Z.; O'Reilly, S. E.; Hao, X.; Zhao, D. *Mar. Pollut. Bull.* **2014**, *79*, 16-33.

(5) Lessard, R. R.; DeMarco, G. *Spill. Sci. Technol. B.* **2000**, *6*, 59-68.

(6) Passow, U.; Ziervogel, K.; Asper, V.; Diercks, A. *Environ. Res. Lett.* **2012**, *7*, 035301.

(7) Ramsden, W. *Proc. R. Soc. London* **1903**, *72*, 156-164.

(8) Pickering, S. U. *J. Chem. Soc., Trans.* **1907**, *91*, 2001-2021.

(9) Aveyard, R.; Binks, B. P.; Clint, J. H. *Adv. Colloid Interface Sci.* **2003**, *100–102*, 503-546.

(10) Melle, S.; Lask, M.; Fuller, G. G. *Langmuir* **2005**, *21*, 2158-2162.

(11) Teas, C.; Kalligeros, S.; Zanikos, F.; Stournas, S.; Lois, E.; Anastopoulos, G. *Desalination* **2001**, *140*, 259-264.

(12) Zhu, Q.; Pan, Q.; Liu, F. *J. Phys. Chem. C* **2011**, *115*, 17464-17470.

(13) Calcagnile, P.; Fragouli, D.; Bayer, I. S.; Anyfantis, G. C.; Martiradonna, L.; Cozzoli, P. D.; Cingolani, R.; Athanassiou, A. *ACS Nano* **2012**, *6*, 5413-5419.

(14) Gui, X.; Cao, A.; Wei, J.; Li, H.; Jia, Y.; Li, Z.; Fan, L.; Wang, K.; Zhu, H.; Wu, D. *ACS Nano* **2010**, *4*, 2320-2326.

(15) Yuan, J.; Liu, X.; Akbulut, O.; Hu, J.; Suib, S. L.; Kong, J.; Stellacci, F. *Nat. Nanotechnol.* **2008**, *3*, 332-336.

(16) Cong, H.; Ren, X.; Wang, P.; Yu, S. *ACS Nano* **2012**, *6*, 2693-2703.

(17) Korhonen, J. T.; Kettunen, M.; Ras, R. H.; Ikkala, O. *ACS Appl. Mater. Interfaces* **2011**, *3*, 1813-1816.

(18) Basak, S.; Nanda, J.; Banerjee, A. *J. Mater. Chem.* **2012**, *22*, 11658-11664.

(19) Zhu, L.; Li, C.; Wang, J.; Zhang, H.; Jian, Z.; Shen, Y.; Li, C.; Wang, C.; Xie, A. *Appl. Surf. Sci.* **2012**, *258*, 6326-6330.

(20) Zhu, Q.; Tao, F.; Pan, Q. *ACS Appl. Mater. Interfaces* **2010**, *2*, 3141-3146.

(21) Pavía-Sanders, A.; Zhang, S.; Flores, J. A.; Sanders, J. E.; Raymond, J. E.; Wooley, K. L. *ACS Nano* **2013**, *7*, 7552-7561.

(22) Huang, H.; Kowalewski, T.; Remsen, E. E.; Gertzmann, R.; Wooley, K. L. *J. Am. Chem. Soc.* **1997**, *119*, 11653-11659.

(23) Zhang, S.; Li, Z.; Samarajeewa, S.; Sun, G.; Yang, C.; Wooley, K. L. *J. Am. Chem. Soc.* **2011**, *133*, 11046-11049.

(24) O'Reilly, R. K.; Joralemon, M. J.; Hawker, C. J.; Wooley, K. L. *Chem. Eur. J.* **2006**, *12*, 6776-6786.

(25) Zhang, F.; Zhang, S.; Pollack, S. F.; Li, R.; Gonzalez, A. M.; Fan, J.; Zou, J.; Leininger, S. E.; Pavía-Sanders, A.; Johnson, R.; Nelson, L. D.; Raymond, J. E.; Elsabahy, M.; Hughes, D. M. P.; Lenox, M. W.; Gustafson, T. P.; Wooley, K. L. *J. Am. Chem. Soc.* **2015**, *137*, 2056-2066.

(26) O'Reilly, R. K.; Joralemon, M. J.; Wooley, K. L.; Hawker, C. J. *Chem. Mater.* **2005**, *17*, 5976-5988.

(27) Rahm, B. G.; Bates, J. T.; Bertoia, L. R.; Galford, A. E.; Yoxtheimer, D. A.; Riha, S. J. *J. Environ. Manage.* **2013**, *120*, 105-113.

(28) Lutz, B. D.; Lewis, A. N.; Doyle, M. W. *Water Resour. Res.* **2013**, *49*, 647-656.

(29) Rahm, B. G.; Riha, S. J. *Environ. Sci.: Processes Impacts* **2014**, *16*, 1400-1412.

(30) Chen, N.; Pan, Q. *ACS Nano* **2013**, *7*, 6875-6883.

(31) Yang, Y.; Zhang, X.; Wang, Z. *Water Sci. Technol.* **2002**, *46*, 165-170.

(32) Li, Y. S.; Yan, L.; Xiang, C. B.; Hong, L. J. *Desalination* **2006**, *196*, 76-83.

(33) Maguire-Boyle, S. J.; Barron, A. R. *J. Membr. Sci.* **2011**, *382*, 107-115.

(34) Palchoudhury, S.; Lead, J. R. *Environ. Sci. Technol.* **2014**, *48*, 14558-14563.

(35) Handlin, D. L.; Thomas, E. L. *Macromolecules* **1983**, *16*, 1514-1525.

(36) Williams, D. B.; Carter, C. B. *Transmission Electron Microscopy: A Textbook for Materials Science*; 2nd ed.; Springer Science+Business Media, LLC 1996: New York, NY, **2009**; Vol. *3*.

(37) Rancourt, J. D.; Taylor, L. T. *Macromolecules* **1987**, *20*, 790-795.

(38) Chiang, P.-C.; Whang, W.-T. *Polymer* **2003**, *44*, 2249-2254.

(39) Agarwal, T.; Gupta, K. A.; Alam, S.; Zaidi, M. G. H. *International Journal of Composite Materials* **2012**, *2*, 17-21.

(40) Hsu, S.-C.; Whang, W.-T.; Hung, C.-H.; Chiang, P.-C.; Hsiao, Y.-N. *Macromol. Chem. Phys.* **2005**, *206*, 291-298.

(41) Lehr, B.; Bristol, S.; Possolo, A., Oil Budget Calculator: Deepwater Horizon, http://noaa.ntis.gov/view.php?pid=NOAA:ocn690106535, (accessed November, 2014).

(42) Zhou, J.; Qiao, X.; Binks, B. P.; Sun, K.; Bai, M.; Li, Y.; Liu, Y. *Langmuir* **2011**, *27*, 3308-3316.

(43) Kaiser, A.; Liu, T.; Richtering, W.; Schmidt, A. M. *Langmuir* **2009**, *25*, 7335-7341.

(44) Brown, P.; Butts, C. P.; Cheng, J.; Eastoe, J.; Russell, C. A.; Smith, G. N. *Soft Matter* **2012**, *8*, 7545-7546.

(45) Carls, M. G.; Holland, L.; Larsen, M.; Collier, T. K.; Scholz, N. L.; Incardona, J. P. *Aquat. Toxicol.* **2008**, *88*, 121-127.

(46) Carls, M. G.; Thedinga, J. F. *Mar. Environ. Res.* **2010**, *69*, 318-325.

(47) Peterson, C. H.; Rice, S. D.; Short, J. W.; Esler, D.; Bodkin, J. L.; Ballachey, B. E.; Irons, D. B. *Science* **2003**, *302*, 2082-2086.

(48) Allan, S. E.; Smith, B. W.; Anderson, K. A. *Environ. Sci. Technol.* **2012**, *46*, 2033-2039.

(49) Du, R.; Zhao, Q.; Li, P.; Ren, H.; Gao, X.; Zhang, J. *ACS Appl. Mater. Interfaces* **2016**, *8*, 1025-1032.

(50) Feng, L.; Zhang, Z.; Mai, Z.; Ma, Y.; Liu, B.; Jiang, L.; Zhu, D. *Angew. Chem., Int. Ed.* **2004**, *43*, 2012-2014.

(51) Tian, D.; Zhang, X.; Tian, Y.; Wu, Y.; Wang, X.; Zhai, J.; Jiang, L. *J. Mater. Chem.* **2012**, *22*, 19652-19657.

(52) Dudchenko, A. V.; Rolf, J.; Shi, L.; Olivas, L.; Duan, W.; Jassby, D. *ACS Nano* **2015**, *9*, 9930-9941.

(53) Zhu, H.; Qiu, S.; Jiang, W.; Wu, D.; Zhang, C. *Environ. Sci. Technol.* **2011**, *45*, 4527-4531.

(54) Choi, S.-J.; Kwon, T.-H.; Im, H.; Moon, D.-I.; Baek, D. J.; Seol, M.-L.; Duarte, J. P.; Choi, Y.-K. *ACS Appl. Mater. Interfaces* **2011**, *3*, 4552-4556.

(55) Yang, Y.; Tong, Z.; Ngai, T.; Wang, C. *ACS Appl. Mater. Interfaces* **2014**, *6*, 6351-6360.

(56) Wang, C.-F.; Lin, S.-J. *ACS Appl. Mater. Interfaces* **2013**, *5*, 8861-8864.

(57) Carreno, N. L. V.; Escote, M. T.; Valentini, A.; McCafferty, L.; Stolojan, V.; Beliatis, M.; Mills, C. A.; Rhodes, R.; Smith, C. T. G.; Silva, S. R. P. *Nanoscale* **2015**, *7*, 17441-17449.

(58) Zhuang, Y.-T.; Gao, W.; Yu, Y.-L.; Wang, J.-H. *Carbon* **2016**, *108*, 190-198.

(59) Hu, L.; Li, Y.; Zhang, X.; Wang, Y.; Cui, L.; Wei, Q.; Ma, H.; Yan, L.; Du, B. *Sci. Rep.* **2016**, *6*, 28924.

(60) Jabbari, V.; Veleta, J. M.; Zarei-Chaleshtori, M.; Gardea-Torresdey, J.; Villagrán, D. *Chem. Eng. J.* **2016**, *304*, 774-783.

(61) Brigante, M.; Pecini, E.; Avena, M. *Micropor. Mesopor. Mater.* **2016**, *230*, 1-10.

(62) Flores, J. A.; Pavía-Sanders, A.; Chen, Y.; Pochan, D. J.; Wooley, K. L. *Chem. Mater.* **2015**, *27*, 3775-3782.

(63) He, Y.; Liu, Y.; Wu, T.; Ma, J.; Wang, X.; Gong, Q.; Kong, W.; Xing, F.; Liu, Y.; Gao, J. *J. Hazard. Mater.* **2013**, *260*, 796-805.

(64) Zhang, S.; Shao, T.; Bekaroglu, S. S. K.; Karanfil, T. *Environ. Sci. Technol.* **2009**, *43*, 5719-5725.

(65) Xiao, J.; Du, J. *Polym. Chem.* **2016**, *7*, 4647-4653.

(66) Shi, L.; Chen, K.; Du, R.; Bachmatiuk, A.; Rümmeli, M. H.; Xie, K.; Huang, Y.; Zhang, Y.; Liu, Z. *J. Am. Chem. Soc.* **2016**, *138*, 6360-6363.

(67) Loche, D.; Malfatti, L.; Carboni, D.; Alzari, V.; Mariani, A.; Casula, M. F. *RSC Adv.* **2016**, *6*, 66516-66523.

(68) Bi, H.; Xie, X.; Yin, K.; Zhou, Y.; Wan, S.; He, L.; Xu, F.; Banhart, F.; Sun, L.; Ruoff, R. S. *Adv. Funct. Mater.* **2012**, *22*, 4421-4425.

(69) Coleman, W. E.; Munch, J. W.; Streicher, R. P.; Ringhand, H. P.; Kopfler, F. C. *Arch. Environ. Contam. Toxicol.* **1984**, *13*, 171-178.

(70) Anderson, J. W.; Neff, J. M.; Cox, B. A.; Tatem, H. E.; Hightower, G. M. *Mar. Biol.* **1974**, *27*, 75-88.

(71) Weaver, J. W., Chacteristics of Spilled Oils, Fuels, and Petroleum Products: 1. Composition and properties of selected oils, https://nepis.epa.gov/Exe/ZyNET.exe/P1000AE6.TXT?ZyActionD=ZyDocument&Client=EPA&Index=2000+Thru+2005&Docs=&Query=&Time=&EndTime=&SearchMethod=1&TocRestrict=n&Toc=&TocEntry=&QField=&QFieldYear=&QFieldMonth=&QFieldDay=&IntQFieldOp=0&ExtQFieldOp=0&XmlQuery=&File=D%3A%5Czyfiles%5CIndex%20Data%5C00thru05%5CTxt%5C00000013%5CP1000AE6.txt&User=ANONYMOUS&Password=anonymous&SortMethod=h%7C-&MaximumDocuments=1&FuzzyDegree=0&ImageQuality=r75g8/r75g8/x150y150g16/i425&Display=hpfr&DefSeekPage=x&SearchBack=ZyActionL&Back=ZyActionS&BackDesc=Results%20page&MaximumPages=1&ZyEntry=1&SeekPage=x&ZyPURL, (accessed October, 2016).

(72) Boehm, P. D.; Fiest, D. L.; Mackay, D.; Paterson, S. *Environ. Sci. Technol.* **1982**, *16*, 498-505.

(73) What is Weathering?, http://response.restoration.noaa.gov/oil-and-chemical-spills/significant-incidents/exxon-valdez-oil-spill/what-weathering.html, (accessed July, 2016).

(74) Dwarakish, G. S.; Mishra, A. K.; Kumar, G. S. *Aquatic Procedia* **2015**, *4*, 435-442.

(75) Saeed, T.; Al-Mutairi, M. *Environ. Int.* **1999**, *25*, 117-129.

(76) In *Emulsions: Fundamentals and Applications in the Petroleum Industry*; 1 ed.; Schramm, L. L., Ed.; American Chemical Society: Washington DC, 1992, p 1 - 129.

(77) Le Floch, S.; Guyomarch, J.; Merlin, F.-X.; Stoffyn-Egli, P.; Dixon, J.; Lee, K. *Spill. Sci. Technol. B.* **2002**, *8*, 65-71.

(78) Sacanna, S.; Kegel, W. K.; Philipse, A. P. *Phys. Rev. Lett.* **2007**, *98*, 158301.

(79) Tambe, D. E.; Sharma, M. M. *Adv. Colloid Interface Sci.* **1994**, *52*, 1-63.

(80) Ashby, N. P.; Binks, B. P. *Phys. Chem. Chem. Phys.* **2000**, *2*, 5640-5646.

(81) Greenspan, P.; Fowler, S. D. *J. Lipid Res.* **1985**, *26*, 781-789.

(82) Dutta, A. K.; Kamada, K.; Ohta, K. *J. Photochem. Photobiol., A* **1996**, *93*, 57-64.

(83) Datta, A.; Mandal, D.; Pal, S. K.; Bhattacharyya, K. *J. Phys. Chem. B* **1997**, *101*, 10221-10225.

(84) Ghoneim, N. *Spectrochim. Acta, Part A* **2000**, *56*, 1003-1010.

(85) Sangster, J. *J. Phys. Chem. Ref. Data* **1989**, *18*, 1111-1229.

(86) Blanco, E.; Lam, S.; Smoukov, S. K.; Velikov, K. P.; Khan, S. A.; Velev, O. D. *Langmuir* **2013**, *29*, 10019-10027.

(87) Fameau, A.-L.; Lam, S.; Velev, O. D. *Chem. Sci.* **2013**, *4*, 3874-3881.

(88) Lam, S.; Blanco, E.; Smoukov, S. K.; Velikov, K. P.; Velev, O. D. *J. Am. Chem. Soc.* **2011**, *133*, 13856-13859.

(89) Williams, M.; Warren, N. J.; Fielding, L. A.; Armes, S. P.; Verstraete, P.; Smets, J. *ACS Appl. Mater. Interfaces* **2014**, *6*, 20919-20927.

(90) Cunha, A. G.; Mougel, J.-B.; Cathala, B.; Berglund, L. A.; Capron, I. *Langmuir* **2014**, *30*, 9327-9335.

(91) Bon, S. A. F.; Colver, P. J. *Langmuir* **2007**, *23*, 8316-8322.

(92) Teixeira, R. F. A.; McKenzie, H. S.; Boyd, A. A.; Bon, S. A. F. *Macromolecules* **2011**, *44*, 7415-7422.

(93) Colver, P. J.; Colard, C. A. L.; Bon, S. A. F. *J. Am. Chem. Soc.* **2008**, *130*, 16850-16851.

(94) Yan, H.; Zhao, B.; Long, Y.; Zheng, L.; Tung, C.-H.; Song, K. *Colloids Surf., A* **2015**, *482*, 639-646.

(95) Mejia, A. F.; Diaz, A.; Pullela, S.; Chang, Y.-W.; Simonetty, M.; Carpenter, C.; Batteas, J. D.; Mannan, M. S.; Clearfield, A.; Cheng, Z. *Soft Matter* **2012**, *8*, 10245-10253.

(96) Lin, Y.; Skaff, H.; Böker, A.; Dinsmore, A. D.; Emrick, T.; Russell, T. P. *J. Am. Chem. Soc.* **2003**, *125*, 12690-12691.

(97) Lin, Y.; Skaff, H.; Emrick, T.; Dinsmore, A. D.; Russell, T. P. *Science* **2003**, *299*, 226-229.

(98) Glogowski, E.; He, J.; Russell, T. P.; Emrick, T. *Chem. Commun.* **2005**, 4050-4052.

(99) Sacanna, S.; Philipse, A. P. *Adv. Mater.* **2007**, *19*, 3824-3826.

(100) Russell, J. T.; Lin, Y.; Böker, A.; Su, L.; Carl, P.; Zettl, H.; He, J.; Sill, K.; Tangirala, R.; Emrick, T.; Littrell, K.; Thiyagarajan, P.; Cookson, D.; Fery, A.; Wang, Q.; Russell, T. P. *Angew. Chem., Int. Ed.* **2005**, *44*, 2420–2426.

(101) Dinsmore, A. D.; Hsu, M. F.; Nikolaides, M. G.; Marquez, M.; Bausch, A. R.; Weitz, D. A. *Science* **2002**, *298*, 1006-1009.

(102) Wang, Z.; van Oers, M. C. M.; Rutjes, F. P. J. T.; van Hest, J. C. M. *Angew. Chem., Int. Ed.* **2012**, *51*, 10746-10750.

(103) Walther, A.; Hoffmann, M.; Müller, A. H. E. *Angew. Chem., Int. Ed.* **2008**, *47*, 711-714.

(104) Passas-Lagos, E.; Schüth, F. *Langmuir* **2015**, *31*, 7749-7757.

(105) Fujii, S.; Cai, Y.; Weaver, J. V. M.; Armes, S. P. *J. Am. Chem. Soc.* **2005**, *127*, 7304-7305.

(106) Yu, S.; Tan, H.; Wang, J.; Liu, X.; Zhou, K. *ACS Appl. Mater. Interfaces* **2015**, *7*, 6745-6753.

(107) Wei, Y.; Chen, J.; Zhang, Y.; Lu, Z. *RSC Adv.* **2015**, *5*, 71824-71829.

(108) Rayner, M.; Timgren, A.; Sjöö, M.; Dejmek, P. *J. Sci. Food Agric.* **2012**, *92*, 1841-1847.

(109) Gupta, R.; Rousseau, D. *Food Funct.* **2012**, *3*, 302-311.

(110) Dora Tang, T. Y.; Rohaida Che Hak, C.; Thompson, A. J.; Kuimova, M. K.; Williams, D. S.; Perriman, A. W.; Mann, S. *Nature Chem.* **2014**, *6*, 527-533.

(111) Skaff, H.; Lin, Y.; Tangirala, R.; Breitenkamp, K.; Böker, A.; Russell, T. P.; Emrick, T. *Adv. Mater.* **2005**, *17*, 2082-2086.

(112) Thompson, K. L.; Chambon, P.; Verber, R.; Armes, S. P. *J. Am. Chem. Soc.* **2012**, *134*, 12450-12453.

(113) Yuan, Q.; Cayre, O. J.; Fujii, S.; Armes, S. P.; Williams, R. A.; Biggs, S. *Langmuir* **2010**, *26*, 18408-18414.

(114) Pakdel, A.; Pourmahdian, S.; Eslami, H. *Macromol. Chem. Phys.* **2012**, *213*, 1944-1952.

(115) Thompson, K. L.; Armes, S. P.; Howse, J. R.; Ebbens, S.; Ahmad, I.; Zaidi, J. H.; York, D. W.; Burdis, J. A. *Macromolecules* **2010**, *43*, 10466-10474.

(116) Shen, M.; Resasco, D. E. *Langmuir* **2009**, *25*, 10843-10851.

(117) Crossley, S.; Faria, J.; Shen, M.; Resasco, D. E. *Science* **2010**, *327*, 68-72.

(118) Shabani Afrapoli, M.; Crescente, C. M.; Li, S.; Alipour, S.; Torsater, O. In *Oil and Gas West Asia*; Society of Petroleum Engineers: Muscat, Oman, 2012.

(119) Altundas, Y. B.; Li, J.; Chugunov, N.; Ramakrishnan, T. S.; Society of Exploration Geophysicists: 2015, p 5472-5476.

(120) Gao, B.; Sharma, M. M. In *SPE Annual Technical Conference and Exhibition* Society of Petroleum Engineers: San Antonio, TX, 2012.

(121) Bourbiaux, B.; Fourno, A.; Nguyen, Q.-L.; Norrant, F.; Robin, M.; Rosenberg, E.; Argillier, J.-F. *SPE-169140-PA* **2015**.

(122) Chen, Y.; Elhag, A. S.; Poon, B. M.; Cui, L.; Ma, K.; Liao, S. Y.; Reddy, P. P.; Worthen, A. J.; Hirasaki, G. J.; Nguyen, Q. P.; Biswal, S. L.; Johnston, K. P. *SPE-154222-PA* **2014**.

(123) Inoue, M.; Hashizaki, K.; Taguchi, H.; Saito, Y. *J. Dispersion Sci. Technol.* **2010**, *31*, 1648-1651.

(124) Xu, H.; Cui, L.; Tong, N.; Gu, H. *J. Am. Chem. Soc.* **2006**, *128*, 15582-15583.

(125) Binks, B. P.; Rodrigues, J. A. *Langmuir* **2007**, *23*, 7436-7439.

(126) Cheng, J.; Teply, B. A.; Jeong, S. Y.; Yim, C. H.; Ho, D.; Sherifi, I.; Jon, S.; Farokhzad, O. C.; Khademhosseini, A.; Langer, R. S. *Pharm. Res.* **2006**, *23*, 557-564.

(127) Cao, N.; Liu, S.; Wu, M.; Deng, R.; Wang, J.; Zhang, Z.; Zhu, J. *Eur. Polym. J.* **2013**, *49*, 3691-3701.

(128) Dunstan, T. S.; Fletcher, P. D. I.; Mashinchi, S. *Langmuir* **2012**, *28*, 339-349.

(129) Hunter, T. N.; Jameson, G. J.; Wanless, E. J.; Dupin, D.; Armes, S. P. *Langmuir* **2009**, *25*, 3440-3449.

(130) Dupin, D.; Howse, J. R.; Armes, S. P.; Randall, D. P. *J. Mater. Chem.* **2008**, *18*, 545-552.

(131) Felipe, V.; Hawe, A.; Jiskoot, W. *Pharm. Res.* **2010**, *27*, 796-810.

(132) Demeester, J.; De Smedt, S. S.; Sanders, N. N.; Haustraete, J. In *Methods for Structural Analysis of Protein Pharmaceuticals*; Jiskoot, W., Crommelin, D. J. A., Eds.; AAPS: Arlington, VA, 2005, p 245-275.

(133) Nallamilli, T.; Binks, B. P.; Mani, E.; Basavaraj, M. G. *Langmuir* **2015**, *31*, 11200-11208.

(134) Ridel, L.; Bolzinger, M.-A.; Gilon, N.; Dugas, P.-Y.; Chevalier, Y. *Soft Matter* **2016**, *12*, 7564-7576.

(135) Tadros, T. F. In *Emulsion Formation and Stability*; Wiley-VCH Verlag GmbH & Co. KGaA: 2013, p 1-75.

(136) Kosif, I.; Cui, M.; Russell, T. P.; Emrick, T. *Angew. Chem., Int. Ed.* **2013**, *125*, 6752-6755.

(137) Sawawi, M.; Wang, T. Y.; Nisbet, D. R.; Simon, G. P. *Polymer* **2013**, *54*, 4237-4252.

(138) Li, Y.; Niu, Z.; Burdyńska, J.; Nese, A.; Zhou, Y.; Kean, Z. S.; Dobrynin, A. V.; Matyjaszewski, K.; Craig, S. L.; Sheiko, S. S. *Polymer* **2016**, *84*, 178-184.

(139) Zhang, K.; Fang, H.; Chen, Z.; Taylor, J.-S. A.; Wooley, K. L. *Bioconjugate Chem.* **2008**, *19*, 1880-1887.

(140) Guérin, G.; Wang, H.; Manners, I.; Winnik, M. A. *J. Am. Chem. Soc.* **2008**, *130*, 14763-14771.

(141) Yan, X.; Liu, G.; Li, H. *Langmuir* **2004**, *20*, 4677-4683.

(142) Wang, X.; Guerin, G.; Wang, H.; Wang, Y.; Manners, I.; Winnik, M. A. *Science* **2007**, *317*, 644-647.

(143) Massey, J.; Power, K. N.; Manners, I.; Winnik, M. A. *J. Am. Chem. Soc.* **1998**, *120*, 9533-9540.